OPTICAL FILTERS BASED ON MICROFIBER KNOT RESONATOR STRUCTURES

SOMAYEH NODEHI

DISSERTATION SUBMITTED IN FULFILMENT OF THE REQUIREMENTS OF THE DEGREE OF DOCTOR OF PHILOSOPHY

INSTITUTE OF GRADUATE STUDIES
UNIVERSITY OF MALAYA
KUALA LUMPUR

2016

University of Malaya

ORIGINAL LITERARY WORK DECLARATION

Name of Candidate: **SOMAYEH NODEHI**

Registration/Matric No: **HHE120003**

Name of Degree: **Doctor of Philosophy (Ph.D)**

Title of Project Paper/Research Report/Dissertation/Thesis ("this Work"):

OPTICAL FILTERS BASED ON MICROFIBER KNOT RESONATOR STRUCTURES

Field of Study: **PHOTONICS**

I do solemnly and sincerely declare that:

1. I am the sole author/writer of this Work;
2. This Work is original;
3. Any use of any work in which copyright exists was done by way of fair dealing and for permitted purposes and any excerpt or extract from, or reference to or reproduction of any copyright work has been disclosed expressly and sufficiently and the title of the Work and its authorship have been acknowledged in this Work;
4. I do not have any actual knowledge nor do I ought reasonably to know that the making of this work constitutes an infringement of any copyright work;
5. I hereby assign all and every rights in the copyright to this Work to the University of Malaya ("UM"), who henceforth shall be owner of the copyright in this Work and that any reproduction or use in any form or by any means whatsoever is prohibited without the written consent of UM having been first had and obtained;
6. I am fully aware that if in the course of making this Work I have infringed any copyright whether intentionally or otherwise, I may be subject to legal action or any other action as may be determined by UM.

Candidate's Signature Date

Subscribed and solemnly declared before,

Witness's Signature Date

Name:

Designation:

University of Malaya

ABSTRACT

Microfiber Resonators are considered as an alternative waveguide due to their low-cost and accessible fabrication technology. This dissertation investigates combination of microfiber resonators for filter application. Also in this work thermal effect on complex structure is used to tune and modify filter factors. In the first section of this research this approach is applied to tune the extinction ratio of a microfiber Mach-Zhender-knot structure output. The same approach is used in a double-knot resonator to correct its optical path and increase the finesse. Then, a period pass-band filter based microfiber structure is proposed. The structure is made of successive microfiber knot resonators. As a result a periodical spectral filtering is obtained. In addition, an experimental investigation of the thermal effect on the spectral modulation of the structure is demonstrated.

Several novel simple types of microfiber knot structures are introduced. These structures generate a periodic output spectrum with an adjustable band-pass using Vernier effect. The structures are combination of knot resonators with semi ring. It is calculated that the obtained finesse from the structure is bigger than that of a single knot. The structures with different size are fabricated in order to obtain various spectra with different bandwidth and increase the suppression ratio that resulted from Vernier effect.

Finally, a single knot is used to investigate the nonlinearity (Kerr effect). The results are used to design an XOR gate. A comparison between thresholds power of stimulation this nonlinearity at passive and active microfiber are shown.

University of Malaya

ABSTRAK

Resonator-resonator gentian mikro dipertimbangkan sebagai satu pandu gelombang yang kos rendah dan teknologi fabrikasi boleh akses. Disertasi ini menyiasat gabungan resonator-resonator gentian mikro untuk aplikasi penapis. Dalam kerja ini juga kesan haba pada struktur yang komplek diguna untuk menala dan ubahsuai faktor-faktor penapis. Dalam seksyen pertama penyelidikan ini, pendekatan ini dikenakan untuk menala nisbah kejatuhan satu gentian mikro struktur keluaran Mach-Zhender-simpulan. Pendekatan yang sama juga dikenakan dalam satu resonator simpulan-ganda untuk memperbetulkan laluan optiknya dan meningkatkan kehalusan tersebut. Kemudian, satu tempoh penapis jalur-lulus berdasarkan struktur gentian mikro diperkenalkan. Stuktur tersebut dibuat dengan resonator-resonator berturut simpulan gentian mikro. Sebagai satu keputusan, satu spektrum pentempohan ditentukan. Tambahan lagi, satu ujikaji penyiasatan terhadap kesan haba pada spektrum modulasi struktur tersebut dipamerkan. Beberapa jenis struktur simpulan gentian mikro yang baru dan ringkas dipernekalkan. Struktur-struktur ini menjana satu keluaran bertempoh dengan jalur-lulus boleh laras menggunakan kesan Vernier. Struktur-struktur tersebut adalah gabungan resonator-resonator simpulan dengan separuh lingkaran. Ia dikira penentuan kehalusan daripada struktur yang lebih besar daripada simpulan tunggal. Sturktur-struktur tersebut dengan saiz yang berbeza difabrikasi untuk menentukan pelbagai spektrum dengan perbezaan lebarjalur dan meningkatkan nisbah yang memberi keputusan daripada kesan Vernier. Akhir sekali, satu simpulan tunggal diguna untuk menyiasat ketidaklinearan (kesan Kerr). Keputusannya diguna untuk merekabentuk satu pintu XOR. Satu perbandingan antara simulasi kuasa ambang dengan menunjukan ketidaklinearan pada gentian mikro pasif dan aktif.

University of Malaya

ACKNOWLEDGMENT

I would like to thank my advisors Prof. Sulaiman Wadi Harun and Prof. Harith Ahmad for their constant support and help during the course of my Ph.D work. Special appreciation goes to my co-Supervisor, Dr. Waleed Mohammad for his precious help and constructive comments during my thesis work. I would like to deliver special thanks to my colleagues at the PRC. I would like also to thank the team at BU-CROCCS for providing a great opportunity to be part of their team as a visiting researcher. Special thanks to Dr. Romuld Jolivot for his priceless help to edit my thesis. Finally, I would like to thank my family and friends who were continuously there for me.

University of Malaya

TABLE OF CONTENTS

University of Malaya

University of Malaya

LIST OF FIGURES

University of Malaya

University of Malaya

University of Malaya

University of Malaya

University of Malaya

University of Malaya

ABBREVIATIONS

WDM	Wavelength Division Multiplexing
3D	Three Dimensional
Tb/s	Terabit per Second
MZ	Mach-Zender
MZI	Mach-Zneder Interferometer
DC	Direct Current
ER	Extinction ratio
FSR	Free Spectral Range
FWHM	Full Width at Half Maximum
FE	Field Enhancement
QF	Quality Factor
EDFA	Erbium Doped Fiber Amplifier
OSA	Optical Spectrum Analyzer
ASE	Amplified Spontaneous Emission
µm	Micrometer
nm	Nanometer
pm	Picometer
MKR	Microfiber Knot Resonator
MLR	Microfiber Loop Resonator
^{0}C	Degree Centigrade
dB	Decibel
dBm	Decibel-milliwatt

University of Malaya

Er	Erbium
W	Watt
mW	milliWatt

University of Malaya

CHAPTER 1

INTRODUCTON

1.1 Background of Microfiber

Optical microfibers have attracted attentions in recent decades because of their wide applications in sensing (Liao et al., 2014; Shao et al., 2014; P. Wang et al., 2011), optical communication (Y. Wu et al., 2008; Zou et al., 2014), nonlinear optics (Gouveia et al., 2013; Vienne et al., 2008) and signal processing (Y. Zhang et al., 2009). Increasing the rate of data communication and demanding for faster data transmissions motivated the fabrication of optical components with smaller dimensions and shorter time scale response. It has been estimated that optical devices in the range of micrometers to nanometers can handle and process optical signals highly efficiently. For instance, it is predicted that to reach an optical transmission rate of about 10 Tb/s, a photonic matrix switching device of the order of 100 nanometer is required (Kawazoe, 2006). Reducing the dimensions reduces as well the power consumption of the device (Guo et al., 2013;Limin Tong et al., 2011; X. Wu et al., 2013). Implementation of small size components such as light sources and active elements requires a mean of transmitting data from one end to another. Hence, waveguides play a key role in future micro- and nano-photonic integrated systems. When waveguide dimensions reach the order of wavelength and sub-wavelength, less power is confined in the guiding region. High fractional of the light becomes in the form of evanescence field (Guo et al., 2013; J. Lou et al., 2005).

Silicon on isolator waveguide (Tien et al., 2011), semiconductor crystalline nanowires (Tian et al., 2009), plasmatic waveguides (Durfee III et al., 1995), and microfibers (Sumetsky, 2010) are few examples of waveguides with micrometer to nanometer

University of Malaya

dimensions. Among these guides, microfiber has the advantages of low loss, easy fabrication, simple structure, high flexibility, and it is easy to manipulate (Sumetsky et al., 2005). Their capabilities for doping and coating opens the way in various fields of microscopic optical devices such as micro-lasers (Z. S. Zhang et al., 2013) and micro-sensors (G. Y. Chen et al., 2013). Microfibers with cladding diameter of about tens of micrometers and its corresponding core diameter of several micrometers, with low refractive index, have been developed as a promising waveguides with applications such as optical couplers (Bo et al., 2014), sensors (Jin, et al., 2013; Kou et al., 2012; J. X. Wu et al., 2014), filters (X. D. Jiang et al., 2007), and lasers (Zhou et al., 2011).

Stable evanescent field, smaller dimensions, higher sensitivity and lower power consumption in micro-fibers allowed them to be considered as basic elements in photonic components (X. D. Jiang et al., 2007; Ma et al., 2012; Y. Zhang et al., 2009). It is also easy to use these fibers in order to fabricate microresonators or 3D structures such as micro coil and microball. Their performances are comparable with microring (Sumetsky, 2005) and optical planar waveguides (Sumetsky, 2008). Accordingly, this dissertation uses flame-brushing method to draw a conventional single mode fiber into a microfiber. This is due to the noticeable good compatibility of microfiber with the commercial single mode fiber compared to other waveguides (J. Zhang et al., 2012). Fabrication of high quality factor microfiber components such as resonators, couplers and interferometers is the next target in microfiber technology.

University of Malaya

1.2 Microfiber Elements and Applications

Microfibers can be employed as both freestanding (Limin Tong et al., 2003) and supported waveguides (Limin Tong et al., 2005) which do not involved substrate distortion and airflow effect respectively. Also, these structures are efficient coupler due to their micro-waist that obtains strong evanescent field. Microfiber can be assembled as different couplers with tuning coupling coefficient by changing the physical coupling length. In addition, microfiber couplers can be fabricated using different methods such as fusing two fibers (G. Kakarantzas et al., 2001) while they are heated during the process. In another method Van Der Waals force is used to couple two microfibers when they are brought in contact (Sumetsky et al., 2005).

These microfiber couplers can be used as building blocks for interferometer based systems. Interferometers are widely used for telecommunication applications (Jerman et al., 1991), spectroscopy (Lepetit et al., 1995) and medical applications (Morgner et al., 2000). Mach-Zender and Sagnac interferometers are two common interferometers which have been employed in many areas such as optical sensors (J. Li et al., 2012), modulators (S. D. Lim et al., 2010; Wong et al., 2002) and filters (Aryanfar et al., 2012). Change in the refractive index of the medium around arms causes phase difference that makes these devices phase sensitive (Aryanfar et al., 2012). Using microfibers in forming these interferometers allows more evanescent wave into the sensing region. That enhances the light environment interaction and hence high sensitivity is expected.

Mach-Zneder interferometer (MZI) for example can be formed by placing two microfiber couplers in series (Y. H. Chen et al., 2010). Another interferometer can be formed due to irregularities in one microfiber (a non-adiabatic microfiber). In this case a

University of Malaya

blub of silica occurs between two segments of the microfiber as shown in Figure 1.1. The figure shows two kinds of Mach-Zender, an inline MZI with a bulb inside the microfiber (Figure 1.1 (a)) and a two-arm MZI (Figure 1.1 (b)).

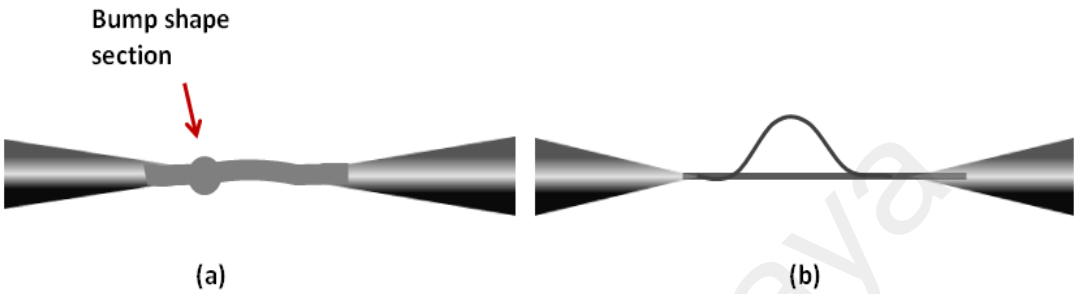

Figure 1.1: The sketch from (a) an in line Mack-Zender, (b) a two arms Mach-Zender.

The originally single mode fiber then excites two or few modes in the bulb. The change of environment then causes relative phases between the modes to change and hence beating fringes are observed in the output spectrum. This is referred to as in line MZI (Liao et al., 2013). Sagnac interferometer can be fabricated when a microfiber is arranged in a shape of loop or coil that couples back to itself (Y. Chen et al., 2013).

Resonators are the basic optical elements that have been employed as building blocks in photonic integrated circuits. There are a few resonators which have been fabricated for sensing (N. K. Chen et al., 2013; Wei et al., 2014; J. X. Wu et al., 2014), laser (Fan et al., 2012) and filter (Y. Wu et al., 2008) applications. Microfiber knot (X. S. Jiang, Tong, et al., 2006) and loop (Sumetsky et al., 2006) are two basic resonator elements which can be designed and fabricated by macro manipulation. Twisting microfiber can form a loop easily (Sumetsky et al., 2005). Microfiber knot has more stability compared to the microfiber loop and it is easier to manipulate. While making a knot, a microfiber should be cut into two parts. One of the microfiber parts is looped around two non-stick separated bars before a knot is formed via micro-manipulation. The two bars are then pressed close to

University of Malaya

each other to separate the sticky microfiber from the bars and then pulled up to form the knot. Both processes are performed in free space, while microcoil and microfiber needs to be wrapped around a central rod (Sumetsky, 2004).

As mentioned earlier, graphen and gold coated and dopant microfiber may be used for laser application (Sulaiman et al., 2014; Ta et al., 2014). There are a few methods to design a microfiber laser. Erbium doped microfiber laser has been demonstrated by using erbium doped microfiber loop as a doped cavity structure (Y. H. Li et al., 2006; Sulaiman et al., 2013). Also, a combination of a straight erbium doped microfiber and a microball can be used to construct a laser (Sulaiman et al., 2012). In addition to doped and co-doped microfiber lasers, some dye lasers are designed based on microfiber knot immersed into a dye solution (X. S. Jiang et al., 2007).

Nonlinearity in microfiber has been studied since 2008 by Vienne, et al (Vienne et al., 2008; Vienne et al., 2008). The study shows a nonlinear phase shift in a silica microfiber resonator (Vienne, Li, et al., 2008). Following this research, nonlinearity in a high Q-value microfiber coil has been investigated to demonstrate a bistable nonlinear resonator (Broderick, 2008). In 2012, the potential of microfiber has been studied (Arjmand et al., 2012; Ismaeel et al., 2012) and nonlinear device based on microfiber resonator has been introduced and demonstrated theoretically and experimentally. A microfiber loop resonator has been considered for field enhancement through the loop by Ismaeel, et al (Ismaeel et al., 2012). The study investigated the third harmonic generation enhancement in microfiber loop. Stimulation of the second harmonic generation inside a microfiber has been done by the same group in 2013 in which they demonstrated how to enhance the phenomena using microfiber loop resonators (Gouveia et al., 2013).

University of Malaya

Recently, microfiber filters has been receiving an increasing interest in telecommunication as add/drop (X. D. Jiang et al., 2007) and short pass filter (Yuan Chen et al., 2008). Add drop filters are basic photonic component with simple design and various forms. Microfiber loop and knot have been considered as add drop filters, which show good compatibility with optical fiber systems. Micro fiber Mach Zender has been employed as band pass filter (Aryanfar et al., 2012).

In addition to all the structures mentioned, there are a few complex microfiber structures which combine different resonators and interferometers and connect them in cascade for sensing (Y. Wu et al., 2011) and laser (Fan et al., 2012; Yang et al., 2009) applications.

1.3 Objective and Scope of Thesis

This research focuses on design and fabrications of new optical filters to employed in telecommunication system, laser and photonics circuits. Both first order filter and high order filter are fabricated using microfiber structures such as microfiber knots and Mach-Zender interferometer. Combination of these structures provides a high qualified optical filters which the results noticeably remarkable. The objective of the research presents a brief theory and design of the structures, which is followed by fabrication and characterization and analysis of the responses. The main objective is the investigation of Vernier effect in filters and how to take advantage of this effect to improve the filter performance. A few multi microfiber resonators are proposed and presented as high order filter in communication system. A Mach-Zender and knot combination is presented as a complex filter. Also there are a few structures are studied including knots with different position to each others. A double cascade knot is one of the structures that investigate

University of Malaya

Vernier effect using thermal effect. To study capability of microfiber filters as stop band filters, two structures with double coupled knots and triple coupled knot are presented and their output spectrum characterized at the end. A hybrid structure including knots and semi-loop is demonstrated in order to modify the filter roll-off factor. Also a new design of optical gate using erbium doped microfiber is investigated theoretically. The capability of active microfiber as a promising element in photonics circuits is demonstrated.

1.4 Thesis Organization

This thesis investigates microfiber structures for filtering applications and proposes some structures as filter for communication systems. The research starts with a brief introduction about microfiber structures and their application in chapter 1. Chapter 2 explains the development of microfiber technology in the recent decades. It also covers the achieved progress to clarify state of the microfiber structures, the fabrication process and their applications. Chapter 3 starts with a complex Mach-Zender-knot structure where thermal effect is induced through the application of a DC current. The output spectrum changes are recorded by passing a different amount of current through a copper wire inserted in the knot structure. A double cascaded microfiber knot is introduced in this chapter as well. Thermal effect is utilized to achieve a tunable high order filter that improves the filter factors using Vernier effect. With proper control of the phase relation between the different rings, the superposition of the individual spectra can result in a net enhancement of the resonance peaks. This effect causes an increase of the finesse at some peaks while suppressing others. Chapter 4 focuses on the introduction of a new hybrid structure as high order filter. The structure has been designed using one knot and a semi loop. To improve and boost its

University of Malaya

performance, another knot is added to the hybrid structure and the output spectrum is characterized. Through the characterization of the new structures, the advantages of their performance compared to a single knot have been listed. Some of the structure factors are investigated to understand how to modify and improve its performance as a filter by engineering of the structures.

Chapter 5 investigates as a new structure, several multi coupled knots are proposed and demonstrated as band stop filter with capability of a few nanometer wavelength filtering. Thermal effect has been examined on the structure. The structure generates a stop-band, pass-band filter. Changing at characteristics of the spectrum is possible by using thermal effect on the structure. The dependency of the response such as stop band width, pass bandwidth, the resonance wavelength and suppression ratio on the structure characteristics, size of the knots, the number of the knots and coupling length are investigated.

Also in this chapter the modeling of an optical gate using a microfiber knot and an erbium doped microfiber knot is demonstrated. A comparison has been done among the results. In this chapter Kerr effect as nonlinear phenomena is investigated in the proposed structure. The threshold power to stimulate the nonlinearity is studied. Finally, chapter 6 includes results and discussion and notices the fault and gap related to structure that end the discussion up with some suggestion for future work.

University of Malaya

CHAPTER 2

LITERATURE REVIEW

2.1 Introduction

This chapter reviews the progress of microfiber technology in terms of design and fabrication of different structures for a variety of applications. First, different techniques used to fabricate microfiber are presented. This is followed by illustration of some microfiber components such as microfiber resonators, couplers, and interferometer for laser, modulator and filter applications. The last section explains the application of microfiber for spectral filtering.

2.2 Microfiber Fabrication Techniques

Recently, fabrication of microfiber has progressed remarkably to provide high quality waveguides. Following these developments, it became possible to fabricate microfibers with different waist, uniformity and length for the different relevant applications. Controlling the fabrication parameters can be achieved using chemical, mechanical or thermal methods. One common method, the thermal- mechanical approach, is followed in this part. It is commonly referred to as taper drawing. In any taper drawing approach, an original single mode (SMF) optical fiber needs to be heated and pulled in order to reduce the structure diameter. Several sources can be used to produce and control the required temperature such as flame, laser and electricity. These three methods are typically referred to as flame heated, laser heated and electrical heated taper drawing.

University of Malaya

Some researches on microfibers have been fabricated using flame-heated method. With this method microfiber is drawn directly from conventional single mode fibers. The waist of the obtained microfiber using this method is in the order of a few micrometers with a length of few millimeters. Two images, an up-down and a side one, of a typical flame heated taper drawing system is illustrated in Figure 2.1 (a) and (b) respectively.

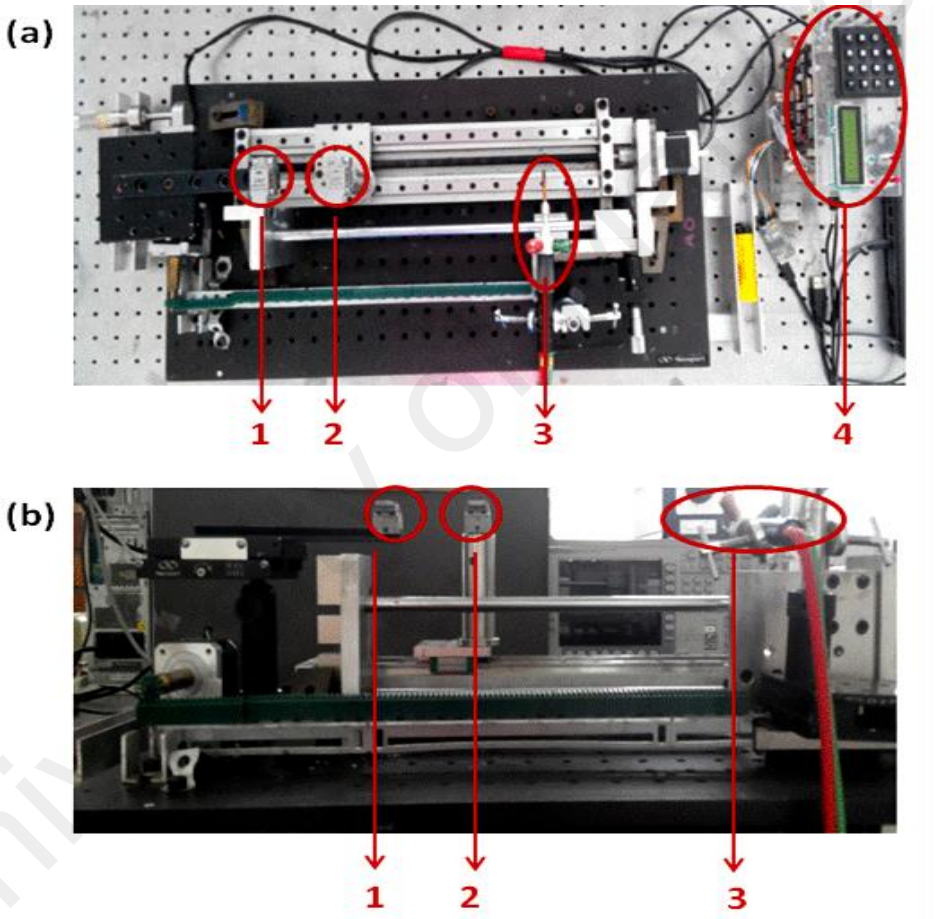

Figure 2.1: Two images of a typical flame heated taper drawing system (a) top and (b) side view.

For the tapering setup, two translation stages are used to hold the SMF fiber during the drawing process. For this method a scanning flame connected to cooking gas (Liquefied

Petroleum Gas) and oxygen canisters has been used as heating source. Figure 2.1 (a and b) show the translation stages, the torch and the motor localization. The softening temperature of the glass fiber is about 2000 K. The flame heats the fiber up until the softening temperature during the drawing. The pulling process is controlled by two motorized translation stages with steady speed. The speed of the translations, traveling distance and pulling force are programmed based on the desired geometric parameters of the microfiber. It is difficult to precisely predict the diameter and length of the microfiber using this process. To monitor the transmission of light through the fiber during the pulling process, an infrared laser and an optical spectrum analyzer are connected at the two ends of the SMF. With proper control, this approach can be used to reduce the fiber waist down to hundreds nanometers (X. Wu et al., 2013).

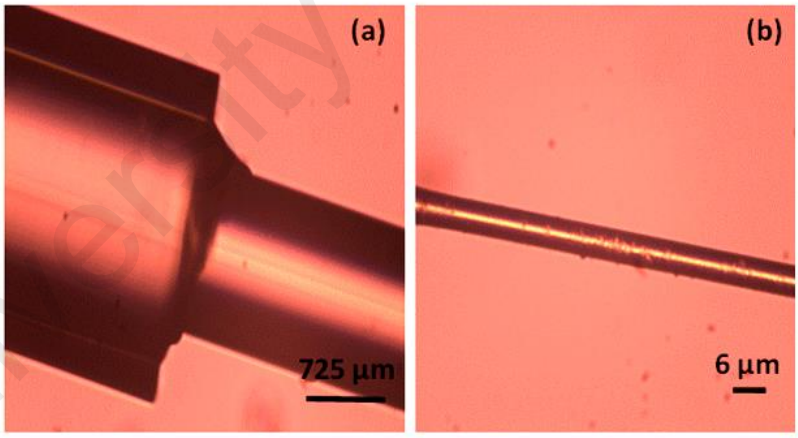

Figure 2.2: (a) A microscopic image of a SMF fiber with and without jacket, (b) a fabricated microfiber with 6 µm using flame heated method.

Figure 2.2 shows the SMF with a jacket covered section (Figure 2.2.a) and fabricated microfiber using the flame heated method with 6 µm diameter and 13 mm length (Figure

University of Malaya

2.2.b). There are drawbacks by using flame as a heating however, this can be overcome. One drawback is that it is hard to control the temperature gradient during the pulling process. This causes a distortion in the uniformity and it makes the repeatability of the fiber fabrication difficult to obtain. There are some ways to improve the pulling condition. Since the flame is coming from a torch, decreasing the size of the torch can allow controlling the size of flame. Controlling the oxygen and methanol gas with low pressure helps to provide a small stable flame. Another technique can be done by programming the stages with controllable speed during the pulling time instead of using a steady speed. The speed change is tuned depending on the microfiber waist.

Conventionally prepared microfiber from flame scanning method comprises of four sections: untapered, two transition regions which connect the untapered to the tapered sections and uniform tapered region. Figure 2.3 illustrates a schematic (top) and a microscopic picture of a microfiber fabricated (bottom) using this scheme. The transition region has been indicated in microscopic image.

University of Malaya

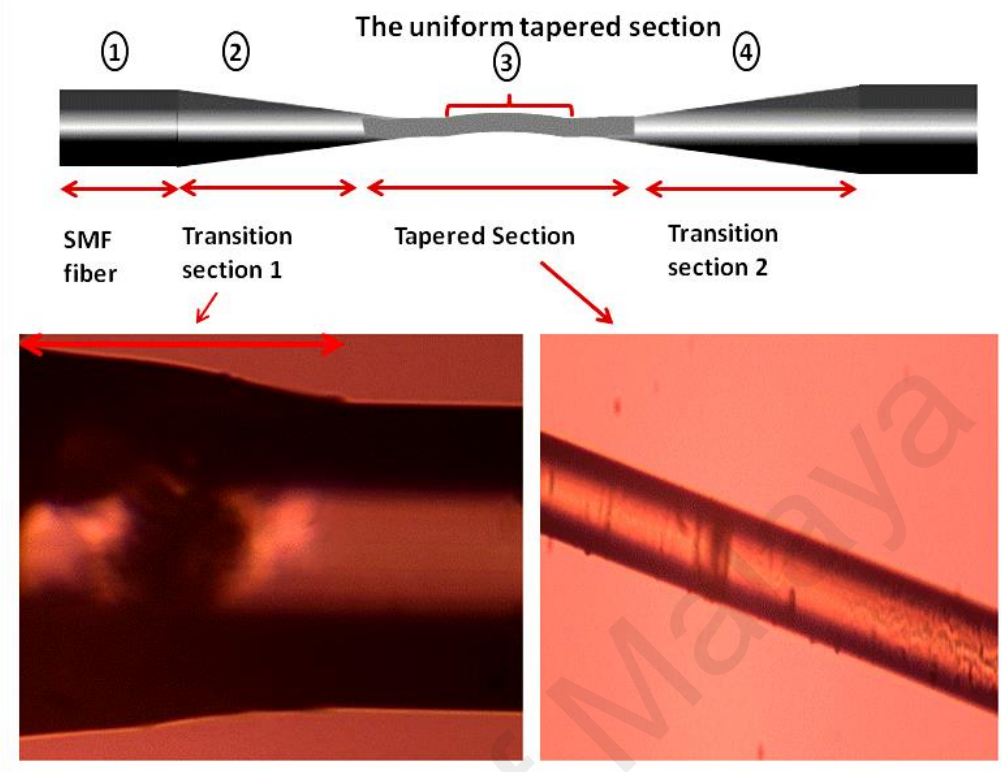

Figure 2.3: A schematic and two microscopic images of tapered fiber including the transition and tapered regions.

The transition region can reach up to few millimeters in length, while the uniform tapered length can be of few centimeters depending on the application of interest. The method can provide large length and uniform microfiber with smooth surface.

As it has already been mentioned stability in temperature, uniformity and repeatability for microfiber fabrication are difficult to obtain. The use of a more stable source is useful for the precise fabrication of microfiber.

Laser heated drawing is a more reliable but expensive alternative. There are a several advantages of using laser source such as the elimination of the burning gas (cleaner), the reduction of the air convection and most importantly, achieving reproducibility. CO_2 laser is commonly used which provides the fabrication process by indirect melting. In the

University of Malaya

experimental setup by Sumetsky et al (Sumetsky et al., 2004), a lens is used to focus and control the beam diameter along the fiber (G. Kakarantzas et al., 2001). Four translation stages are used in the fabrication such that the diameter of the fabricated microfiber can be predictable (estimated). It is worth mentioning that the produced temperature can be tuned by controlling the laser power which is a great advantage of this source. The required laser power depends on the desired fiber diameter. The power drops proportionally to the area of the fiber cross-section. Power dissipation by the fiber drops linearly with the fiber radius. The temperature of the fiber increases linearly with the laser power (A.J.C.Grellier, 1998). It is also possible to control the waist of the microfiber by the laser power as mentioned by Dimmick et al (Dimmick, 1999). Electrical heater is another source for fiber drawing that is presented due to its simplicity, cleanliness, controllability and being commercial available. The main limitation of this source is the fact that it cannot reach high temperature because of the tolerance of the heater material. Hence this method is the least favorable among the three. These sources can be used to taper low softening point materials such as polymers and compound glass. In an experimental setup, the electrical heated technique based on graphite microheater has been used as the source (Shi et al., 2006). The setup includes one fixed and one rotary stage. The stage pulls the fiber at the softening temperature. Using this method, it is possible to fabricate microfiber of few centimeter (Shi et al., 2006).

2.3 Microfiber as a Waveguide

A single mode fiber with a core diameter of 9 μm and a cladding diameter of 128 μm is detailed in this section. The fiber is a cylindrically symmetric step index waveguide. It has a small circular cross section, infinitely long length and a uniform air-cladding interface.

University of Malaya

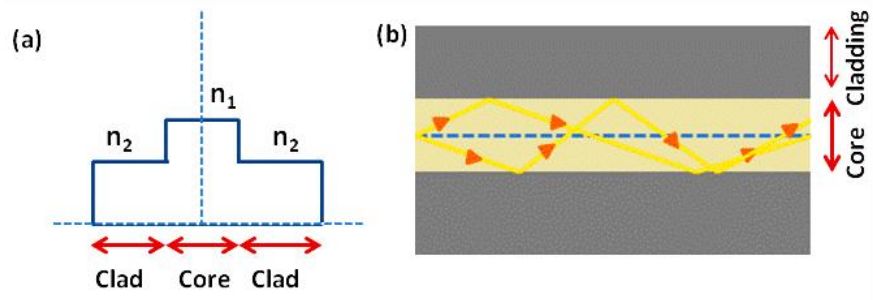

Figure 2.4: (a) A general cylindrical step index profile, (b) light behavior inside the core region from ray-optics point of view

A general cylindrical step index profile is shown in Figure 2.4 (a), where the refractive index is expressed by equation (2.1)

$$n(r) = \begin{cases} n_1, & 0 < r < a, \\ n_2 & a \leq r < \infty \end{cases} \tag{2.1}$$

Here n_1, n_2 and a are respectively the refractive indices of the microfiber, air and the radius of the fiber. Figure 2.4 (b) presents the light behavior inside the core region from ray-optics point of view. The light is guided in the fiber through total internal reflection. When the light hits the interface between the core and the air-cladding, a fraction of confined light penetrates through the air cladding and propagates as an evanescence field in the cladding. Due to the lack of momentum (imaginary components of the propagation constant normal to the interface), the light comes back to the core boundary causing a slight shift along the direction of propagation. This is referred to as the Goos-Hanchien effect (Snyder et al., 1976). Due to the fact that the core radius of the fiber decreases during the drawing process, the extension of the evanescent wave increases outside the core in the air along the fiber. When the core radius is smaller than the wavelength of the light, ray-optics is not applicable anymore to explain the light behavior. When reaching these limits, Maxwell's equations of the electromagnetic fields are used. Theory of microfiber as a

University of Malaya

cylindrical wavelength-diameter waveguides has been analyzed based on applying the boundary conditions such as cross section, length, effective index and uniformity using Maxwell's equations. As illustrated in Figure.2.3, a general microfiber includes four regions which affect the guided modes. Region one is the single mode fiber that is considered as a non-dissipative and source free waveguide with dielectric core and cladding media. Equation (2.2) expresses Maxwell's equations for the defined waveguide:

$$\begin{cases} \boldsymbol{\nabla} \times \boldsymbol{E} = -\frac{1}{c}\frac{\partial \boldsymbol{B}}{\partial t} \\ \boldsymbol{\nabla} \times \boldsymbol{H} = \frac{1}{c}\frac{\partial \boldsymbol{D}}{\partial t} \end{cases} \qquad \begin{cases} \boldsymbol{D} = \varepsilon \boldsymbol{E} \\ \boldsymbol{B} = \mu \boldsymbol{H} \end{cases} \tag{2.2}$$

where $\mu = \mu_0 \mu_r,\ \varepsilon = \varepsilon_0 \varepsilon_r,\ c = \frac{n}{\sqrt{\mu\varepsilon}}$ which are respectively the magnetic permeability, electric permittivity and light speed in dielectric medium with refractive index of n. To decouple the electric and magnetic fields components, the following relation (equation (2.3)) is applied to simplify equation (2.4):

$$\boldsymbol{\nabla} \times \boldsymbol{\nabla} \times \boldsymbol{A} = \boldsymbol{\nabla}(\boldsymbol{\nabla}.\boldsymbol{A}) - \boldsymbol{\nabla}^2 \boldsymbol{A} \tag{2.3}$$

$$\begin{cases} \boldsymbol{\nabla} \times \boldsymbol{\nabla} \times \boldsymbol{E} = -\boldsymbol{\nabla} \times (\frac{1}{c}\frac{\partial \boldsymbol{B}}{\partial t}) \\ \boldsymbol{\nabla} \times \boldsymbol{\nabla} \times \boldsymbol{H} = \boldsymbol{\nabla} \times (\frac{1}{c}\frac{\partial \boldsymbol{D}}{\partial t}) \end{cases} \rightarrow \begin{cases} \boldsymbol{\nabla}^2 \boldsymbol{E} = \varepsilon\mu \frac{\partial^2 \boldsymbol{E}}{\partial t^2} \\ \boldsymbol{\nabla}^2 \boldsymbol{H} = \varepsilon\mu \frac{\partial^2 \boldsymbol{H}}{\partial t^2} \end{cases} \tag{2.4}$$

Both electric and magnetic fields are assumed to be harmonic time dependent. Hence, the first and second time derivatives are reduced to $-i\omega$ and $-\omega^2$ respectively. Equation (2.4) is reduced to Helmholtz equations as below:

$$\begin{cases} \left(\boldsymbol{\nabla}^2 - \frac{n^2\omega^2}{c^2}\right)\boldsymbol{E} = 0 \\ \left(\boldsymbol{\nabla}^2 - \frac{n^2\omega^2}{c^2}\right)\boldsymbol{H} = 0 \end{cases} \tag{2.5}$$

Exact solutions of equation (2.5) for single mode fiber and microfiber boundary conditions have been obtained using Bessel functions (Snyder et al., 2012). Based on these solutions, the eigenvalue equations are expressed for the HE_{ml} and EH_{ml} modes as:

University of Malaya

$$\left\{\frac{J_m^{'}(U)}{UJ_m(U)}+\frac{K_m^{'}(W)}{WK_m(W)}\right\}\left\{\frac{J_m^{'}(U)}{UJ_m(U)}+\frac{n_2^2K_m^{'}(W)}{n_1^2WK_m(W)}\right\}=\left(\frac{m\beta}{kn_1}\right)^2\left(\frac{V}{UW}\right)^4 \quad (2.6)$$

For TE_{0l} modes:

$$\frac{J_1(U)}{UJ_0(U)}+\frac{K_1(W)}{WK_0(W)}=0 \quad (2.7)$$

And for TM_{0l} modes:

$$\frac{n_1^2J_1(U)}{UJ_0(U)}+\frac{n_2^2K_1(W)}{WK_0(W)}=0 \quad (2.8)$$

J_m and K_m are the Bessel function of the first kind and the modified Bessel function of the second kind. The parameters U, W and V are defined in follow $U=a(k_0^2n_1^2-\beta^2)^{1/2}$, $W=a(-k_0^2n_2^2+\beta^2)^{1/2}$, $V=k_0.a(n_1^2-n_2^2)^{1/2}$. Based on these analytical solutions, it is possible to determine the guided modes inside SMF and a defined uniform microfiber (Snyder et al., 2012). One important parameter of interest in equation (2.6) is the V-number. The fiber is single-mode when the V number is less than 2.40 (Snyder et al., 2012). At that limit, only the fundamental mode HE_{11} is guided through the core of the untapered fiber.

Regions two and four (the conical sections in Figure 2.3) are referred to as the transition regions. The transition regions can be shaped in an adiabatic form with slow taper-down/up.

University of Malaya

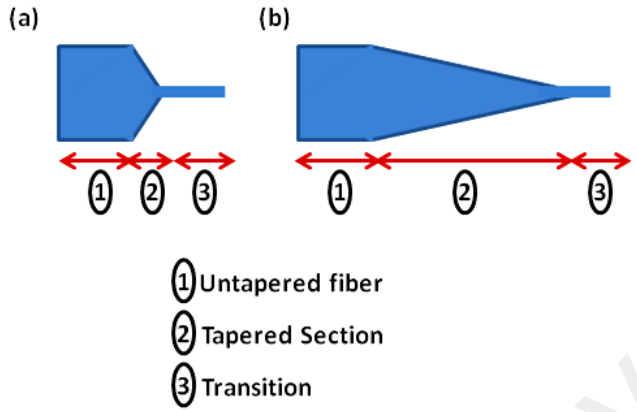

Figure 2.5: (a) Fast taper-down/up (nonadiabatic transition region), (b) slow taper-down/up (adiabatic transition region).

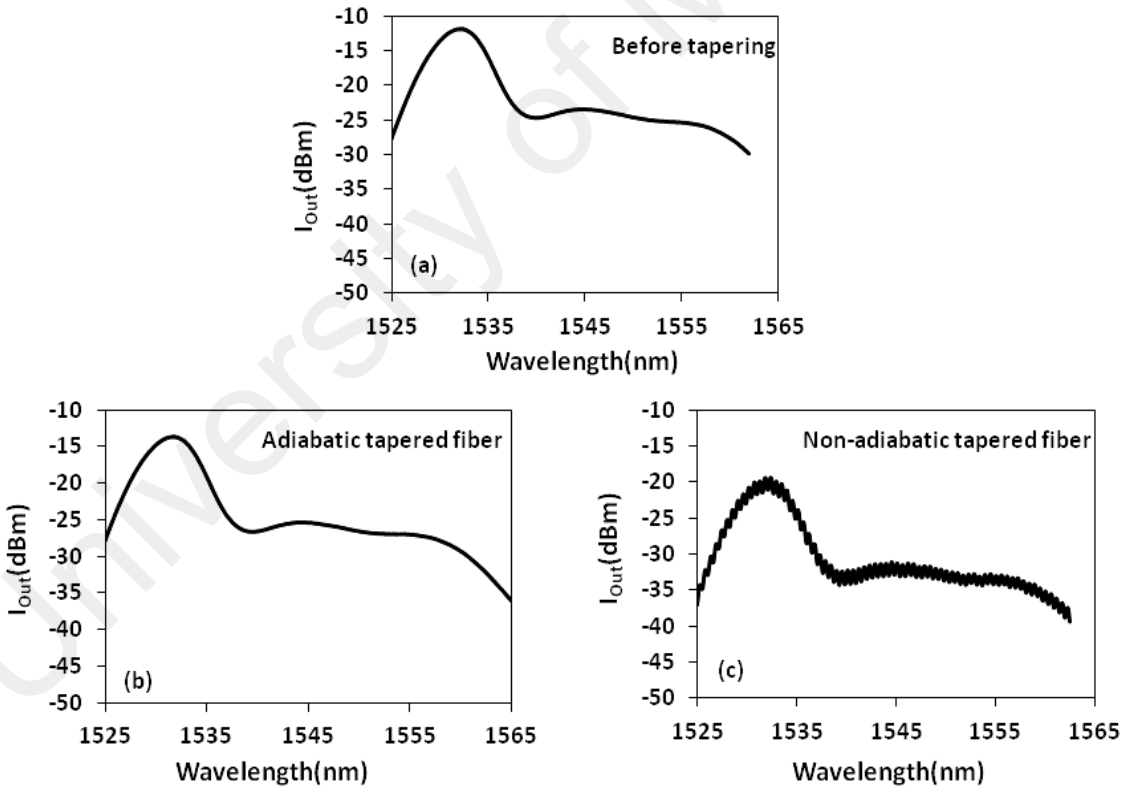

Figure 2.6: (a) Spectra from the fiber before and (b) after tapering when the transition regions are adiabatic or (c) nonadiabatic tapered fiber.

University of Malaya

Nonadiabatic form can be achieved with fast taper-down/up. These two forms are shown in Figure 2.5 (a) and Figure 2.5 (b). Adiabatic transition regions guide the fundamental HE_{11} similar to SMF core-guided mode. Then the fundamental HE_{11} propagates into the core of the uniform tapered fiber (section three in Figure 2.3). Figure 2.6 (a) and (b) shows the spectra from the fiber before and after tapering when the transition regions are adiabatic. As shown in Figure 2.6 (b), the adiabatic tapered fiber has a smooth and uniform spectrum with lower power due to loss during the tapering process. But nonadiabatic transition sections can excite high-order fiber modes in addition to the fundamental HE_{11}. These modes have the same frequency but different propagation constants. Figure 2.6 (c) shows a nonuniform output from a nonadiabatic tapered fiber due to the interference between different modes.

2.4 Microfiber Components: Introduction, Fabrication and Applications

Various types of microfiber elements have been fabricated and investigated for several applications. These elements can be categorized in three groups: resonators, couplers and interferometers. This section introduces some new structures and reviews the method of their fabrication and their application.

2.4.1 Microfiber Resonators

Microfiber resonators, such as microfiber loop, knot, coil and multi-resonator structure, have been fabricated by different methods in several sizes depending on their applications. Their optical properties were investigated theoretically and experimentally in literature (F. Xu et al., 2007b; Y. P. Xu et al., 2014). Demonstration of microfiber ring resonator has

University of Malaya

been first published in 2005 with the fabrication of a loop using subwavelength fiber in free space with Q factor of 15000 and extinction ratio 34 dB (Sumetsky et al., 2005). More studies on microfiber loop and its sensing applications have been done by Sumetsky et al. in 2006 (Sumetsky et al., 2006). This structure has been used to design other components such as a Fabry-Perot resonator (S. S. Wang et al., 2009), millimeter-wave ultra-wideband signal generator (Y. Zhang et al., 2011) and UV detector (K. S. Lim et al., 2013). Broderick studied in 2008 the capability of the structure in nonlinearity (Broderick, 2008). A microfiber resonator has been demonstrated to generate a nonlinear phase shift (Vienne, Li, et al., 2008). Microfiber coil has been introduced and demonstrated as a nonlinear resonator due to high field enhancement inside it (Broderick, 2008). A microfiber loop resonator has been used to generate the second harmonic and the third harmonic through the ring (Gouveia et al., 2013; Ismaeel et al., 2012).

In addition to microfiber loop, microfiber knot has similar structure with better stability and it has been demonstrated and investigated in literature (J. Y. Lou et al., 2014). It has been fabricated as a freestanding structure with a Q factor of 57000 and a finesse of 22 (X. S. Jiang et al., 2006). The structure has been studied in different areas such as the host polymer and polarization effects on the structure (Vienne et al., 2007; G. H. Wang et al., 2010), resonance condition (K. S. Lim et al., 2011) and the investigation of its thermal properties (X. L. Li et al., 2013). Different designs of microfiber have been demonstrated to obtain high finesse and good performance (Y. P. Xu et al., 2014).

Using MgF_2 slot and coating polymers have been suggested and demonstrated as a way to make robust structure (T. Li et al., 2012). Microfiber ring structures have been applied for sensing application such as current (K. S. Lim et al., 2011), magnetic field (X. L. Li et al., 2012), temperature (Y. Wu et al., 2011), humidity (Y. Wu et al., 2011), refractive index

University of Malaya

(Shi et al., 2007) and acoustic (Sulaiman et al., 2013) sensors. There are also few examples of laser systems such as dye laser and rare- earth ion doped been demonstrated utilizing microfiber knot and loop cavities (X. S. Jiang et al., 2007).

The first design of microcoil as a 3D microresonator has been demonstrated in 2004. It has been fabricated by twisting a microfiber around a bar (Sumetsky, 2004). Packaging the coil resonator, in 2007 an embedded microfiber coil in Teflon has been fabricated (F. Xu et al., 2007a). Theoretical and numerical studies on microfiber coil resonators output and their characterization have also been done Sumetsky et al.(Sumetsky, 2005). A multi-port microfiber resonator has been demonstrated by Ismaeel et al. (Ismaeel et al., 2012).

2.4.2 Microfiber Couplers and Interferometers

Microfiber couplers can be used to split power as well as channels multiplexing for sensing (Bo et al., 2014), laser and biomedical applications (Bo et al., 2014; Sulaiman et al., 2013). The fabrication technique of a 2 by 2 microfiber coupler has been demonstrated in 2012 by Jasmin et al. (Jasim et al., 2012). The microfiber coupler has been fabricated through the fusion of two fibers during simultaneous tapering (Jasim et al., 2012). A microfiber coupler based Sagnac loop has been introduced and employed as a temperature sensor (S. D. Lim et al., 2010). Bo et al. demonstrated microfiber coupler used as a biomedical sensor in 2014 (Bo et al., 2014).

Two cascaded microfiber couplers form a microfiber interferometer. There are two types of microfiber interferometers demonstrated so far: Mach-Zender and Sagnac interferometers. The performance of these interferometers is based on the interference of two light beams, which are split from one beam and traveled different distances.

University of Malaya

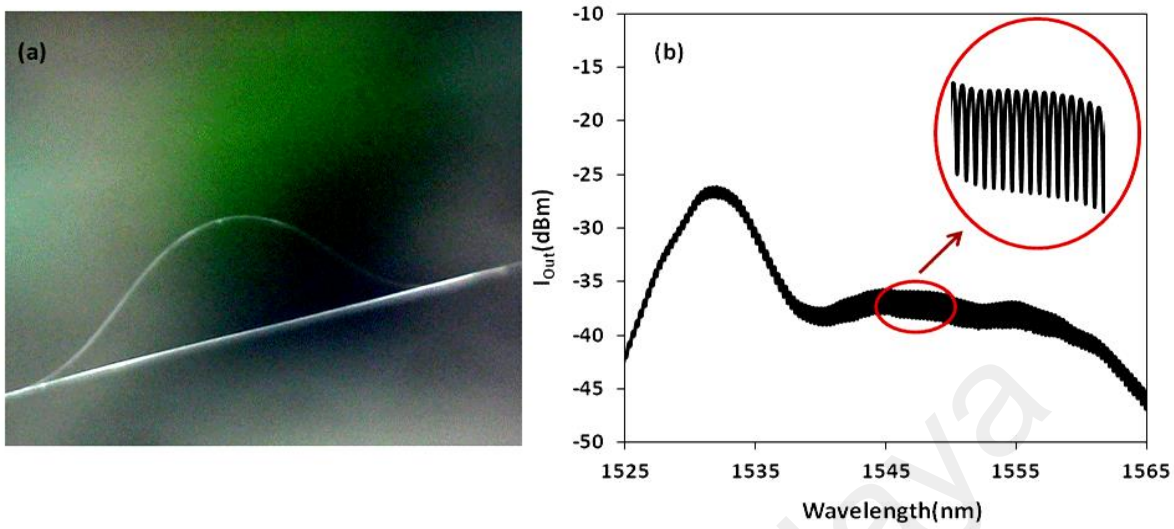

Figure 2.7: (a) Fabricated MZI and (b) resultant spectrum.

Figure 2.7 shows the fabricated MZI and the resultant spectrum. In 2010, a combination of MZI with a knot inside it has been used as high quality factor interferometer (Y. H. Chen et al., 2010). In the same year an interferometer based on microfiber Sagnac loop has been demonstrated by Lim et al. (S. D. Lim et al., 2010). A combination of MZI and Sagnac loop mirror interferometer has been fabricated as an add drop filter (Aryanfar et al., 2012). Microfiber MZI has been employed in a variety of sensors such as refractive index (Tan et al., 2013), strain (Liao et al., 2013) and rotation angle sensors (Digonnet, 2011). The microfiber MZI refractive index sensor has been fabricated to measure the complex refractive index of Graphen waveguide (Yao et al., 2013). In 2014, a double sensor has been demonstrated including dual microfiber MZI for simultaneous refractive index and temperature sensing (Liao et al., 2014).

University of Malaya

2.5 Filter Based Microfiber Structure

There exist few microfiber structure designs that are proposed and fabricated for filter applications (Zou et al., 2014). Microfiber resonators such as knot, loop and coil are good examples of structures used for such application due to their intrinsic comb spectrum. As mentioned before, microfiber knot has been introduced as add-drop filter (X. D. Jiang et al., 2007). Later a tunable all-fiber filter based on microfiber loop has been proposed and demonstrated in 2008 (Y. Wu et al., 2008). A notch filter has been investigated using a microfiber ring laser with the rejection ratio about 35 dB (Y. Zhang et al., 2010). A microfiber loop embedded in a low refractive index material has been demonstrated in 2011 (K. S. Lim et al., 2011). Also the same group suggested and investigated a microfiber Mach-Zender interferometer as an add-drop filter (Aryanfar et al., 2012). Birefringent microfiber based filter has been introduced by Jin and employed as both tunable comb filter and refractive index sensor (Jin et al., 2013). A new design of two linearly chirped Bragg gratings has been proposed for channel-spacing tunable filter in 2014 (Zou et al., 2014). All these filters behave as first order filters with one filtering structure. With such order, it is difficult to improve the extinction ratio and finesse at the same time. The spectrum characteristics are dependent on a single structure, which has limited characteristics so the possibility of tuning the spectrum is limited. This research suggests some high order filter structure as a solution to improve the filter spectrum characteristic such as finesses, FSR, band ripple and extinction ratio simultaneously and robustness and increases tuning capability for variety of filter applications.

University of Malaya

CHAPTER 3

COMPLEX MICROFIBER STRUCTURE FILTER APPLICATION

3.1 Introduction

This chapter presents an overview of the coupled mode theory, which is used to model the performance of the proposed micro-fiber structures. Some of the most important characteristics of the output spectrum of a knot resonator are introduced in this chapter such as free spectral range (FSR), full width at half maximum (FWHM) and extinction ratio (ER). High quality filter can be defined through sharp fineness, wide FSR and large ER. These filter characteristics depend strongly on the microfiber knot parameters such as ring radius and coupling coefficient. This dependency limits the spectral tuning of the resonator, finesse and ER. To overcome these limitations, three approaches are presented: using thermal effect, multi- microfiber resonators and taking advantage of nonlinearity in rare earth doped microfiber. Following these solutions, a complex structure is proposed consisting of microfiber Mach-Zender and knot. This structure has been designed to increase the extension ratio via optical path correction. Another structure consisting of a double-knot resonator is proposed and fabricated. With proper control of the phase relation between the different rings, the superposition of the individual spectra can result in a net enhancement of the resonance peaks due to Vernier effect. This effect causes an increase of the finesse at some peaks while suppressing others. The present chapter demonstrates a comparison between the output of a single knot and the proposed structures.

University of Malaya

3.2 Coupled Mode Theory

This section derives a closed form expression for single knot output based on coupled mode theory. The theory defines how the field elements inside different adjacent waveguides interact with each other and exchange energy. Here the field elements include elements in a straight microfiber and curved microfiber at the knitted section of the knot. A sketch of the area, including the related filed components, is shown in Figure 3.1.

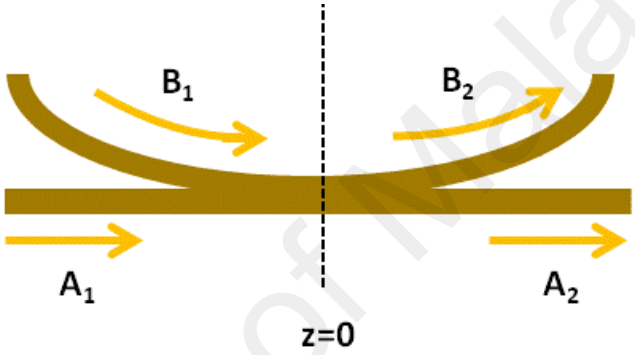

Figure 3.1: sketch of the coupling region including the related field elements

The coupling theory is expanded based on polarization perturbation that has been investigated by Yariv in 1973.

Maxwell's equations in section (2.3) can be simplified due to the time dependence term ($e^{-i\omega t}$) of the mode fields as:

$$\begin{cases} \nabla \times \boldsymbol{E} = i\omega\mu_0 \boldsymbol{H} \\ \nabla \times \boldsymbol{H} = -i\omega\varepsilon_0 \boldsymbol{E} - i\omega\Delta \boldsymbol{P} \end{cases} \tag{3.1}$$

$\Delta \boldsymbol{P}(\boldsymbol{r})$ is the spatially dependent perturbation polarization to the microfiber sections A and B in Figure 3.1.

The following explanations aim to formulate the desired equations which using the desired coupling terms. The first step is to rewrite equation (3.1) for waveguide A and the complex conjugate of the equation is rewritten for waveguide B (as it is shown in Figure 3.1):

University of Malaya

$$\begin{cases} \boldsymbol{\nabla} \times \boldsymbol{E}_A = i\omega\mu_0 \boldsymbol{H}_A \\ \boldsymbol{\nabla} \times \boldsymbol{H}_A = -i\omega\varepsilon_0 \boldsymbol{E}_A - i\omega\Delta \boldsymbol{P}_A \end{cases} \tag{3.2a}$$

$$\begin{cases} \boldsymbol{\nabla} \times \boldsymbol{E}_B^* = -i\omega\mu_0 \boldsymbol{H}_B^* \\ \boldsymbol{\nabla} \times \boldsymbol{H}_B^* = +i\omega\varepsilon_0 \boldsymbol{E}_B^* + i\omega\Delta \boldsymbol{P}_B^* \end{cases} \tag{3.2b}$$

Where $\boldsymbol{E}_{A,B}$ and $\boldsymbol{H}_{A,B}$ are the electric and magnetic fields of the guided modes inside A and *B* sections of the microfiber respectively. To form the coupled terms, $\boldsymbol{H}_B^*$ and $\boldsymbol{E}_B^*$ are vectors multiplied (dot product) of equation in (3.3a). For equations (3.2b), $\boldsymbol{H}_A$ and $\boldsymbol{E}_A$ are vectors multiplied the ones in (3.2b):

$$\begin{cases} \boldsymbol{H}_B^* . \boldsymbol{\nabla} \times \boldsymbol{E}_A = i\omega\mu_0 \boldsymbol{H}_B^* . \boldsymbol{H}_A \\ \boldsymbol{E}_B^* . \boldsymbol{\nabla} \times \boldsymbol{H}_A = -i\omega\varepsilon_0 \boldsymbol{E}_B^* . \boldsymbol{E}_A - i\omega \boldsymbol{E}_B^* . \Delta \boldsymbol{P}_A \end{cases} \tag{3.3a}$$

$$\begin{cases} \boldsymbol{H}_A . \boldsymbol{\nabla} \times \boldsymbol{E}_B^* = -i\omega\mu_0 \boldsymbol{H}_A . \boldsymbol{H}_B^* \\ \boldsymbol{E}_A . \boldsymbol{\nabla} \times \boldsymbol{H}_B^* = +i\omega\varepsilon_0 \boldsymbol{E}_A . \boldsymbol{E}_B^* + i\omega \boldsymbol{E}_A . \Delta \boldsymbol{P}_B^* \end{cases} \tag{3.3b}$$

From the combination equation 3.3a and 3.3b, the following expressions are obtained by:

$$\begin{cases} \boldsymbol{H}_B^* . \boldsymbol{\nabla} \times \boldsymbol{E}_A - \boldsymbol{E}_A . \boldsymbol{\nabla} \times \boldsymbol{H}_B^* = i\omega\mu_0 \boldsymbol{H}_B^* . \boldsymbol{H}_A - i\omega\varepsilon_0 \boldsymbol{E}_A . \boldsymbol{E}_B^* - i\omega \boldsymbol{E}_A . \Delta \boldsymbol{P}_B^* \\ \boldsymbol{H}_A . \boldsymbol{\nabla} \times \boldsymbol{E}_B^* - \boldsymbol{E}_B^* . \boldsymbol{\nabla} \times \boldsymbol{H}_A = -i\omega\mu_0 \boldsymbol{H}_A . \boldsymbol{H}_B^* + i\omega\varepsilon_0 \boldsymbol{E}_B^* . \boldsymbol{E}_A + i\omega \boldsymbol{E}_B^* . \Delta \boldsymbol{P}_A \end{cases} \tag{3.4}$$

For these equations, the following formalism is assumed: mode orthogonality and orthonormality as well power conservation as its basic tenets. Orthonormality and orthogonality relations are defined as follow:

Orthonormality for TE mode: $\int \boldsymbol{E}_i . \boldsymbol{E}_j^* da = \delta_{ij}$, $\delta_{ij} = \begin{cases} 1 & i = j \\ 0 & i \neq j \end{cases}$ (3.5)

Orthonormality for TM mode: $\int \boldsymbol{H}_i . \boldsymbol{H}_j^* da = \delta_{ij}$ (3.6)

Orthogonality: $\int (\boldsymbol{E}_i \times \boldsymbol{H}_j^* + \boldsymbol{E}_j^* \times \boldsymbol{H}_i) . \hat{z}\, da = \pm P_i \delta_{ij}$ (3.7)

where $\boldsymbol{E}_{i,j}$ and $\boldsymbol{H}_{i,j}$ are the normalized electric and magnetic field for the *i*th and *j*th waveguided modes respectively. P_i is the power of the i*th* waveguide mode. Based on the defined relations, equation (3.4) can be reduced to:

$$\nabla . (\boldsymbol{E}_A \times \boldsymbol{H}_B^* + \boldsymbol{E}_B^* \times \boldsymbol{H}_A) = -i\omega (\boldsymbol{E}_A . \Delta \boldsymbol{P}_B^* - \boldsymbol{E}_B^* . \Delta \boldsymbol{P}_A) \tag{3.8}$$

University of Malaya

The linear expansion of any optical field at a given frequency ω in the waveguides is given by:

$$\begin{cases} \boldsymbol{E}_A(r) = \sum_a F_a \hat{E}_a(x,y) e^{i\beta_a z} \\ \boldsymbol{H}_A(r) = \sum_a F_a \hat{H}_a(x,y) e^{i\beta_a z} \end{cases} \tag{3.9a}$$

$$\begin{cases} \boldsymbol{E}_B(r) = \sum_b F_b \hat{E}_b(x,y) e^{i\beta_b z} \\ \boldsymbol{H}_B(r) = \sum_b F_b \hat{H}_b(x,y) e^{i\beta_b z} \end{cases} \tag{3.9b}$$

In which $F_{a,b}$ are the modal amplitude of the electric and magnetic field through A and B sections.

Substituting equations (3.9a) and (3.9b) in equation (3.8) and using orthogonality obtains equations (3.10a) and (3.10b) as the coupled equations:

$$\frac{dF_a}{dz} = ik_{ab}F_b e^{i\Delta z} + ik_{aa}F_a \tag{3.10a}$$

$$\frac{dF_b}{dz} = ik_{ba}F_a e^{-i\Delta z} + ik_{bb}F_b \tag{3.10b}$$

Where $\Delta = (\beta_a - \beta_b)$ and $k_{ab} = \frac{\omega}{P_a} \int \Delta\varepsilon \hat{E}_a^* . \hat{E}_b \, da$ are propagation and the coupling coefficient between modes a and b from the microfiber sections A and B respectively. The coupled equations can be rewritten as a matrix in equation (3.11):

$$\begin{bmatrix} \frac{dF_a}{dz} \\ \frac{dF_b}{dz} \end{bmatrix} = \begin{bmatrix} ik_{aa} & ik_{ab}e^{i\Delta z} \\ ik_{ba}e^{-i\Delta z} & ik_{bb} \end{bmatrix} \begin{bmatrix} F_a \\ F_b \end{bmatrix} \rightarrow \begin{bmatrix} A_2 \\ B_2 \end{bmatrix} = \begin{bmatrix} ik_{aa} & ik_{ab}e^{i\Delta z} \\ ik_{ba}e^{-i\Delta z} & ik_{bb} \end{bmatrix} \begin{bmatrix} A_1 \\ B_1 \end{bmatrix} \tag{3.11}$$

This matrix is solved analytically by finding the eigenvalue. Equation (3.12) expresses the solution of (3.11):

$$\begin{bmatrix} A_2 \\ B_2 \end{bmatrix} = \begin{bmatrix} r & ik \\ ik & r \end{bmatrix} \begin{bmatrix} A_1 \\ B_1 \end{bmatrix} \tag{3.12}$$

In which r and k are the transmission and coupling coefficients. $r^2 + k^2 = 1$ in a lossless medium. Also the relation between B_1 and B_2 in a ring structure is

$$B_1 = e^{\frac{-i2\pi nL}{\lambda} - \alpha L} \; B_2 \tag{3.13}$$

University of Malaya

Where λ, n, α are wavelength, refractive index and the round trip loss. Also L is considered as effective length, the difference of between the length of the ring with radius of R and the coupling length. In this chapter the following method, transfer matrix, is used to simulate and analyze the output spectrum of the structures.

3.3 Single Knot Structure

A single knot structure is a straight microfiber that is knitted to form a shape of a ring as shown in figure 2.a.

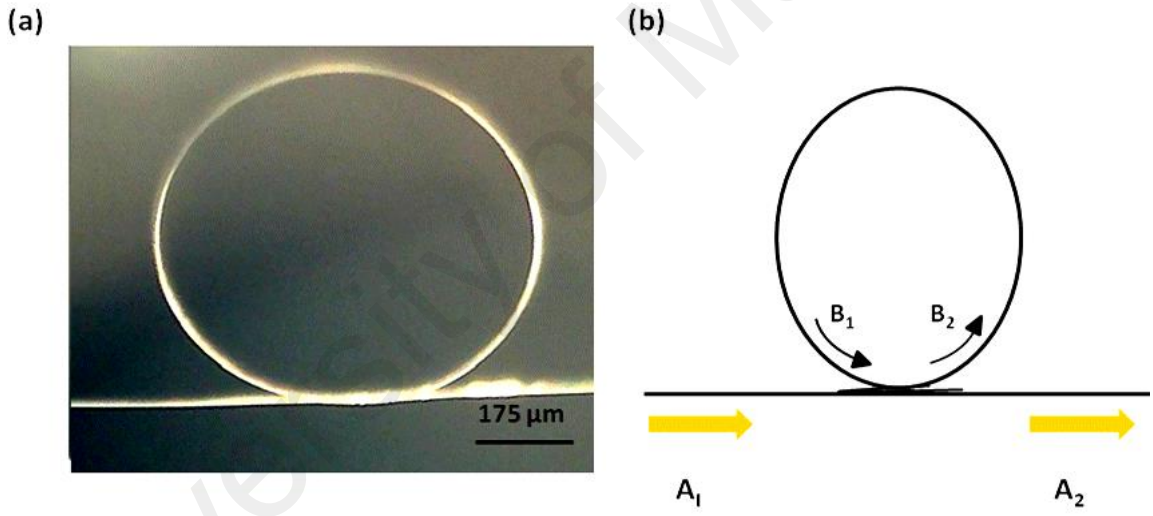

Figure 3.2: (a) A microscopic image of a microfiber knot with 350 µm radius, (b) a sketch of a knot.

For the field components in figure 3.2b, when an input electric field (A_1) is coupled to the curved section (B_2), at some certain wavelength the field inside the knot enhances (B_1) and the output (A_2) shows a comb spectrum. Therefore, there are a few parameters to define how much power is coupled or built-up through the knot such as coupling length and knot radius. In the following section these parameters are discussed.

University of Malaya

3.3.1 Design and Characterization

This section presents an overview of the basic concepts related to ring resonator. The aim of this section is to understand the operation of such structure. At resonance, the excitation wavelength is defined by the following relation:

$$m\lambda_m = nL\ , \tag{3.14}$$

where m is the mode number, n is the refractive index and L is the circumference of the knot. As previously deduced from equation (3.12), the strength of the different field components can be expressed as follows:

$$\begin{cases} A_2 = rB_1 + \mathrm{i}kA_1 \\ B_2 = rA_1 + \mathrm{i}kB_1 \\ B_1 = \mathrm{e}^{-\propto\frac{\mathrm{L}}{2}} e^{-i(\frac{2\pi n}{\lambda})\mathrm{L}} B_2 \end{cases} \tag{3.15}$$

In equation (3.15), the round trip phase is defined as $\varphi = \frac{2\pi n}{\lambda}\mathrm{L}$. Resonance occurs when the round trip phase is a multiple of $(2m+1)\pi/2$. To measure the field intensity inside the resonator, B_2 is extracted from equation (3.15):

$$\frac{B_1}{A_1} = \frac{ik}{1-r\mathrm{e}^{\propto\frac{\mathrm{L}}{2}}} \tag{3.16}$$

At resonance, the strength of the circulating field inside the knot increases, it is referred to as field enhancement (FE). Higher FE causes lower input power requirement, sharper roll-off and larger extension ratio.

University of Malaya

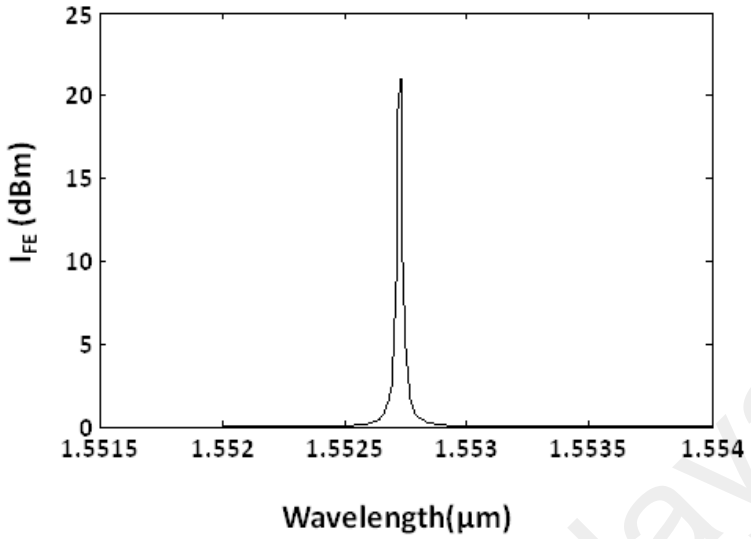

Figure 3.3: Simulation of the normalized field enhancement of knot with of 100 μm.

Figure 3.3 shows a simulation of the normalized field enhancement $I_{inside\ ring}/I_{input}$ for a ring resonator with radius of 100 μm. As shown in the figure, the amount of field enhancement obtained a circulating power about 23 times bigger than the input power. At certain wavelength, the field enhancement compensates the loss inside the knot, it induces a large and deep ER on the wavelength of the output spectrum.

Equation (3.16) shows that FE has a strong dependency on the coupling coefficient. This dependency is theoretically illustrated in Figure 3.4. It shows a structure with a radius of 120 μm at resonance wavelength of 1.5535 μm.

University of Malaya

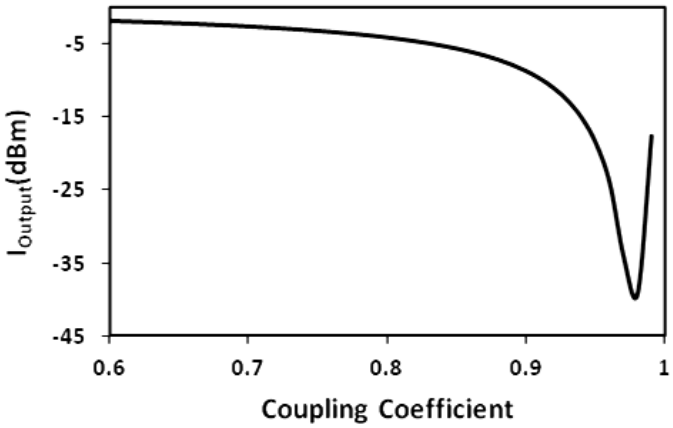

Figure 3.4: Simulation of a normalized output from a microfiber knot versus coupling coefficient.

Based on Figure 3.4 for a specified knot, the maximum FE occurs at a certain coupling coefficient, which is 0.98 in this case. Considering equation (3.15) the normalized output intensity is defined as follow:

$$\left|\frac{A_2}{A_1}\right|^2 = \left|\frac{ike^{\propto\frac{L}{2}}e^{i(\frac{2\pi n}{\lambda})L}+1}{e^{\propto\frac{L}{2}}e^{i(\frac{2\pi n}{\lambda})L}-ik}\right|^2 \tag{3.17}$$

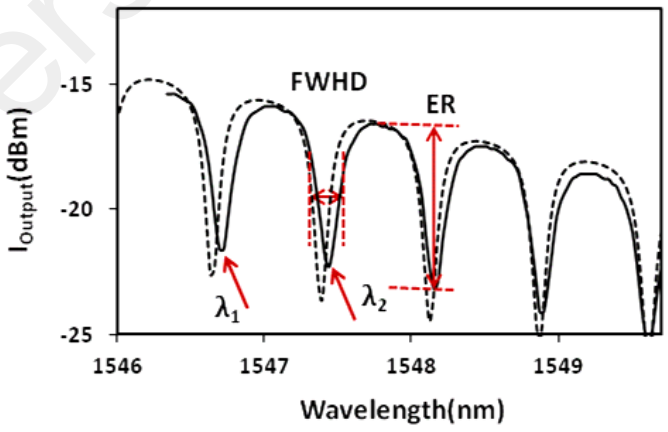

Figure 3.5: Experimental (bold line) and simulation (dashed line) output of a microfiber with radius of 357 µm.

University of Malaya

Figure 3.5 shows experimental (bold line) and simulation (dashed line) output from a knot structure with 357 μm radius. The performance analysis of the designed knot filter requires several definitions, which are introduced in the following sections.

3.3.2 Resonator Bandwidth and Free Spectral Range (FSR)

For a knot resonator, bandwidth is the main factor determining the optical data processing speed. It is measured using the full width at half maximum (FWHM) of the resonance:

$$\delta\lambda_{FWHM} \approx \frac{\lambda^2(1-re^{-\frac{L}{2}})}{\pi nL\sqrt{re^{-\frac{L}{2}}}} \tag{3.18}$$

where $\delta\lambda_{FWHM}$ is the bandwidth.

The difference between two successive resonant wavelengths is called free spectral range (FSR), which is defined as follows:

$$\Delta\lambda_{FSR} = \frac{\lambda^2}{nL} \tag{3.19}$$

In Figure 3.5, two successive resonant wavelengths are indicated (λ_1 and λ_2). The FSR for this output spectrum is, λ_2 - λ_1= 715 pm.

Based on equation (3.19), FSR has an inverse relationship with the circumference of the resonator. Figure 3.6 presents the experimental result (a) and the simulation spectra (b) of two knots. The bold line shows the output of the knot with a radius of 1110 μm (FSR = 175 pm). The dashed line represents the spectrum of the knot with 800 μm radius and FSR of 325 pm.

University of Malaya

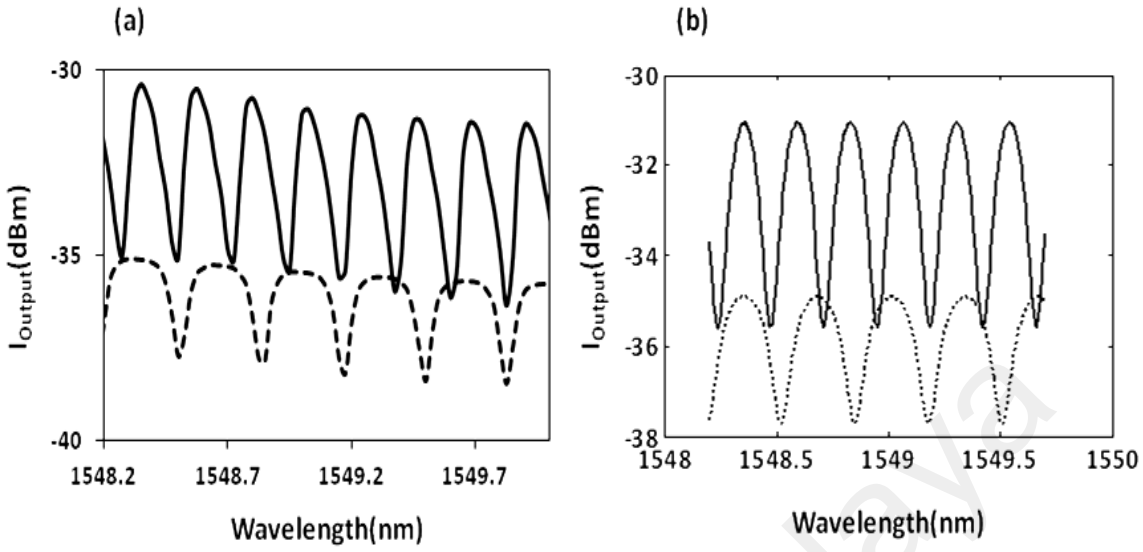

Figure 3.6: (a) Experimental results of two knots with 1110 µm (bold line) and 800 µm radii, (b) simulation result from the same knots.

3.3.3 Resonator Finesse and Quality Factor

Finesse is one important characteristic of any resonator. Finesse is the ratio between the free spectral range (FSR) and FWHM and it is defined as follows:

$$F = \frac{\Delta\lambda_{FSR}}{\Delta\lambda_{FWHM}} = \frac{\pi\sqrt{re^{-\frac{L}{2}}}}{1-re^{-\frac{L}{2}}} \tag{3.20}$$

Equation (3.20) shows that the finesse is not dependent on the dimensions of the resonator. It is a function of the coupling coefficient and loss. The spectrum in Figure 3.5 shows a FWHM of 137 pm. Based on the definition in equation (3.20), the spectrum has a finesse of 5. As illustrated in Figure 3.5, the extinction ratio (ER) of the spectrum defined as the difference between the maximum and minimum normalized power. The quality factor (Q) is the ratio of the stored energy inside the resonator to the dissipated one. Based on this definition, the following expression is deduced for Q in terms of the resonance wavelength, λ, and the bandwidth of the resonance, $\delta\lambda_{FWHM}$:

University of Malaya

$$Q = \frac{\lambda}{\delta\lambda_{FWHM}} \tag{3.21}$$

The calculated quality factor of the spectrum in Figure 3.5 is 11000.

3.3.4 Fabrication of a Single Knot Filter

The fabrication and the main characteristics of microfiber such as the uniformity and guided modes have been covered in chapter 2. Microfiber knot is fabricated from a uniform straight microfiber. The diameter of the microfiber depends on the application and the light source used (George Y et al., 2013).

To realize such structure, a standard single mode fiber (SMF) is tapered adiabatically by using flame brushing method. To form a single knot individually with different radii, it is required to cut the tapered microfiber into two parts: one part for bending and inter-twisting and the other one for coupling the free end to the first part. This process has been done by two small pieces of cleaved fiber or tweezers. It is difficult to control the diameter of the microfiber knot as the microfiber tends to stick to itself and causes the structure to break.

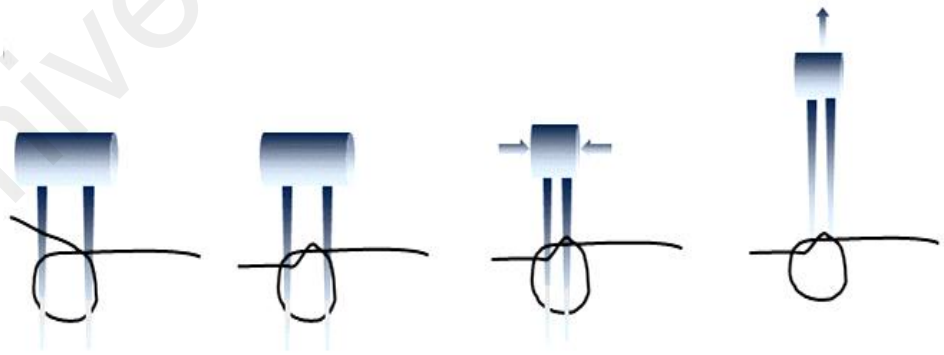

Figure 3.7: Schematic of microfiber knitting to fabricate a knot.

University of Malaya

To avoid this problem, two nonstick bars are used in the process. Each tapered fiber part is individually twisted around the bars, then they are separated to form a knot. The two bars are pressed close to each other to detach the sticky microfiber. They are then pulled up as shown in Figure 3.7. By using this technique, the knot is made almost to the desired radii. At the end, this part of microfiber is attached to another part of tapered fiber via van der Waal and electrostatic forces.

As mentioned in the previous chapter, this work focuses on filter applications of microfiber resonators. The simplest filter structure includes a single microfiber knot that is considered as both all-pass and add-drop filters. Figure 3.2 shows a microfiber all-pass filter. This filter includes a knot and a coupled straight waveguide. As illustrated in Figure 3.5, a single knot shows a periodic cavity resonance spectrum.

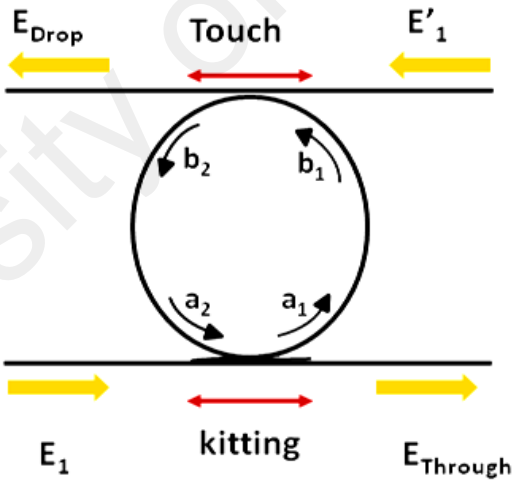

Figure 3.8: Schematic of an add-drop filter including all the related field elements.

The geometry of the knot allows more than one straight microfiber to be coupled to it. Figure 3.8 shows an add drop filter in which the knot is coupled from two sides. Based on the defined transfer matrix in section 3.2, the field elements of the figure are related as follows:

University of Malaya

$$\begin{cases} a_1 = r_1 E_1 + \mathrm{i}\mathrm{k}_1 a_2 \\ E_{through} = r_1 a_2 + \mathrm{i}\mathrm{k}_1 E_1 \\ b_2 = r_2 b_1 + \mathrm{i}\mathrm{k}_2 E_1' \\ E_{drop} = r_2 E_1' + \mathrm{i}\mathrm{k}_2 b_1 \\ b_1 = \mathrm{e}^{-\propto\frac{\mathrm{L}}{2}} e^{-i(\frac{2\pi n}{\lambda})\mathrm{L}} a_1 \\ b_2 = \mathrm{e}^{\propto\frac{\mathrm{L}}{2}} e^{i(\frac{2\pi n}{\lambda})\mathrm{L}} a_2 \end{cases} \tag{3.22}$$

$$\begin{bmatrix} a_1 \\ a_2 \end{bmatrix} = T_1 \begin{bmatrix} E_1 \\ E_{through} \end{bmatrix}, \begin{bmatrix} b_1 \\ b_2 \end{bmatrix} = T_2 \begin{bmatrix} a_1 \\ a_2 \end{bmatrix}, \begin{bmatrix} E_1' \\ E_{drop} \end{bmatrix} = T_3 \begin{bmatrix} b_1 \\ b_2 \end{bmatrix} \tag{3.23}$$

Substituting equations (3.22) into equation (3.23), the following matrices are obtained:

$$T_1 = \begin{bmatrix} \frac{1}{r_1} & \frac{i\mathrm{k}_1}{r_1} \\ \frac{-i\mathrm{k}_1}{r_1} & \frac{1}{r_1} \end{bmatrix}, T_2 = \begin{bmatrix} \mathrm{e}^{-\propto\frac{\mathrm{L}}{2}} e^{-i(\frac{2\pi n}{\lambda})\mathrm{L}} & 0 \\ 0 & \mathrm{e}^{\propto\frac{\mathrm{L}}{2}} e^{i(\frac{2\pi n}{\lambda})\mathrm{L}} \end{bmatrix}, T_3 = \begin{bmatrix} \frac{i\mathrm{k}_2}{r_2} & \frac{-i}{\mathrm{k}_2} \\ \frac{i}{\mathrm{k}_2} & \frac{-i\mathrm{k}_2}{r_2} \end{bmatrix} \tag{3.24}$$

Following the illustrated concept of ER in Figure 3.5, it can be expressed as (McKinnon et al., 2009):

$$ER \equiv \frac{|A_2|^2{}_{max}}{|A_2|^2{}_{min}} \tag{3.25}$$

In addition to ER, filter quality is affected by in band ripple and roll off. Band ripple considers the axial roughness of the spectrum between two successive resonance wavelengths. The roll off factor defines the trend of the spectrum in the proximity of the resonance wavelength. The slope of the output spectrum near resonance wavelength becomes very steep. This fact makes the device spectrum very sensitive to phase variation.

University of Malaya

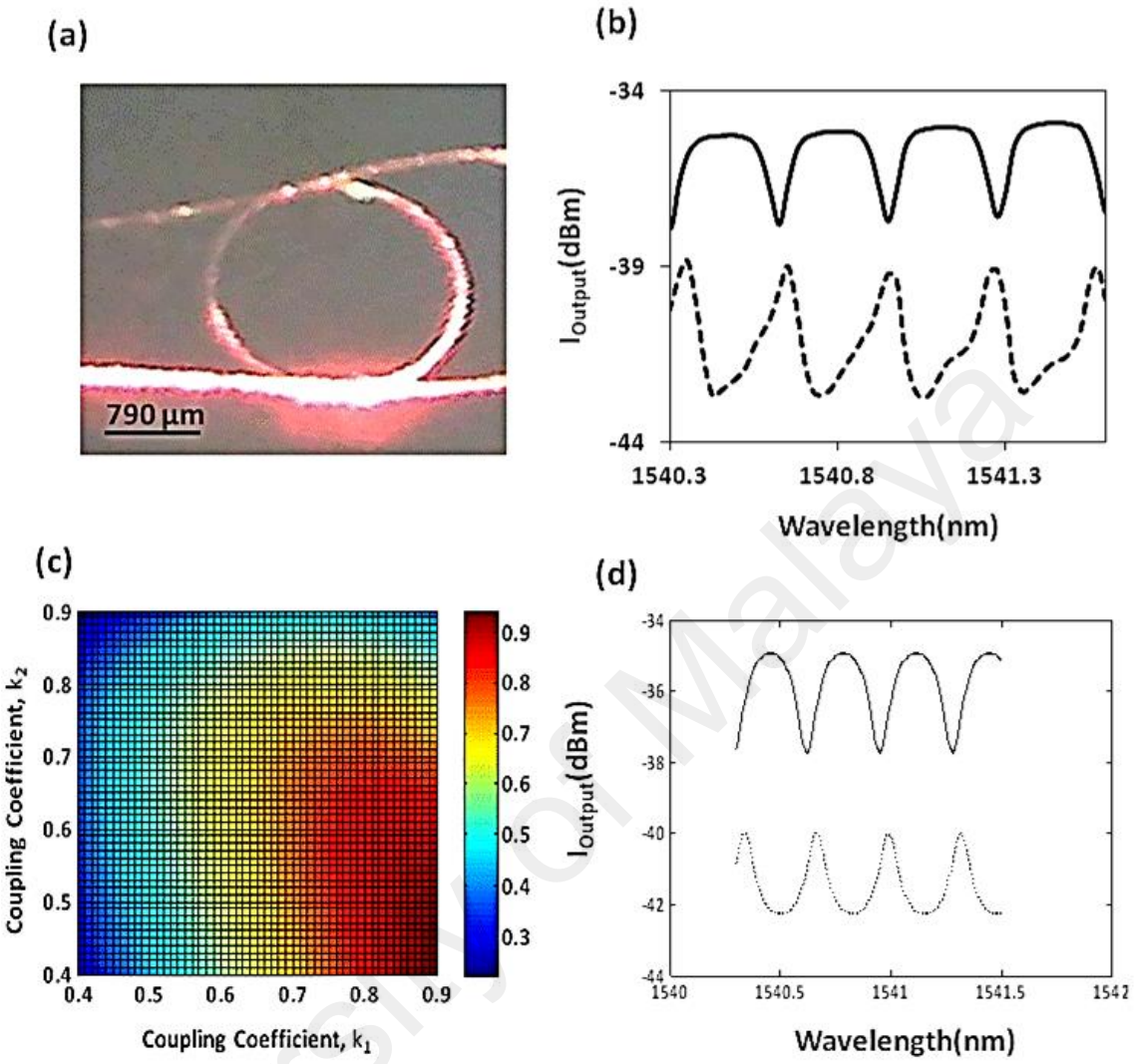

Figure 3.9: (a) microscopic image of an add-drop filter with radius of 790 µm, (b) experimental through port (bold line) and drop port (dashed line) spectrum of the knot, (c) simulation of drop port of the knot versus two coupling coefficients, (d) simulation results, through (bold line) and drop (dashed line) port of the knot.

Figure 3.9 (a) presents a microscopic image of an add-drop filter with radius of 790 µm, a red light source has been used to take the picture. The bright section indicates the knitting section, which obtains stronger coupling. The light is lunched from the right side, inside the through port of the microfiber. The experimental results of the proposed structure are

University of Malaya

shown in Figure 3.9 (b). Using the definitions in section 3.3.1, the spectrum has FSR of 325 pm, QF of 20000, FWHD 0f 75 pm, finesse of 4.3 and ER of 3.5 dB. In the Figure 3.9 (b), the through output is depicted in a bold line and shows higher power compared to the drop output (dashed line). Theoretical simulation of the drop port of the knot versus two coupling coefficients is shown in Figure 3.9 (c). It is noticeable from the figure that the drop port shows maximum ER in the blue region. Figure 3.9 (d) depicts the calculated spectra for the through (bold line) and drop (dashed line) port of a 790 μm radius knot with a coupling coefficients of 0.9.

3.3.5 Limitations and Solutions

A microfiber knot and its characters have been introduced in the previous sections. The resonance wavelengths in the output spectrum depend on the induced phase. By changing the induced phase, it can tune the resonator such that some resonant wavelengths are modified. In this structure, the induced phase directly depends on the length of the resonator. Any change of the length causes optical path variation, which alters the resonance condition. It can be utilized to tune the resonance wavelength for the output spectrum. Based on this concept, fine tuning of the resonator circumference can be provided by controlling of the environment (Zeng et al., 2009). Temperature is one of the environment variables that can be used for tuning the resonance spectrum (Zeng et al., 2009). If the process is reversed, one can tune the characteristics of the resonance spectrum by controlling the physical variables that affect its extinction and suppression ratio, bandwidth and resonance wavelength. This tuning ability is useful when developing filter, laser, and modulators with specific features or characteristics.

University of Malaya

In this chapter, thermal effect is employed to tune the resonant wavelength through changing the optical path. A research has been done to determine water temperature by a micro fiber knot. A 500 µm radius knot has been obtained from a 6 µm microfiber. The knot was placed on a glass slab and coated with a low refractive index polymer to increase the robustness of the structure under water as shown in Figure 3.10 (b). The coated knot measures the temperature of the water from 40 to 80 ^{o}C. The resonance wavelength changes linearly compared to the water temperature. In Figure 3.10 (a) the spectrum shift is related to 4 different temperatures: 60 ^{o}C (yellow, dashed line), 65^{o}C (blue, dashed line), 70 ^{o}C (purple, dashed line) and 80 ^{o}C (red, continued line). As it is shown figure 3.10 (c), the resonant wavelength changes with a slope of 85 picometer per 10 ^{o}C.

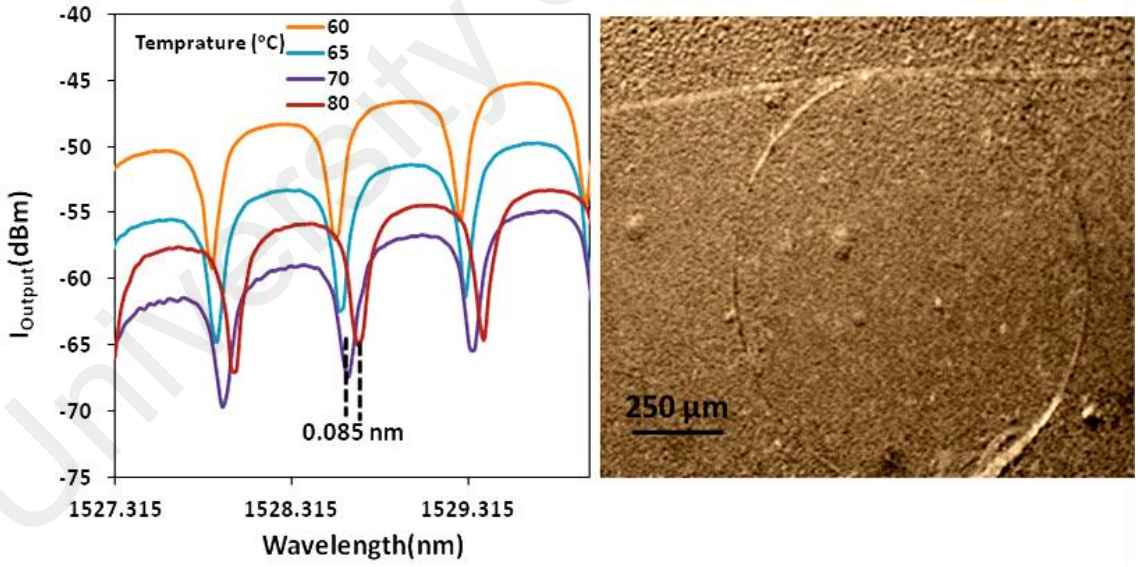

Figure 3.10: (a) Experimental result of a microfiber knot water temperature sensor (knot radius: 500 µm), (b) microscopic image of the prepared coated microfiber knot.

The linear expansion relation of any material is defined by:

$$\Delta L = \alpha L_1 \Delta T \tag{3.26}$$

University of Malaya

In which α is the linear expansion coefficient, L_1 is the initial length and ΔT is the temperature difference. Using this definition, it is possible to calculate the range of the linear expansion of the microfiber. Considering $\Delta T = 1$, the linear expansion coefficient of glass is in the range of $10^{(-6)}$ and the initial length of the structures is in the range of $10^{(-3)}$ which provides a ΔL in the range of a nanometer. Such increase leads to a few picometer changes at a certain resonance wavelength which is noticeable. As a result any changes in water temperature, a micro-size heater or a DC current wire can tune the resonant wavelength, FSR and ER.

The quality of resonators is typically determined by their FSR as well as the finesse (the ratio between FSR to FWHM) (J. Niehusmann et al., 2004). A combination of sharper finesse, wider FSR and deeper ER is a desired filter response (Grover et al., 2004; Grover et al., 2002). These filter characteristics depend strongly on the microring parameters such as ring radius and coupling coefficient (Poon et al., 2004). This dependency limits the spectral tuning of the resonator. In a single knot, controlling the finesse and ER independently is not practical (Sumetsky et al., 2005). Improvement in one factor causes a drop in another as shown in Figure 3.11 (Sumetsky et al., 2005). The figure includes experimental (a) and simulation (b) results of two knots with the same radius of 800 μm. Both waveforms at Figure 3.11 show FSR of 320 pm. The bold line spectrum has a quality factor of 20000, finesse of 4.3 and ER of 2.5 dB. The dashed line waveform shows QF of 15000, finesse of 3.2 and extinction ratio of 5.3 dB. These results indicate that an increase in ER leads to a drop in finesse and QF.

University of Malaya

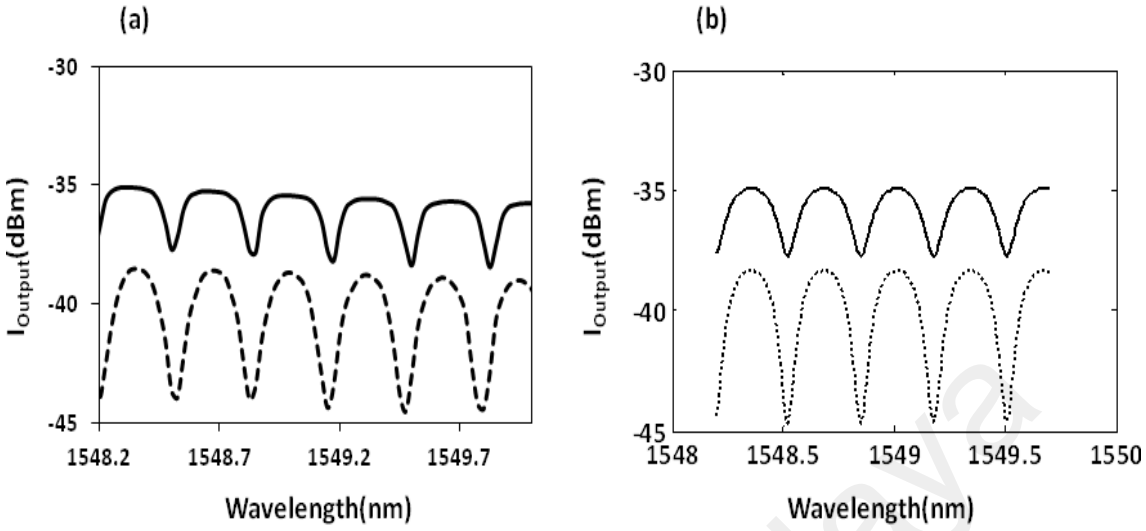

Figure 3.11: (a) experimental result from two microfiber knots with the same radius of 800 µm, (b) simulation result for the microfiber knots, the fitting coupling coefficient for the bold line and dashed line are 0.8 and 0.9 respectively.

To overcome this limitation multi-resonators have been proposed (Grover et al., 2002). With proper control of the phase relation between the different resonators, it is possible to obtain the desired spectrum. This chapter takes advantage of thermal effect and complex structure to improve the filter response.

3.3.6 Using Nonlinearity in Er- doped Microfiber Knot for Switching

Taking advantage of nonlinearity helps to switch the resonant wavelength through change in refractive index by stimulating nonlinear refractive index. Resonators are interesting elements towards the implementation of all optical switches due to their high field enhancement. This effect leads to high power inside the resonators which stimulates the nonlinear effect and decreases the input power threshold for such phenomena. As shown in Figure 3.3, the amount of field enhancement obtained for the circulating power is about 23

University of Malaya

times bigger than the input power. There are a few resonators that were proposed and fabricated (Gouveia et al., 2013; Ismaeel et al., 2012). These structures need high switching power to stimulate low nonlinearity in the material (Ismaeel et al., 2012).

The fabrication process for these elements, which most of the times is silicon based, is complicated and expensive (Poon et al., 2004). Microfiber resonators can provide a low cost alternative. Fiberglass has boosted the nonlinear refractive coefficients through material doping such as rare earth elements. Because the nonlinear refractive coefficient of the EDF (10^{-15}) is much larger than the one of silica fiber (10^{-20}), micro-Er doped-fiber may be a good candidate due to easiness of shaping and low switching power threshold compared to the fabricated structure so far (C. F. Li et al., 2006).

3.4 MZ- knot Structure

This research demonstrates a new approach for tuning the extinction ratio of a complex microfiber structure output using thermal effect. The microfiber filter device comprises of a microfiber Mach-Zhender interferometer followed by a knot structure. There are various microfiber structures including Mach-Zender interferometer (Y. H. Chen et al., 2010), microfiber ring (Sun et al., 2012), knot (X. S. Jiang et al., 2006), coil (F. Xu & Brambilla, 2007a), and some multi-knot structures (Y. Wu, Chen, et al., 2011). By taking advantage of phase sensitivity, these structures have been constructed and used as modulators and convertors (X. L. Zhang et al., 2012; Y. Zhang et al., 2009), mean to provide time delay (Y. P. Xu., et al., 2014) and to generate tunable lasers (Sulaiman et al., 2012b). The characteristics of the resonance spectrum can be controlled by the physical variables that affect its extinction and suppression ratio, bandwidth and resonance wavelength. This

University of Malaya

tuning ability is useful in developing filters, lasers, and modulators with specific features or characteristics.

A simple way to control the temperature of an optical microfiber structure is by passing electrical current through a conductor in its vicinity. The heat generated by the conductor is transferred to the microfiber structure, thereby changing its path length and modifying its resonance spectrum. There is a previous work in which a microfiber knot surrounds a copper wire has been used for current sensing (K. S. Lim et al., 2011). Also a similar structure has been reported as a temperature based microfiber current sensor that employs knot resonator and MZI. Figure 3.12 demonstrates a MZ-knot structure including all the field elements.

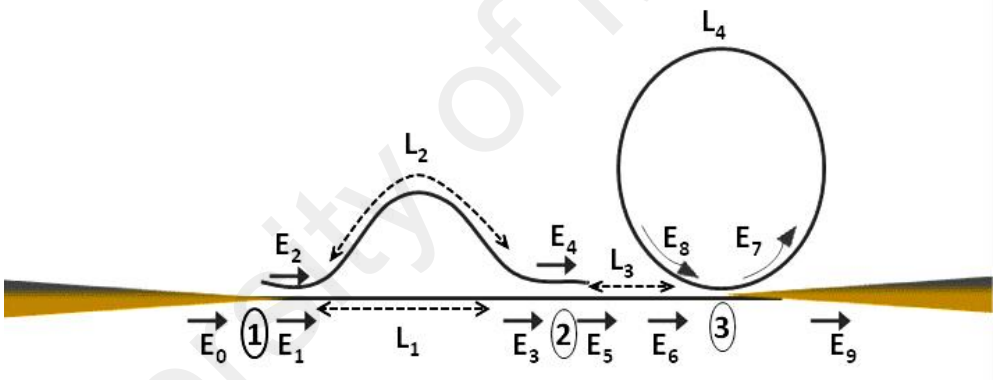

Figure 3.12: Schematic of Mach-Zhender and Knot structure.

This section investigates the use of DC to tune and improve the extinction ratio of the output spectrum of a microfiber filter consisting of Mach-Zhender and Knot structure. The current shifts the resonance wavelength of one of the structure elements that causes a change in the extinction ratio of the superposition output spectrum of the structure.

University of Malaya

3.4.1 Design and Fabrication

This structure relies on the superposition of field elements where changes in the phase lead to destructive or constructive interference. All the related field elements of the structure are indicated in Figure 3.12. It is possible to calculate the output using the coupling equations as follows:

$$\begin{cases} E_1 = t_1 E_0 \\ E_2 = -ik_1 E_0 \\ E_3 = e^{(-i\varphi_2 - \alpha L_2)} E_1 \\ E_4 = e^{(-i\varphi_1 - \alpha L_1)} E_2 \\ E_5 = -ik_2 E_4 + t_2 E_3 \\ E_6 = e^{(-i\varphi_3 - \alpha L_3)} E_5 \end{cases} \tag{3.27}$$

$$\begin{cases} E_7 = -ik_3 E_8 + t_3 E_6 \\ E_8 = e^{(-i\varphi_4 - \alpha L_4)} E_7 \\ E_9 = -ik_3 E_6 + t_3 E_8 \\ E_8 = e^{(-i\varphi_4 - \alpha L_4)}(-ik_3 E_8 + t_3 E_6) \end{cases} \tag{3.28}$$

Based on equations 3.27 and 3.28, expression for E_5 (the output of MZ), E_6 and E_9 are deduced in terms of E_0 as:

$$\begin{cases} E_5 = -ik_2 e^{(-i\varphi_1 - \alpha L_1)}(-ik_1) E_0 + t_2 e^{(-i\varphi_2 - \alpha L_2)} t_1 E_0 \\ E_6 = e^{(-i\varphi_3 - \alpha L_3)}[-ik_2 e^{(-i\varphi_1 - \alpha L_1)}(-ik_1) E_0 + t_2 e^{(-i\varphi_2 - \alpha L_2)} t_1 E_0] \end{cases} \tag{3.29}$$

where:

$$r_{1,2,..}^2 + k_{1,2,..}^2 = 1 - \gamma \ , \ \varphi_{1,2,..} = \frac{2\pi n L_{1,2,..}}{\lambda} \tag{3.30}$$

$r_{1,2,..}$ is the transmission coefficient, $k_{1,2,..}$ is the coupling coefficient, γ is the coupling loss and α is the round trip loss and L is the length related to the indicated regions.

University of Malaya

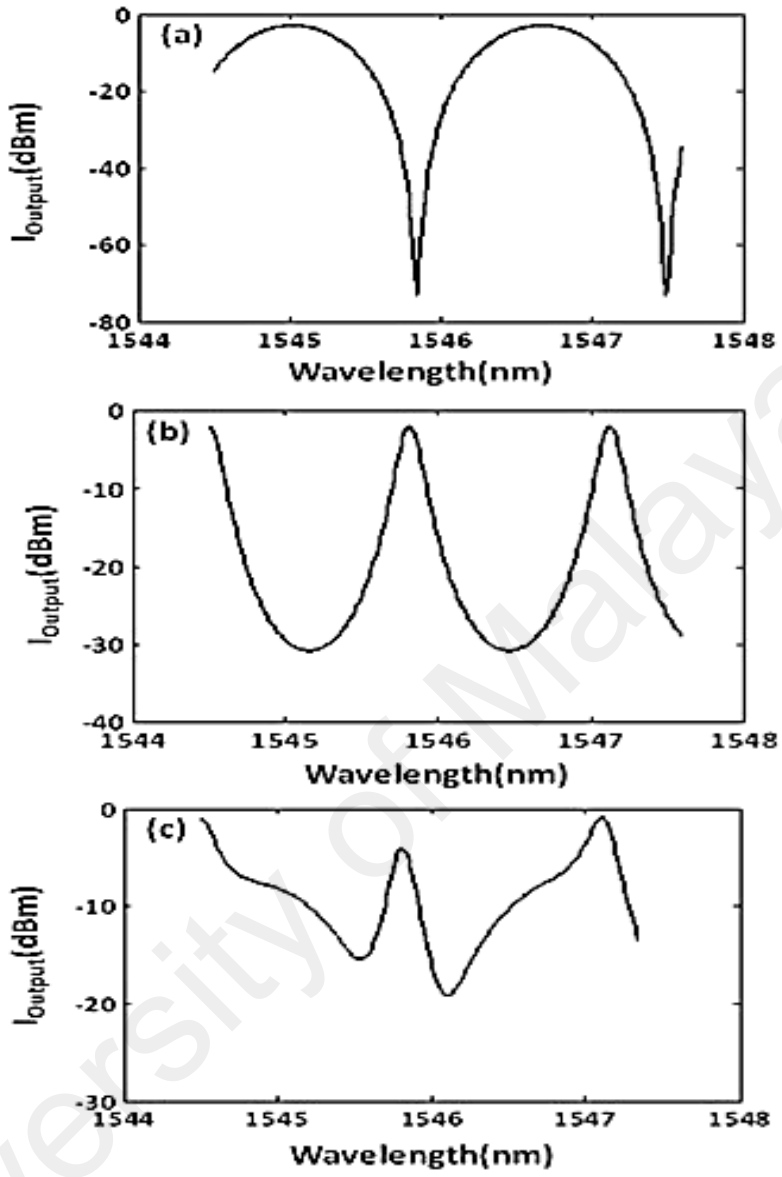

Figure 3.13: Simulation results from (a) a MZ with (L_1= 1000 µm and L_2=2000 µm), (b) a knot with radius of 200 µm and (c) the combination of two structures, value of all the coupling coefficients are 0.7.

Figure 3.13 (a) shows a simulation result from a MZ which including two arms with lengths of 1000 µm and 2000 µm. Also Figure 3.13 (b) shows the output of a knot with a radius of 200 µm. The combination of the two structures has an output as shown in Figure 3.13 (c). In Figure 3.13 (a), the MZ spectrum has an extinction ration of -80 dB at wavelength of 1545.9. Superposition of the modes from MZ and knot causes the power

University of Malaya

value of a certain resonant wavelength drop to -5 dBm. By taking advantage of this effect, it is possible to adjust or eliminate certain resonant wavelengths.

To fabricate these structures, a uniform microfiber must be prepared. A single mode fiber (SMF28) is first tapered using flame-brushing method until the diameter decreases to about 6 μm. To construct the filter with a cascaded MZI and knot structure (as shown in Figure 3.12), the microfiber is first cut into two sections of equal lengths. The first microfiber section is first twisted around two nonstick separated bars to form a knot. Then the two bars are pressed together and pulled out of the knot. The other microfiber section is curved to form an MZI structure. After making the MZI structure, the microfiber ends of the two structures are attached together by Van Der Waals and electrostatic forces so that the combined structure have one input and one output. The transmission spectrum of the structure is monitored by injecting amplified spontaneous emission (ASE) light. This light comes from an erbium doped fiber amplifier (EDFA) through the input port, while the output port is connected to the optical spectrum analyzer (OSA).

3.4.2 Characterization of the Obtained Band-pass Spectrum

The output spectrum from the microfiber shows the amount of reduction and uniformity, which is required in this experiment. Figure 3.14 (a) shows the output spectrum for the laser before and after tapering. This figure reveals that the output experiences a 4 dBm loss due to the tapering process.

Experimentally, a single knot was fabricated and its output was compared with one of the combined structure. The fabricated knot has a radius of 899.5μm that corresponds to the following resonance characteristics: free spectral range (FSR) = 300 pm, quality factor

University of Malaya

≅9000, full-wave half maximum (FWHD) = 175 pm and finesse = 1. 8 and extinction ratio =5 dB as it is shown in Figure 3.14 (b).

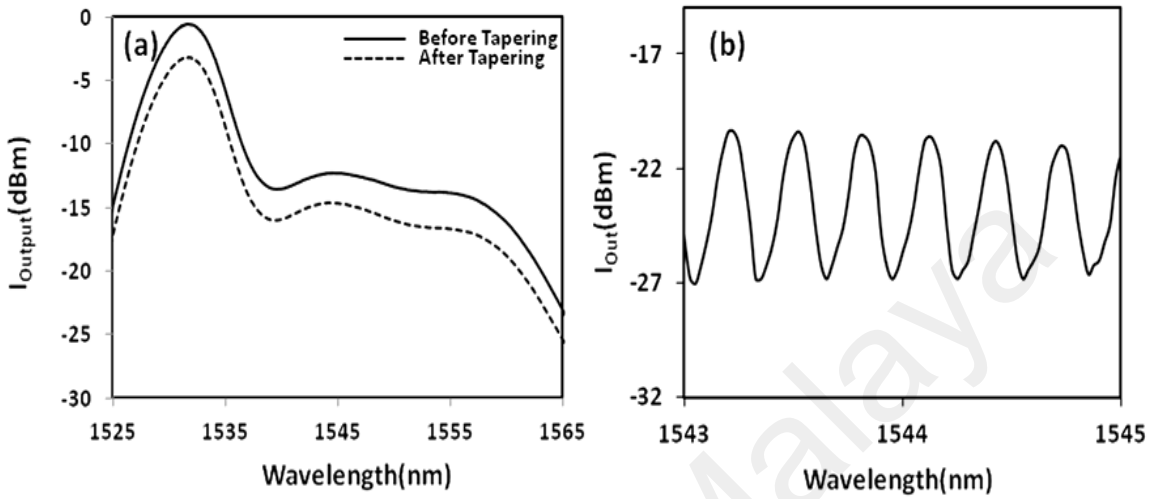

Figure 3.14: (a) Output power of Erbium laser through the fiber before tapering (bold line) and after tapering (dashed line), (b) resonant wavelength of the knot with 899.5μm.

The surrounding environment may affect the resonance spectrum and changes the resonance wavelength. Here, the effect of temperature on the spectrum shift of the knot is examined. A simple way to control the temperature of an optical microfiber structure is by passing an electrical current through a conductor in its vicinity. The heat generated by the conductor is transferred to the microfiber structure. This changes the fiber path length and influences its resonance spectrum. In our experiment, the room temperature was fixed at 28 ^{o}C. The temperature difference produced by the copper wire, with 250 μm diameter, resistivity of 1.68×10^{-8} Ωm and 10 cm length, is calculated for different current values as shown in Figure 3.15 using the following relation:

$$\Delta T = \frac{\rho l I^2}{AmC_w} \tag{3.31}$$

University of Malaya

where ρ is the resistivity, l the length, I the current, A the cross section, m the mass and C_w is the copper heat capacity.

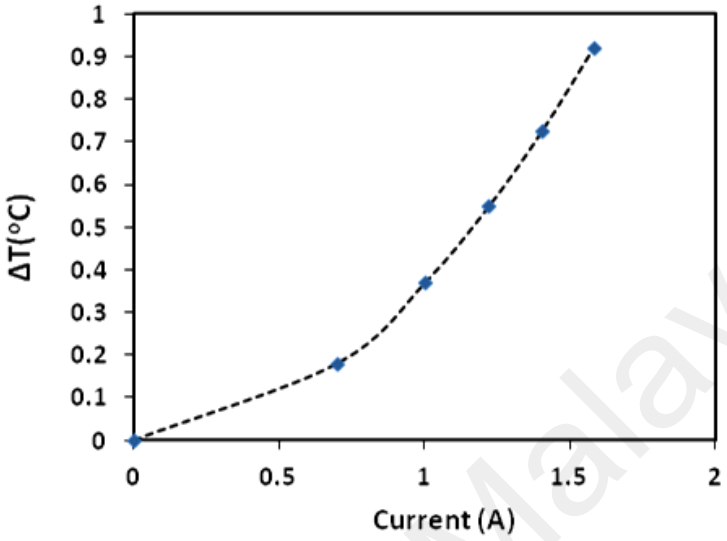

Figure 3.15: Temperature difference (with the room temperature) produced by the copper wire.

To calculate the phase and resonant shift during the heating process, free spectral range of the resonator should be considered. The free spectral range of the knot and its phase are defined as below (Y. Wu etal., 2009):

$$FSR = \frac{\lambda^2}{n_{eff}L} \tag{3.32}$$

$$\varphi_4 = \frac{2\pi n\, L_4}{\lambda} \tag{3.33}$$

where λ is the operating wavelength, n_{eff} and L indicates the effective index of the microfiber and the length of the resonator, respectively. Thermal effect caused by the current flow influences n_{eff} and L. This causes shift in the resonance as described in the following expression:

$$\frac{\Delta\lambda}{\lambda} = \left(\frac{\Delta n}{n} + \frac{\Delta L}{L}\right)_{Temp} \tag{3.34}$$

in which:

University of Malaya

$$\frac{\Delta n}{n} = \alpha \Delta T \, , \frac{\Delta L}{L} = \beta \Delta T \tag{3.35}$$

Here, $\propto$ and β are the thermal expansion coefficient and thermal optic coefficient of the microfibers, respectively. The temperature change is proportional to the resonance wavelength based on the following equation (Sumetsky, 2008; Y. Wu et al., 2009):

$$\frac{\Delta \lambda}{\lambda} \propto \frac{\rho I^2}{A} \tag{3.36}$$

where the constants ρ and A are the conductor resistivity and the cross section area of the conductor rod, respectively. Changing the current flowing through the copper rod from 0 A to 1.22 A, the output comb spectrum from the knot structure experiences a red wavelength shift of about 0 to 150 pm as shown in Figure 3.16 (a). The wavelength shift versus current is illustrated in Figure 3.16 (b).

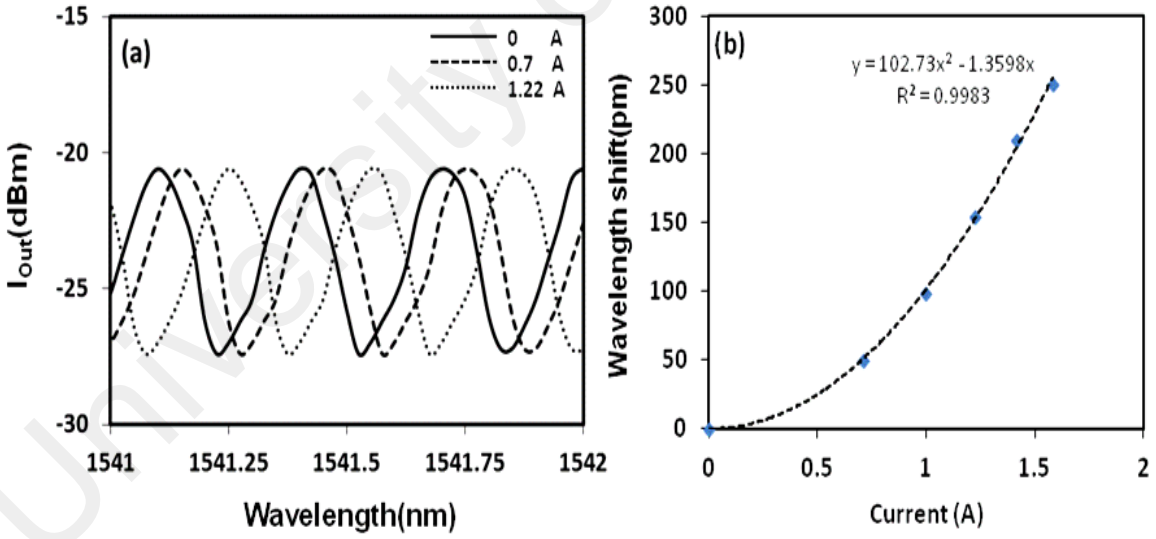

Figure 3.16: (a) Resonant wavelength shift of the knot spectrum, (b) resonant wavelength shift of the knot spectrum versus current.

University of Malaya

3.4.3 Controlling Extinction Ratio Base on Thermal Effect

The combined structure is depicted in Figure 3.17 (a). It consists of one microfiber mach-zhender interferometer (MZI) and one knot with the defined characteristics. The cascaded structure includes a knot and a MZI with two branches with a length difference of 6000 µm that generates a spectrum with FSR = 300 pm (the same with the knot) and extinction ratio of 4 dB. Microscopic images of the MZI and the knot are shown separately in Figure 3.17 (b) and Figure 3.17 (c) in this order. In the filter, the input light propagates through the MZI and then passes through the microfiber knot. The output spectrum of the filter is a superposition of the two elements.

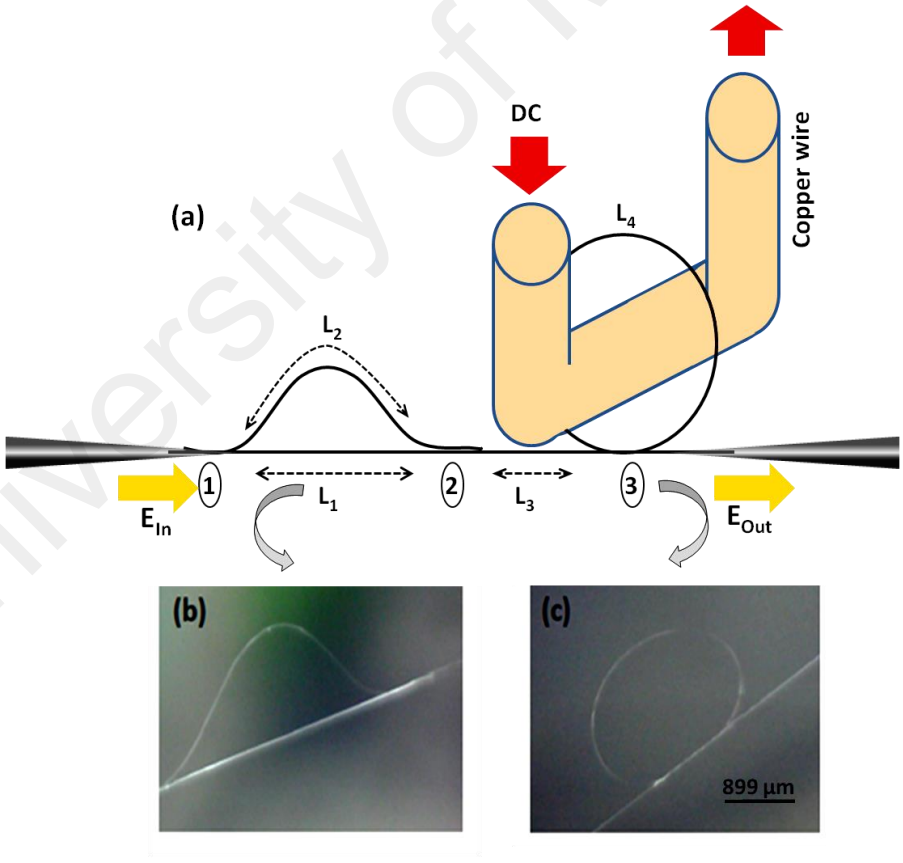

Figure 3.17: (a) Schematic diagram of the proposed structure, (b) microscopic image of the MZI and (c) the knot

University of Malaya

Due to the changes at the knot resonance characteristics caused by the changes in φ_4 , the combined output spectrum is altered according to equation (3.28). The output spectrum from the cascaded structure is shown in Figure 3.18 (a) in bold line, which shows an extinction ratio of about 10 dB at I=1.22 A. By increasing the DC to 1.22 A, the output spectrum of the knot overlaps with the individual MZI output spectrum. This improves the extinction ratio of the output spectrum of the cascading structure to 10 dB. Figure 3.18 (b) shows a sub-plot magnification of the red part. The sub-plot shows an increase in the finesse from 1.8 to 3.2 for a single knot and the structure respectively. It is clear that the spectrum provided from the structure provides sharper roll-off and deeper extinction ratio compared to the single knot.

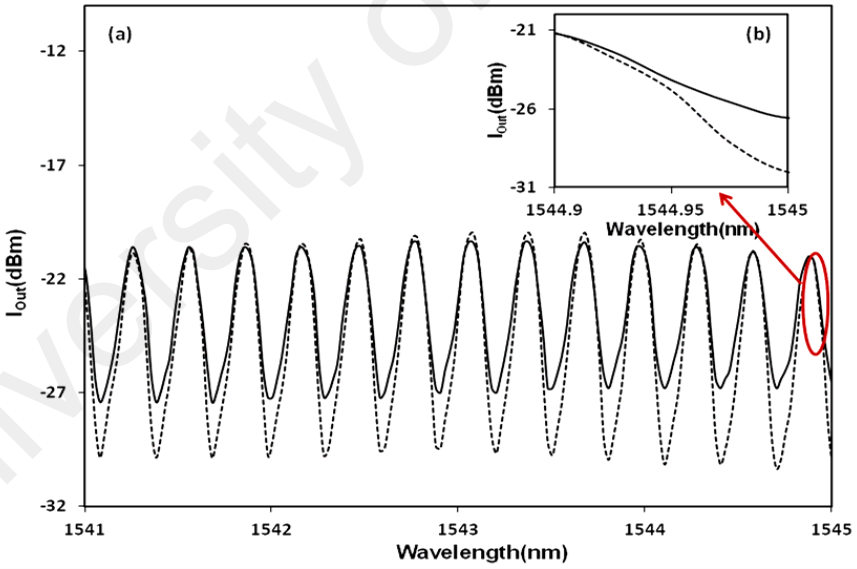

Figure 3.18: (a) Output spectrum from the knot (bold line) and cascade structure (dashed line) with I=1.22 A, (b) magnified sub-plot of the red circle part.

This is attributed to the constructive interference between the output spectra from both structures. The range of tuning in the structure spectrum extinction has been shown in

University of Malaya

Figure 3.19 (a). According to the figure, the highest extinction ratio of 10 dB is obtained when I=1.22 A at wavelength shift of 150 pm. At currents higher than 1.22 A, the resonance wavelength for the knot shifts away from MZI causing a drop in the extinction ratio as shown in Figure 3.19 (b).

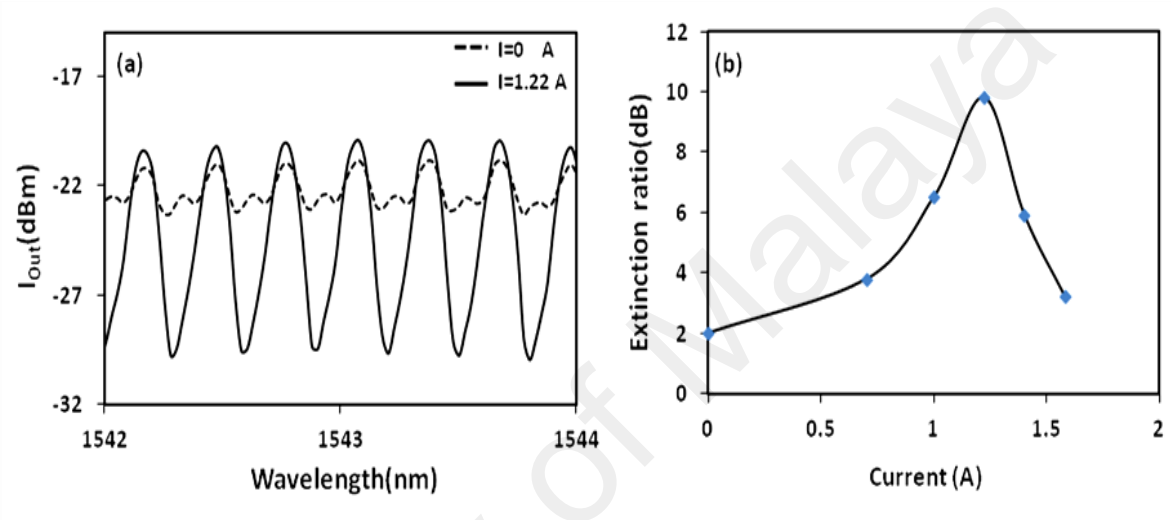

Figure 3.19: (a) Output spectrum from the cascade structure when I=0 A (dashed line) and I=1.22 A (bold line), (b) extinction ratio of the structure versus current square.

Based on Figure 3.19, tuning of the extinction ratio of a cascaded microfiber structure output spectrum is possible by applying an electrical DC current. This is attributed to the applied electrical current, which heats the conductor and affects the optical path of the knot. The change in the optical path shifts the resonance wavelength from one of the knots. That changes the extinction ratio of the superposition in the output spectrum of the cascaded structure. In the following section another structure is examined to overcome the single knot filter limitations by using thermal effect on double knot structure.

University of Malaya

3.5 Double Knot in Series

In 2007 a microfiber knot resonator has been reported for the first time as an all fiber add-drop filter (X. D. Jiang et al., 2007). The knot generates a spectrum with QF of 13000. Though, the produced QF is high, finesse and extension-ratio remains important factors. There are few works that show the finesse of a microfiber knot or loop resonator spectrum drops when the extinction ratio increases (X. D. Jiang et al., 2007; Sumetsky et al., 2005).

In this work a double microfiber knots has been proposed to improve both finesse and extinction ratio simultaneously. The same structure has been demonstrated for multi-point temperature sensing by taking advantage of thermal effect on the structure (Y. Wu., 2012). In this research, the thermal effect is utilized to achieve a tunable high order filter that improves the finesse and extinction ratio using Vernier effect. It is found that the output of the proposed structure can be filtered by controlling the optical path length difference via heating technique. This technique indicates that it is possible to add and eliminate some resonance wavelengths, while obtaining a high extinction ratio. In this section, theoretical analysis is also presented based on transfer matrix to estimate the characteristics of the output spectrum.

3.5.1 Single Knot Structure vs. Double Knot Structure

This part focuses on the performance of the double knot filter compared to single knot. The response of a filter can be expressed as (Madsen et al., 1999):

$$H(K) = \frac{E_{output}(K)}{E_{input}(K)} \tag{3.37}$$

University of Malaya

Which E_{input} and E_{output} are the input and output field elements and $K$is wave number. This describes how the output spectrum behaves away from the resonance wavelength. The output field for a single knot is defined by:

$$E_{output} = E_{input}\left(\frac{-ik+e^{-iKL}e^{-\propto\frac{L}{2}}}{1+ike^{-iKL}e^{-\propto\frac{L}{2}}}\right) \cong \frac{1}{1+ike^{-\propto\frac{L}{2}}(1-iKL)} \tag{3.38}$$

$$K = \frac{2\pi n}{\lambda} \tag{3.39}$$

Therefore the response of a single knot is in the order of $\frac{1}{K}$ and the output port intensity behaves as $\frac{1}{(1+ike^{-\propto\frac{L}{2}}(1-iKL))^2}$. It follows a Lorentzian response with sharp roll-off for higher orders. Coupled mode theory is used to obtain the filter response of a double knot structure. Figure 3.20 shows a couple knot structures including all the field elements inside the knots, input and output field.

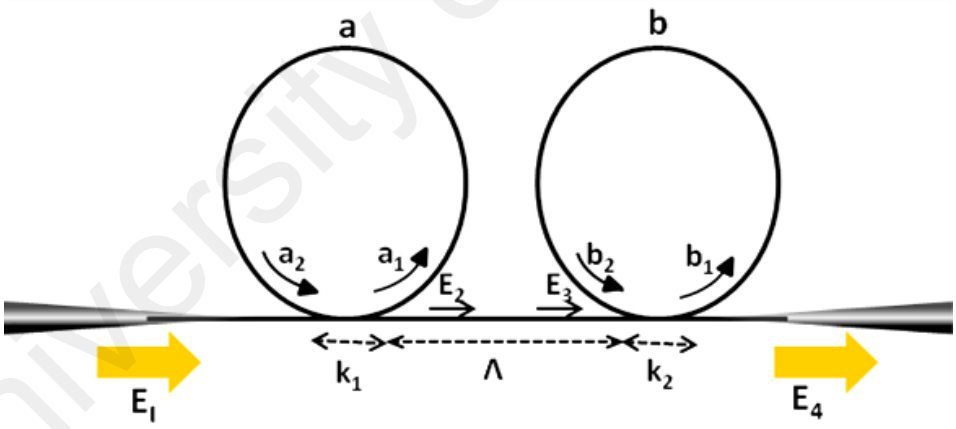

Figure 3.20: Schematic diagram of the proposed microfiber cascaded knots structure.

The following equations lead to the response function of the structure:

University of Malaya

$$\begin{cases} E_2 = ik_1 a_1 + r_1 a_2 \\ a_1 = ik_1 a_2 + r_1 E_1 \\ E_3 = e^{\left(-i\varphi_2 - \alpha\frac{\Lambda}{2}\right)} E_2 \\ b_1 = ik_1 b_2 + r_1 E_3 \\ E_4 = ik_2 b_1 + r_2 b_2 \end{cases} \tag{3.40}$$

The field components E_1 and E_2 represent the input and the output fields, respectively. E_2 and E_3 are the field components inside the structure. The coupling coefficient is defined as $k = \gamma \mathrm{k}$ where $\mathrm{k} = -i \sin\frac{\pi L_c}{2L_\pi}$. k_1 and k_2 are the coupling coefficient of microfiber segment 1 belonging to knot(a) and knot(b), respectively. Also k' is the coupling coefficient of the microfiber segment 2 while L_c and L_π are the physical coupling length and coupling length in order (Delage et al., 2009; McKinnon et al., 2009). The constant γ is the coupling loss. The exponential expression in equation (3.40) represents the round trip loss of the light propagating through the knots while the constant $\propto$ is the loss coefficient. L_a and L_b are the round trip lengths for the knots a and b respectively. The constants λ, n and Λ are the operating wavelength of input light, the effective index of the microfiber and the length between the coupling regions of the two knots. The response filter of a double knot is derived from the set equation (3.40) in the following equation:

$$E_4 = \left(\frac{-ik_a + e^{-i\left(\frac{2\pi n}{\lambda}\right)L_a} e^{-\propto\frac{L_a}{2}}}{1 + ik_a e^{-i\left(\frac{2\pi n}{\lambda}\right)L_a} e^{-\propto\frac{L_a}{2}}}\right)\left(\frac{-ik_b + e^{-i\left(\frac{2\pi n}{\lambda}\right)L_b} e^{-\propto L_b/2}}{1 + ik_b e^{-i\left(\frac{2\pi n}{\lambda}\right)L_b} e^{-\propto L_b/2}}\right) e^{-i\left(\frac{2\pi n}{\lambda}\right)\Lambda} e^{-\propto\Lambda} E_1 \tag{3.41}$$

As shown in equation (3.41), the response of the structure is in the order of $\frac{1}{K^2}$. It has a sharper roll-off than a single knot. The interference between the individual knots responses result in a flatter top compared with single knot filter can be obtained.

University of Malaya

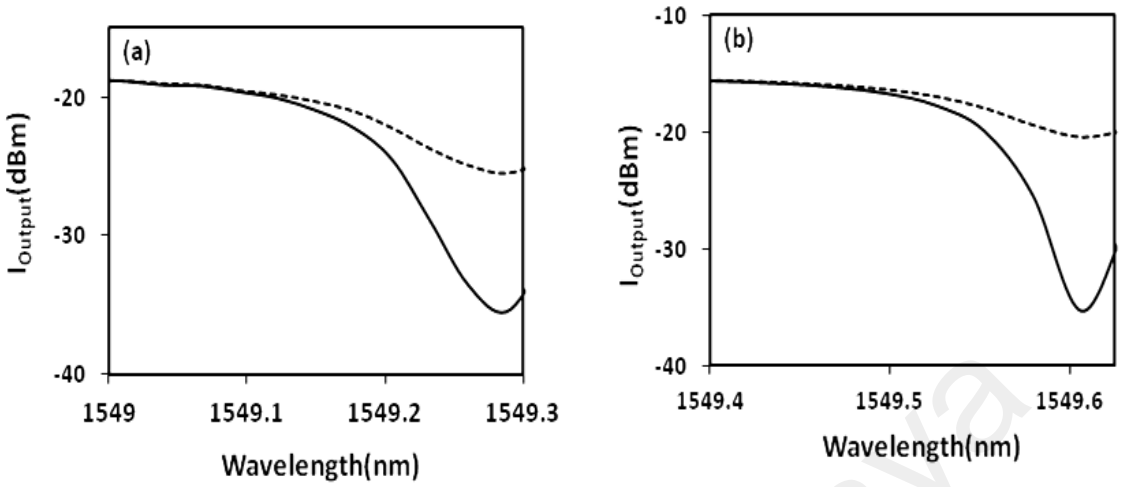

Figure 3.21: (a) Simulation result of output spectrum for a single-knot (dashed line) and double-knot structure (bold line) (b) experimental curves of a single-knot (dashed line) and double-knot structure (bold line) with the same radii of 357.66 µm.

Figure 3.21 compares the simulation results of the double-knot structure spectrum (bold line) and a single knot spectrum (dashed line) filter. Vernier effect delivers sharp roll-off when the number of resonators with similar resonance wavelength increases.

3.5.2 Fabrication and Characterization

Figure 3.20 illustrates the proposed resonator that consists of two cascaded knots in series. The two knots are assembled based on a single tapered microfiber. First, a standard single mode fiber (SMF) is tapered adiabatically down to 8 µm of waist diameter by using flame-brushing method. Then it is cut in the middle and divided into two parts where each part is used to fabricate a single knot. In the experiment, the knots are formed based on the traditional method of knitting a woolen or string. Where one of the microfiber parts is looped around, two nonstick separated bars before a knot is formed via micro-manipulation.

University of Malaya

The two bars are then pressed close to each other to separate the sticky microfiber from the bars and then pulled up to form the knot. The second knot is formed based on the same technique using the other part of microfiber. Both knots are then cascaded together by attaching and coupling two microfibers ends via van der Waals and electrostatic forces and denoted by knot (a) and knot (b). The radii of knot (a) and knot (b) are 357.66 µm and 357.73 µm, respectively. During the fabrication process, the transmission spectrum of the resonance structure is monitored by injecting amplified spontaneous emission (ASE) light. This light comes from an erbium doped fiber amplifier (EDFA) through the input port, while the output port is connected to the optical spectrum analyzer (OSA). At the coupling region of the knot resonator, the microfiber is represented by segments 1 and segments 2. Segment 1 represent the ingoing and outgoing lights respectively and segment 2 the light energy exchange between two segments. Figure 3.22 demonstrates the output spectrum of the knot (a) with the ring radius of 357.66 µm. The spectrum in this figure is monitored separately by attaching another microfiber at the output end of the knot (a) before it was assembled with the second knot. Based on the experimental spectrum (solid line) analysis, the quality factor ($\lambda 0/\Delta\lambda$) of the knot is calculated to be around 11000 while free spectral range (FSR), full-wave half maximum (FWHM), finesse, and extinction ratio are obtained at around 715 pm, 137 pm, 5 and 6 dB, respectively. The theoretical investigation curve is also included in Figure 3.22 as shown by dashed line for comparison.

University of Malaya

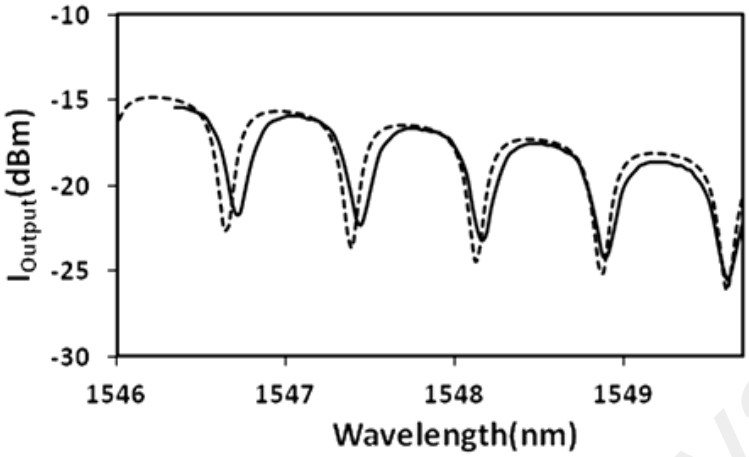

Figure 3.22: Output spectrum of the knot with the ring radius of 357.66 µm and coupling coefficient of 0.7, experimental (bold line), simulation (dashed line) result.

3.5.3 Improvement in Extinction Ratio and Finesse Based on Thermal Effect

Previously, a microfiber knot resonator (MKR) was demonstrated as a temperature sensor with sensitivity of 0.27nm/degree ^{o}C (Zeng et al., 2009). In another work, a microfiber loop resonator (MLR) embedded in low refractive index polymer was demonstrated to exhibit a linear reduction of the extinction ratio against temperature a rate of about 0.043dB/^{o}C (K. S. Lim et al., 2011). In this work, thermal effect is used on the knot to calculate the wavelength shift versus temperature change and correct the optical path of the structure. Figures 3.23 (a) and (a) show a sketch and a microscopic image of the proposed setup for optical path correction. As a result of the temperature increase of the metallic wire from the room temperature of 28^{o}C to 30^{o}C, the round trip length of knot (a) extends by few nanometers.

University of Malaya

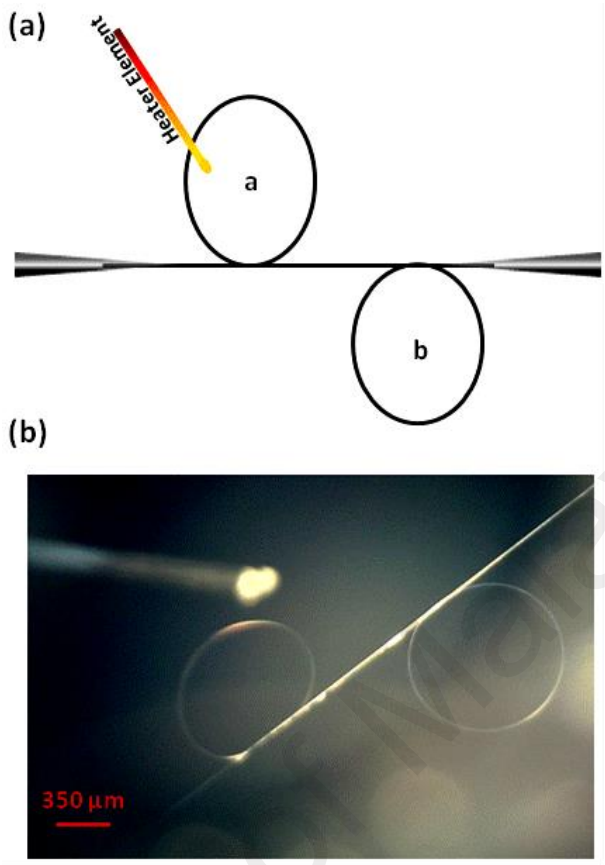

Figure 3.23: (a) Schematic diagram of the proposed setup, (b) microscopic image of the proposed setup for optical path correction .

Combining the two knots in series with a distance Λ, of an estimated 2000 µm, a new comb filter with complex spectrum is obtained at the output (Figure 3.24 (a)), in which two attenuated wavelengths are excited at the peak of each ripple of the original output spectrum (comb) of the single knot. As it can be clearly seen from Figure 3.22, the extinction ratio has diminished from 6 dB to around 3.5 dB compared to the extinction ratio at single knot. This is due to the slight mismatch in the radii of the knots of about ~ 70 nm. That corresponds to a significant phase difference between the two spectra. A simulation result has been shown in the figure with dashed line as well. In which the best-fit curve is obtained at coupling coefficient of 0.70.

University of Malaya

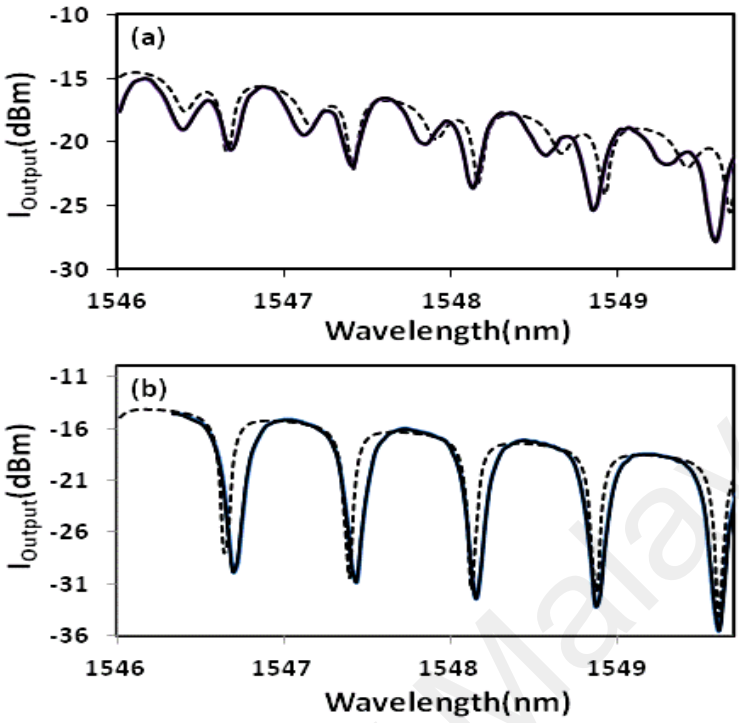

Figure 3.24: Simulation and experimental curves fittings of the output comb spectrum for (a) structure before heating and (b) after heating.

To overcome the radii mismatching, this work proposes a simple solution method for optical path correction by heating up small section from the loop of the smallest knots by placing a hot metallic wire close to the loop with a gap of approximately 60 µm. As shown in Figure 3.24 (a), this eliminates the attenuated wavelengths at the peak of the output comb filter of the double-knot structure; showing a flat comb filter with high extinction ratio of about 15 dB. Such filtering indicates that a proper optical path correction has been achieved. According to Figure 3.24 (b), a significant change in the output spectrum of the structure after heating knot (a) can be clearly observed. Figure 3.24 (b) shows the best fitting (dashed line) from the experimental result uses a coupling coefficient of 0.7 for both

University of Malaya

knots. Based on the calculations, the resonance characteristics of the structure have been changed and the quality factor increases to 20000, with a reduction in FWHM to 85pm. This improves the finesse to 9.5 as well as increases the extinction ratio to 15dB. There is an obvious difference between the calculations and experimental results because of the approximation in estimating the coupling length in each knot. Also, there might be slight error while measuring the actual radii of the two knots. Regardless of the slight difference between the simulation and experiment, the proposed method of optical path correction shows that the extinction ratio can be significantly improved by keeping both resonators in-phase. This approach can be as well used for spectrum manipulation using thermal effect. Thermal effect can help to tune the characteristics of the output spectrum. It can as well possibility eliminates unwanted attenuated wavelengths and enhances some other parts of the spectrum.

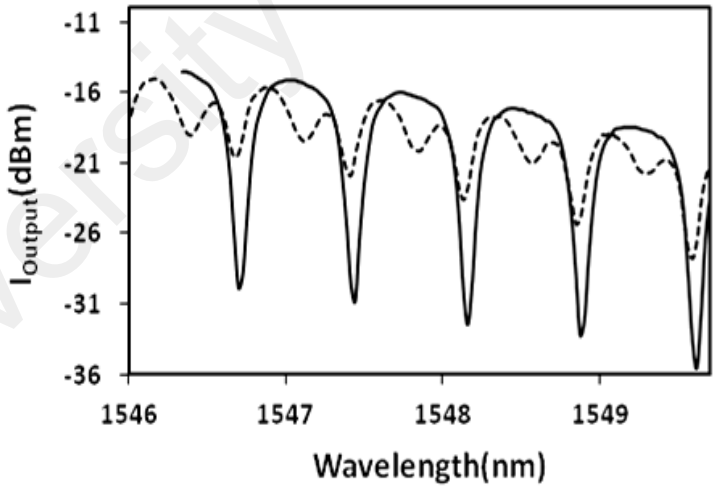

Figure 3.25: Experimental curves of the output spectrum for the cascaded knot structures before heating(dashed line) and after heating(bold line).

It is shown in Figure 3.25 that the double-knot structure (bold line) obtains a sharper roll-off than a single knot (dashed line) filter due to the Vernier effect, where the finesse increases by about twice that of a single knot. Spectrum tuning is shown in Figure 3.25

University of Malaya

when the knots are out of phase (before heating) and when optical temperature is applied to bring the two resonances in phase as shown by the solid line.

3.6 Summary

In this chapter microfiber resonator has been introduced as an optical filter element. A single knot as a filter suffers some limitations. In a single knot structure, the extinction ratio and finesse cannot be controlled at simultaneously. Also, a knot with a defined radius can only generate a fixed bandwidth with certain resonance wavelength. To overcome these limitations, utilization of multi microfiber resonator and employing thermal effect on the structures have been proposed.

A new approach has been demonstrated for tuning the extinction ratio of a complex microfiber structure output using thermal effect. The microfiber filter device comprises of a microfiber Mach-Zhender interferometer followed by a knot structure. The temperature is controlled by a DC current applied to a copper wire placed inside the knot. To control the resonator spectrum characteristics of the microfiber resonators, the effect of the DC current on the spectrum of a complex microfiber structure has been monitored. This enables electrical tuning, applying an electrical current increases the temperature and affects the optical path. The change of temperature facilitates fine-tuning of the resonance output spectrum. The change in the optical path which shifts the resonance wavelength from one of the knot changes the extinction ratio of the output spectrum of the cascaded structure. From the experiment, a comb spectrum can be shifted by roughly 150 pm when increasing the current from 0 A to 1.22 A. It was observed that the extinction ratio of the output comb

University of Malaya

spectrum can be controlled within 2 dB to 10 dB by varying the current rating from 0 A to 1.22 A.

In another combination, two microfiber knots with different radii, in a series, have been considered. Theoretical and experimental investigations of the thermal effect on the resonance conditions of this structure are provided. The double-knot microfiber resonator has been successfully fabricated using a flame brushing technique. The fabricated device consists of two similar knots with radii of 357.66 μm and 357.73 μm with an almost similar individual resonance characteristics of (FSR = 715 pm, Quality factor ~ 11000, FWHM = 137 pm, finesse = 5 and extinction ratio = 6 dB). Here, double-knot microfiber resonator, which utilizes heat for optical path correction, is introduced to increase the finesse. In the proposed structure, the two knots are combined in series with a distance of 2000 μm between two coupling region. The extinction ratio of the comb spectrum at this condition is roughly 3.5. The smallest knot is slightly heated to change its optical path length to match that of the second knot. Consequently, the output spectrum is transformed into a new comb spectrum with an improved quality factor and extinction ratio of 20000 and 15 dB, respectively. In this research, it is found that using thermal effect helps tuning the characteristics of the output spectrum. Such tuning is very useful for different applications specially at filtering and in fiber lasers.

The compatibility of these structures with single mode fiber systems makes it easy to be used as noise filtering in telecommunication and fiber lasers. The proposed designs have advantages of being simple and low cost. That provides a large potential application in photonic integrated circuits such as band-pass and stop-band filters.

University of Malaya

CHAPTER 4

NEW DESIGN OF OPTICAL FILTER USING VERNIER EFFECT ON MULTI-RESONATOR MICROFIBER STRUCTURE

4.1 Introduction

Optical filter ring resonators have been proposed and fabricated as one of the basic photonics components during recent decades. Single ring resonator has been demonstrated as all pass and add-drop filter (Grover et al., 2004; Hryniewicz et al., 2000). According to the literature, the quality of the resonators is typically determined by their FSR as well as the finesse (the ratio between FSR to FWHM) (Niehusmann et al., 2004). As explained in chapter 3, combination of sharp finesse, wide FSR and deep ER are desired filter characteristics (Grover et al., 2002). These characteristics depend strongly on the microring parameters such as ring radius and coupling coefficient (Poon et al., 2004). This dependency limits the spectral tuning of the resonator. To overcome this limitation multi-ring resonators have been proposed (Griffel, 2000; Grover et al., 2002). With proper control of the phase relation between the different rings, the superposition of the individual spectra can result in a net enhancement of the resonance peaks due to Vernier effect. This effect causes an increase in the finesse at some peaks while suppressing others (Griffel, 2000). Achieving higher finesse allows the use of ring resonators in wavelength division multiplexing applications (Little et al., 2004) and the design of advanced filter for notch filter (Popovíc et al., 2006). Applying Vernier effect, verity of high order filters based on multi-microring resonators structures have been demonstrated such as asymmetrical ring resonator array (Griffel, 2000), parallel cascaded microring resonators (Grover et al., 2002), coupled racetrack resonators (Boeck et al., 2010).

University of Malaya

In all these designs, integrated waveguides are used. This requires complicated and expensive fabrication techniques. In the integrated microrings, the loops dimensions are precisely controlled through the lithography and nanotechnology process (Chao et al., 2002; Poon et al., 2004).

This fabrication complexity as well as the desired high quality filter response of the multiring resonators created a demand for an alternative low cost implementation scheme. The current developments of microfiber loop and knot technology seem to provide a practical solution (Jung et al., 2011; Lee et al., 2013; M. Sumetsky et al., 2006; Y. P. Xu et al., 2014) .

Microfiber loops can be realized by twisting a tapered fiber (M. Sumetsky et al., 2006). Using this technique, a 1 μm-microfiber loop with 1mm diameter was obtained. A resultant quality factor (QF) of 630000 has been reported. Theoretically QF value of up to 10^{10} is predicted, which is comparable to the integrated microring resonator (Sumetsky, 2004; M. Sumetsky et al., 2006; Y. P. Xu et al., 2014). Microfiber knot shows stable light coupling and supports single–mode operation readily. Those characteristics have allowed this structure to be considered as modulators and convertors (X. L. Zhang et al., 2012; Y. Zhang et al., 2009), tunable lasers (Chen et al., 2014; Sulaiman et al., 2012) and a wide range of sensors (Liao et al., 2014; Shao et al., 2014; P. Wang et al., 2011).

In this work, we fabricate a microfiber knot structure component, which can be used as a filter in laser, sensor and amplifier applications. These high order filters already have been used to increase field enhancement on desired wavelengths and at the same time suppress other wavelengths. Also increasing the finesse leads to a sharp roll-off is one of their benefits.

In a recent work, a single microfiber knot was used in spectral filtering (Jiang et al., 2007).

University of Malaya

As mentioned in chapter 3, controlling the finesse and ER independently is not practical (Sumetsky et al., 2005). Improvement in one factor causes a drop in another. The previous chapter takes advantage of the thermal effect to correct the optical path. This leads to instructive mode interference. To overcome the limitation where a desired ER is maintained while increasing the finesse, this chapter has borrowed the same concept utilized in multi-ring resonators through the implementation of two knots structure. Using two knots, Vernier effect allows keeping the ER when increasing the finesse. This is not feasible for single knot for some of the resonance peaks. To the best of our knowledge, this is the first time utilization of Vernier effect in microfiber knot structures.

This work investigates this effect theoretically and experimentally. At section 4.2, the structure and the governing theory are mentioned. The section describes the experimental method. Here, the theoretical analysis is based on transfer matrix.

4.2 Single Knot Hybrid Microfiber Structure

This research is based on a microfiber resonator structure, which includes one knot, a semi ring and a straight microfiber. The structure has three ports: input and drop/through ports. As shown in Figure 4.1, the knot is located at the left part of the semi ring structure at the opening of the structure. The part of the structure which contains the semi ring is referred to section A. Section B refers to the knot with a radius as big as the curvature at section A. All the field elements involved in our theoretical analysis are demonstrated in the figure. The figure as well shows a microscopic pictures that show a sample of such structure. The curvature at section A is referred to as curvature A.

University of Malaya

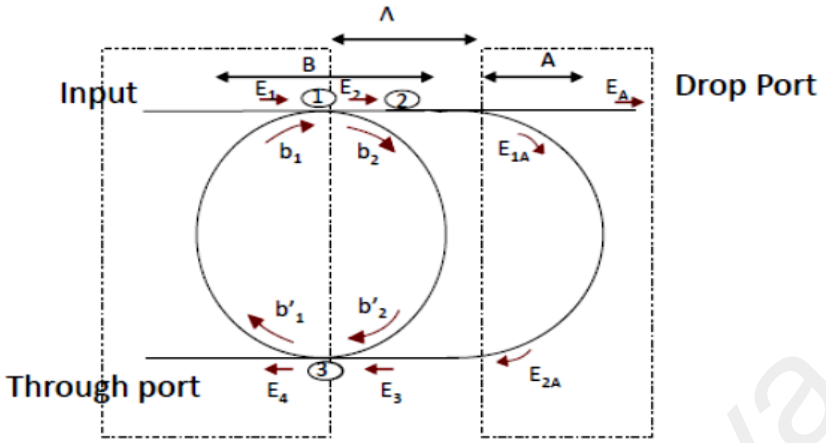

Figure 4. 1: Schematic diagram of the proposed new structure with one microfiber knot surrounded by a semi ring structure.

4.2.1 Concept and Design

Transfer matrix method has been used to analyze the output related to the structure (Yariv et al., 1999). As illustrated in Figure 4.1, the elements E_1, E_4 , E_A express the input and left/right output field components respectively.

$$\begin{cases} E_2 = ikE_1 + rb_1 \\ b_2 = ikb_1 + rE_1 \\ E_A = ikE_2 \end{cases} \tag{4.1}$$

$$\begin{bmatrix} b_1 \\ b_2 \end{bmatrix} = M_1 \begin{bmatrix} E_1 \\ E_2 \end{bmatrix}, \begin{bmatrix} b_1' \\ b_2' \end{bmatrix} = M_2 \begin{bmatrix} b_1 \\ b_2 \end{bmatrix}, \begin{bmatrix} E_4 \\ E_3 \end{bmatrix} = M_3 \begin{bmatrix} b_1' \\ b_2' \end{bmatrix} \tag{4.2}$$

In equations (4.1) and (4.2), the matrices have been defined as as follows:

$$M_1 = \begin{bmatrix} \frac{-ik}{r} & \frac{i}{r} \\ \frac{1}{r} & \frac{ik}{r} \end{bmatrix}, M_2 = \begin{bmatrix} \mathrm{e}^{\propto L_B/4} e^{i(\frac{2\pi n}{\lambda})\frac{L_B}{2}} & 0 \\ 0 & \mathrm{e}^{-\propto L_B/4} e^{-i(\frac{2\pi n}{\lambda})\frac{L_B}{2}} \end{bmatrix}, \; M_3 = \begin{bmatrix} -\frac{ir}{k} & \frac{i}{k} \\ -\frac{i}{k} & \frac{ir}{k} \end{bmatrix}$$

(4.3)

University of Malaya

where $b_1, b_2, b_1^{'}, b_2^{'}, E_{1A}, E_{2A}$ are the field components inside the rings and curvature. Hence the associated transmission matrix between the matrix $\begin{bmatrix} E_1 \\ E_2 \end{bmatrix}$ and matrix $\begin{bmatrix} E_4 \\ E_3 \end{bmatrix}$ is:

$$\begin{bmatrix} E_4 \\ E_3 \end{bmatrix} = M_3 M_2 M_1 \begin{bmatrix} E_1 \\ E_2 \end{bmatrix} \tag{4.4}$$

$$E_3 = e^{-i(\frac{2\pi n}{\lambda})\frac{L_A}{2}} e^{-\propto L_A/4} e^{-i2(\frac{2\pi n}{\lambda})\Lambda} e^{-\propto \Lambda} r_2 E_2 \tag{4.5}$$

$$k = \gamma k^{'}, r = \gamma r^{'}, k^2 + r^2 = \gamma^2 \tag{4.6}$$

where k and r are the coupling and transmission coefficient belonging to sections 1, 2 and 3 (Figure 4.1). The element γ is the coupling loss (Smith, 1976; M. Sumetsky et al., 2006). In equation (4.5), the factor $e^{-\propto L_{A,B,\Lambda}}$ is the round trip loss through curvature A and knots B. The constant $\propto$ is the loss coefficient (Tong et al., 2011). λ is the wavelength of light, n is the effective index related to the microfiber and $L_{A,B} = 2\pi R_{A,B}$ is the length of curvature A and knots B and C. The constant $r_{A,B,C}$ is the knot or curvature radius. Λ represents the length between knot B to semi ring A.

The resonances are from the interference of light with different phase shift, which is obtained from different paths. These paths pass from 1 and 2 points.

4.2.2 Fabrication and Characterization

In the experiment, a single mode fiber (SMF28) is first tapered to 10 µm waist diameter using flame brushing method and a knot with 1763 µm radius was fabricated. In this setup, the transmission spectrum of the structure is monitored by injecting amplified spontaneous emission (ASE) light from an erbium doped fiber amplifier (EDFA) into one end of the input port while the other end is connected to the optical spectrum analyzer.

University of Malaya

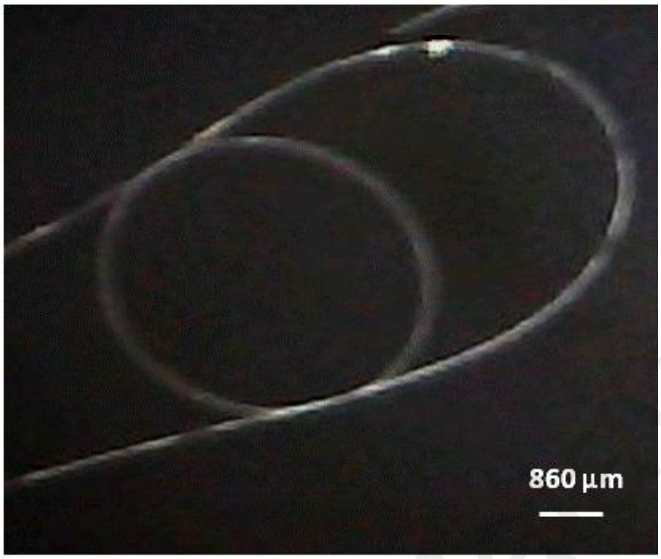

Figure 4.2: Microscopic picture from a fabricated structure.

To fabricate semi ring structure, the microfiber end is looped back to the knot. Another microfiber with the same diameter is used to assemble the drop output port where the second microfiber is coupled to the first microfiber at location between A and B section as shown in Figure 4.1. The final structure has three ports: one input and two outputs (drop/through).

University of Malaya

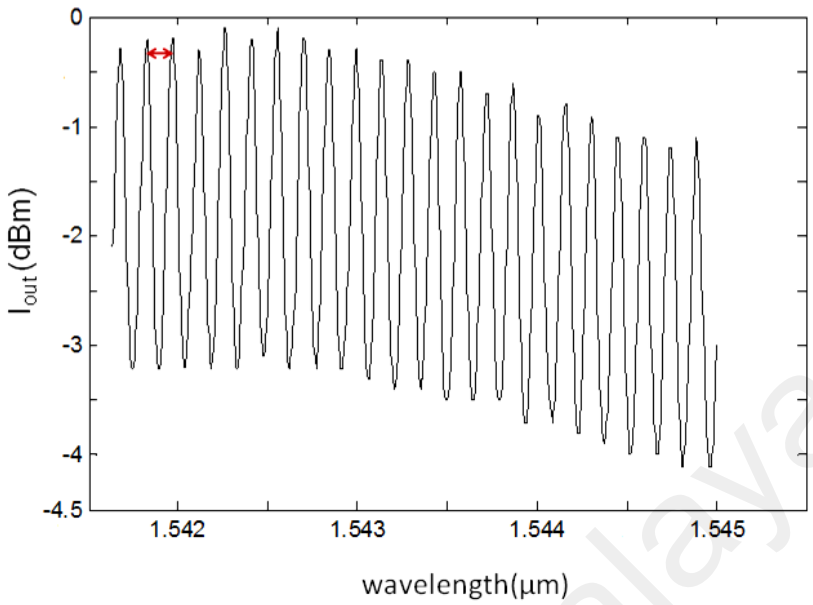

Figure 4.3: Experimental result of drop output of a single knot with $\boldsymbol{r_A = 1763\ \mu m}$ versus wavelength.

Figure 4.3 shows the spectrum of a knot with a radius of 1763 μm. Based on the spectrum analysis, the quality factor ($\lambda_0/\Delta\lambda$) of the knot is of the order of 12300 also a finesse of 1.2 and a FSR of 145 pm have been obtained.

To increase the FSR, a semi ring has been added to the structure as it is shown in Figure 4.2. A structure with the following parameters, $r_B = r_A = 1763\ \mu m$, $\Lambda = 3766\ \mu m$ has been fabricated. Figure 4.4 shows the response spectrum of the structure. From the spectrum one can observe that FSR increases to 440 pm. In the filter E_A/E_1 is called the filter response. In a single knot the Fourier extension of the filter response is in order of $1/k$ while at this structure the response filter is in order of $1/k^2$. This gives sharper roll-off and higher finesse (Madsen et al., 1999) than that of the single knot. The calculated finesse (around 5.17 as obtained from Figure 4.4) is three times bigger than that of a single knot structure.

University of Malaya

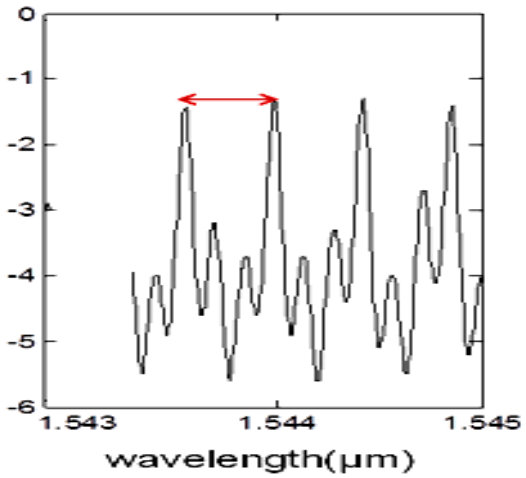

Figure 4.4: Experimental result of drop output of the structure with parameters $\mathbf{r_B} = \mathbf{r_A} =$ $\mathbf{1763\ \mu m}$, $= \mathbf{3766}\ \mu\mathbf{m}$.

The free spectral range of the spectrum can be modified by manipulation of some factors such as radius size and length of the straight microfiber. Figure 4.5 shows the output spectrum from the same structure but increasing the length Λ up to 4000 μm, as shown in Figure 4.5 two different FSR, 300 pm and 430 pm, have been obtained at the same time.

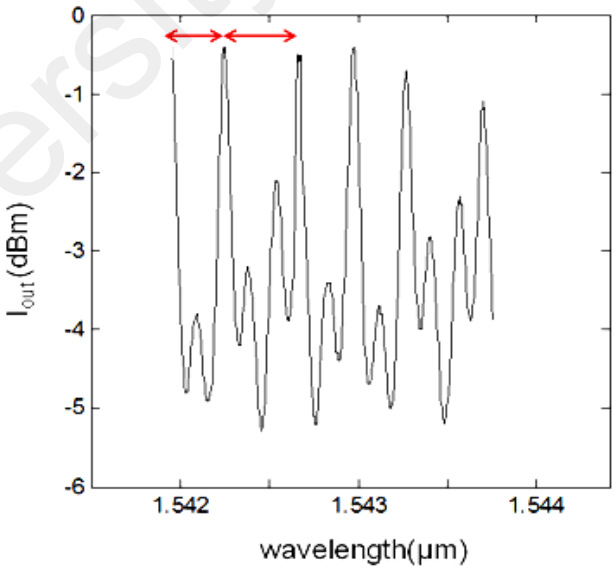

Figure 4.5: Experimental result of drop output of the structure with parameters $\mathbf{r_B} =$ $\mathbf{r_A}$ =1763 μm, =4000μm.

University of Malaya

4.3 Double Knot Hybrid Microfiber Structure

Sharp roll-off and low band ripple are required to reach proper isolation among different channels in order to avoid distortion in the recorded signal. To achieve this goal there are some parameters, which may be engineered such as number of knots, coupling coefficients and size of knot radius. In this section, a hybrid structure, which includes two knots, is demonstrated and shown in figure 4.6. In the figure, the two-microfiber knots are surrounded by a semi ring structure.

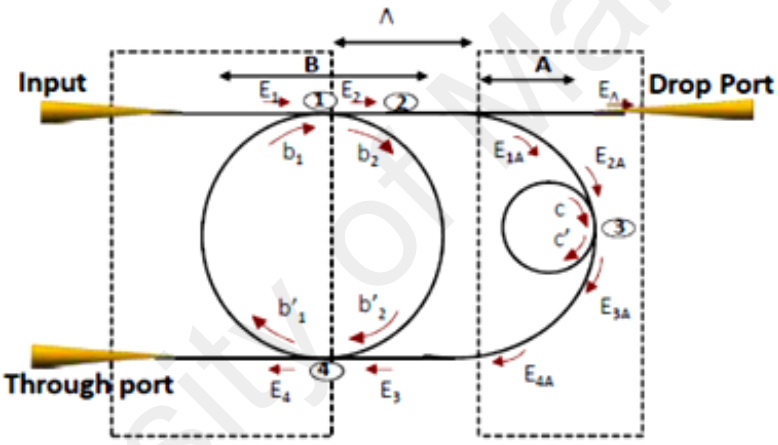

Figure 4.6: Schematic diagram of the proposed new structure with one microfiber knot surrounded by a semi ring structure.

4.3.1 Design of the Structure Using Vernier Effect

The section focuses on the fabrication of a hybrid microfiber resonator structure and on the demonstration of the finesse enhancement at a fixed ER value. In the case of a single resonator (knot) structure, the finesse and ER of the output is limited by the characteristics of one resonator. To compare the performance of a single resonator as a first order filter and a multi-resonator as a high order filter, the filter response (FR) is expressed as a ratio of the drop port power to the input power, $\frac{E_{drop}}{E_{input}}$ (Poon et al., et al., 2004).

University of Malaya

The output spectrum of a single knot has been mentioned in equation (3.37). The equation describes the response of the single knot, which is in the order of $\boldsymbol{\frac{1}{K}}$. The output port intensity behaves as $\frac{1}{(1+ike^{-\propto\frac{L}{2}}(1-iKL))^2}$, which follows Lorentzian response**.** The power of the denominator increases by increasing the number of resonators. That yields a sharper roll-off. The filter response of the structure can be deduced from transfer matrix method (Yariv et al., 1999).

The proposed structure consists of two knots having different radii. These knots are surrounded by a semi loop structure with three input/output (drop and through) ports. As shown in Figure 4.6, the small knot is located at the right part of the semi-loop structure while the big knot is located closer to the opening of the structure. The part of the structure, which contains the small knot, is referred to as section A, while section B refers to the bigger knot in the Figure. The curvature at section A is referred to as curvature A and the knot at the same section is referred to as knot C. The big knot at section B is referred to as knot B. The length S is the length between the two-microfiber knots as shown in the Figure. As illustrated in Figure 4.6, the field components $\mathrm{E_1}$, $\mathrm{E_4}$, $\mathrm{E_A}$ are defined as input, left output and right output respectively. The components labeled as $b_1, b_2, b_1', b_2', E_{1A}, E_{2A}, \mathrm{c}, \mathrm{c}'$ represent the fields inside the rings while E_3, E_2 are the field components inside the curvature. Based on the transfer matrix, the relation between the field elements are expressed as follows:

$$\begin{bmatrix} E_4 \\ E_3 \end{bmatrix} = M_1 \begin{bmatrix} b_1' \\ b_2' \end{bmatrix}, \begin{bmatrix} b_1' \\ b_2' \end{bmatrix} = M_2 \begin{bmatrix} b_1 \\ b_2 \end{bmatrix}, \begin{bmatrix} b_1 \\ b_2 \end{bmatrix} = M_3 \begin{bmatrix} E_1 \\ E_2 \end{bmatrix} \tag{4.7}$$

University of Malaya

$$M_1 = \begin{bmatrix} \frac{-ik_4}{r_4} & -\frac{i}{r_4} \\ \frac{i}{r_4} & -\frac{ik_4}{r_4} \end{bmatrix} \quad (4.8)$$

$$M_2 = \begin{bmatrix} e^{\propto L_B/4} e^{i(\frac{2\pi n}{\lambda})\frac{L_B}{2}} & 0 \\ 0 & e^{-\propto L_B/4} e^{-i(\frac{2\pi n}{\lambda})\frac{L_B}{2}} \end{bmatrix} \quad (4.9)$$

$$M_3 = \begin{bmatrix} \frac{-ir_1}{k_1} & \frac{i}{k_1} \\ \frac{-i}{k_1} & \frac{ir_1}{k_1} \end{bmatrix} \quad (4.10)$$

$$\begin{bmatrix} E_4 \\ E_3 \end{bmatrix} = M_1 M_2 M_3 \begin{bmatrix} E_1 \\ E_2 \end{bmatrix} \quad (4.11)$$

$$E_3 = \frac{-ik_3 + e^{-i(\frac{2\pi n}{\lambda})L_C} e^{-\propto L_C/2}}{1 + ik_3 e^{-i(\frac{2\pi n}{\lambda})L_C} e^{-\propto L_C/2}} e^{-i(\frac{2\pi n}{\lambda})L_A} e^{-\propto L_A/4} e^{-i2(\frac{2\pi n}{\lambda})\Lambda} e^{-\propto \Lambda} r_2 E_2 \quad (4.12)$$

$$E_A = -ik_2 E_2 \, , k = \gamma k' \, , r = \gamma r' , k^2 + r^2 = \gamma^2 \quad (4.13)$$

where $k_{1,2,3,4}$ and $r_{1,2,3,4}$ are the coupling and transmission coefficients belonging to the coupling regions 1, 2, 3 and 4 respectively as shown in Figure 4.6. The constant γ is the coupling loss (Delâge et al., 2009; M Sumetsky et al., 2006). $e^{-\propto L_{A,B,C,\Lambda}}$ represents the round trip loss through curvature A and knots B and C where α is the attenuation coefficient. λ is the wavelength of light and n is the effective index related to the microfiber. $L_{A,B,C} = 2\pi R_{A,B,C}$ is the round trip length of curvature A, knot B and knot C

University of Malaya

respectively, where $R_{A,B,C}$ is knot/curvature radius. Λ represents the length from knot B to the semi ring C. In the structure, resonance occurs due to the constructive interference between the different field components at the coupling regions. These regions are denoted by numbers 1, 2, 3 and 4 in Figure 4.6.

For the proposed scheme, the two loops radii are pre-designed to keep an integer ratio between the FSR ($FSR_{B,C} = \frac{\lambda^2}{nL_{B,C}}$) of the individual knots. This can be achieved by ensuring an integer ratio between the larger and small loops circumferences. Under this condition, the resultant FSR is (Boeck et al., 2010):

$$FSR_{Output} = m_{\mathrm{B}}.FSR_B = m_{\mathrm{C}}.FSR_C \tag{4.14}$$

$$\frac{FSR_B}{FSR_C} = \frac{m_C}{m_B} = \frac{L_C}{L_B} \tag{4.15}$$

where m_B and m_C are integers. The constants L_B and L_C are the circumferences of the loops B and C respectively. In our design, the values of m_B and m_C are set to 3 and 1 respectively. In other words $L_B = 3L_C$. The distance between the two knots, S, can be arbitrary chosen. For simplicity the lenght S is chosen to be equal to the small knot's circumference.

4.3.2 Fabrication from Individual Knots Hybrid Structure

To realize such structure, a standard single mode fiber (SMF) is tapered adiabatically down to a diameter of 10 μm by using flame brushing method. To form a single knot individually with different radii, it is required to cut the tapered microfiber into two parts: one part for bending and intertwisting and the other one is to couple to the free end of the first part. This process has been done by two small pieces of cleaved fiber or tweezers. It is hard to control the diameter of the microfiber knot as the microfiber tends to stick to itself and causes the

University of Malaya

structure to break. To avoid this problem, two nonstick bars are used in the process. Each tapered fiber part is individually twisted around the bars then they are separated to form a knot. The two bars are then pressed close to each other to detach the sticky microfiber and they are then pulled up as shown in Figure 4.7(a). Using this technique, two knots are made to almost the desired radii. These knots are then cascaded together by attaching and coupling the two microfibers ends of each knot via van der Waals and electrostatic forces. To fabricate semi-loop structure with two ports of (input/through output), a microfiber end (carrying two knots) is coupled back to the big knot as illustrated in Figure 4.7(b). The drop port is finally formed by attaching another tapered fiber with a 10 μm diameter to the loop curvature via van der Waal and electrostatic forces as shown in the last step in Figure 4.7(b).

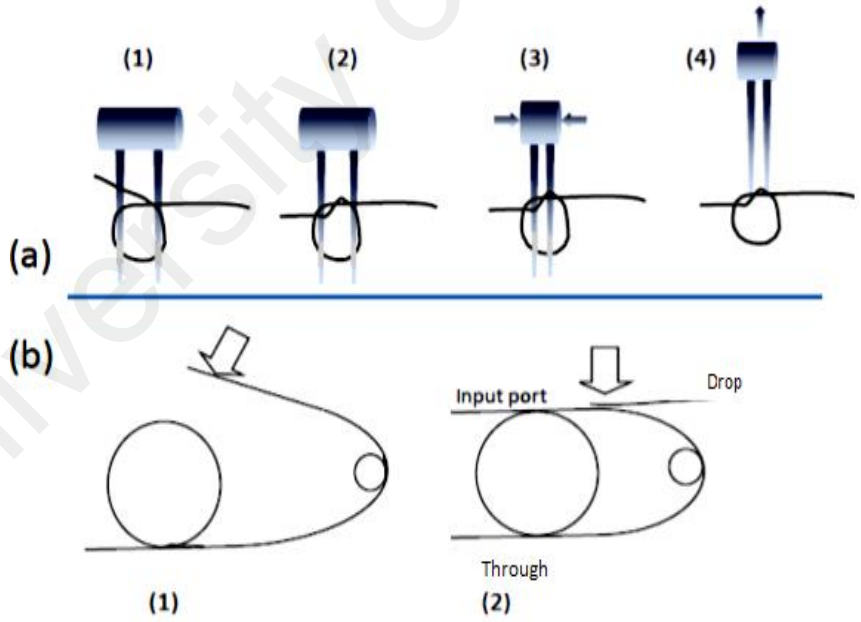

Figure 4.7: (a) Knot formation using Knitting technique (b) double knot formation for (1) first step and (2) adding drop channel.

University of Malaya

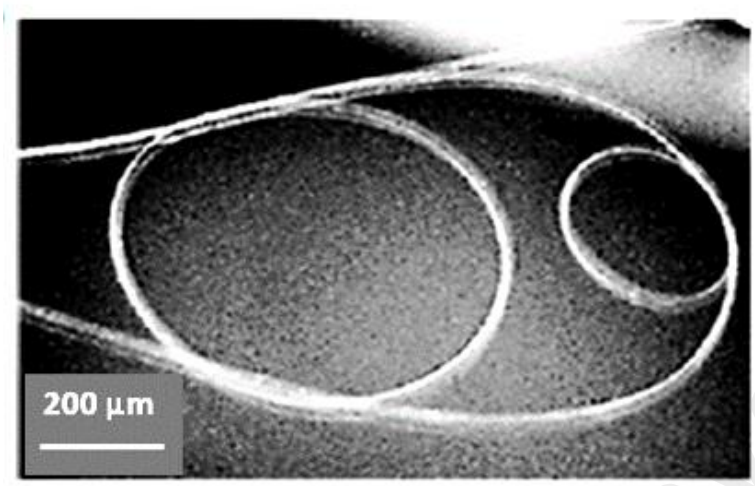

Figure 4.8: Microscopic picture from a fabricated structure including two knots.

It is worth mentioning that the fabrication process was performed in free air at room temperature. Typically a packaging process is needed to enhance the robustness of the system where the microfibers are placed on MgF_2 glass or embedded in low refractive index polymer and materials (S. S. Wang et al., 2009; F. Xu et al., 2008). Here, the system was not packaged though the environment was controlled during the measurement through vibration control and by keeping a constant temperature. To control the whole structure which has a length of a few millimeter, three stage has been used to keep the three port tight and firm. These stages decrease any distraction during the manipulation of the structure.

4.3.3 Characterization and Modification of the Output Spectrum

The output spectra of two individual knots with radii R1 and R2 (ratio of 3) fabricated using the above technique are shown in Figure 4.9. The Figure shows clearly that the peaks of the smaller knot almost overlap every third peak of the bigger knot. This is due to the

University of Malaya

slight difference between the fabrication and the desired radii. To achieve the required precision, a simple approach was used where one loop is fixed. In the other loop, the two sides of the twisted microfiber's ends are pulled with 10 µm resolution translation stages, while observing the output spectrum. Another important observation here is that the small knot with a radius of 549 µm provides higher ER (6 dB) compared to the big loop with a radius of 1643 µm (3 dB). The small knot provides FSR of 465 pm and finesse of 2.73. The big knot has FSR of 150 pm and a finesse of 2.1 (Y.P. Xu et al., 2015). To measure the output spectrum, an erbium doped fiber amplifier (EDFA) was used as a light source. The spectra were recorded using optical spectrum analyzer (OSA).

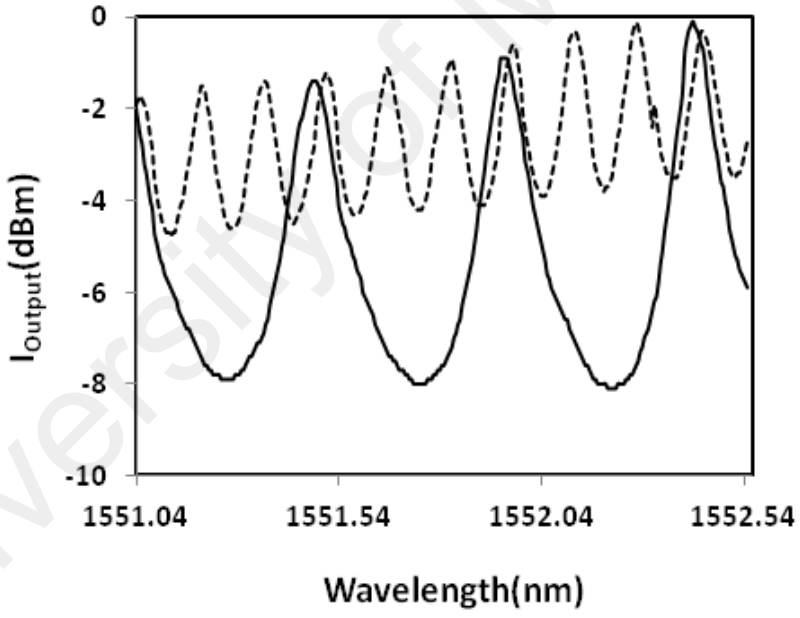

Figure 4.9: Spectra from the incident ASE, and the drop port output spectrum of the knot C with radius of 549 µm (bold line), the knot B with radius of 1643 µm (dashed line).

The output spectrum in Figure 4.10 indicates that the resultant filter has a FSR of 465 pm and a quality factor of approximately 25000. The spectrum shows a suppression of two

University of Malaya

peaks between each two maxima (due to the ratio of the radii). This suppression resulted in a band ripple of 2 dB.

Combining the two knots as proposed with a separation, S, of 3400 µm resulted in an output spectrum with a higher fineness of 8. This is shown by the sharper roll-off in the inset in Figure 4.11 (dashed line) compared to the small knot (cube-point). The ER in this case was kept at a value of 6 dB.

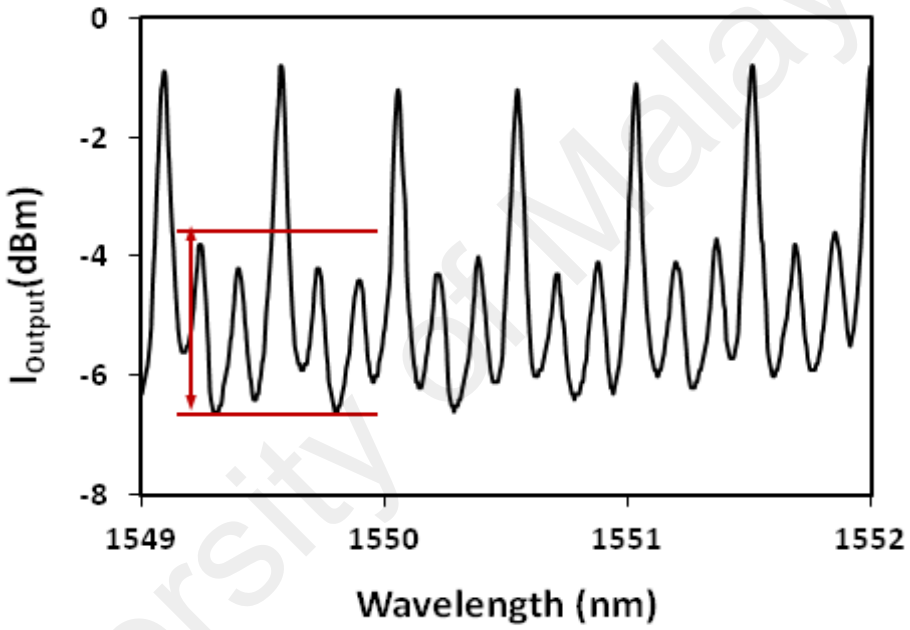

Figure 4.10: Spectra from the incident ASE, and the drop port output spectrum of the hybrid structure including the knot C with radius of 549 µm and the knot B with radius of 1643 µm.

University of Malaya

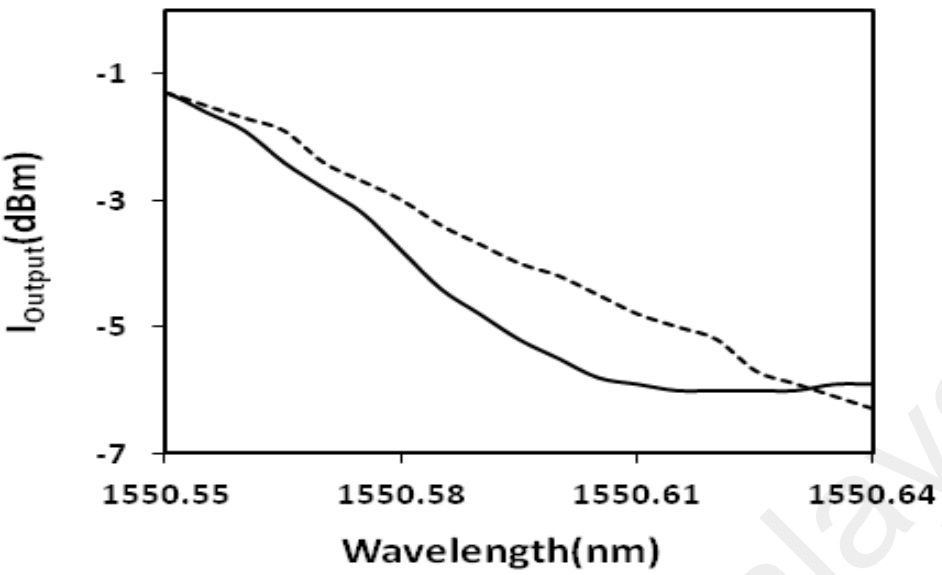

Figure 4.11: Drop port output spectrum from single knot (dashed line) and the hybrid structure (bold line).

To investigate the FSR of the output spectrum, another hybrid microfiber resonance structure is fabricated with different dimensions compared to the previous structure. In this new design, the knots have radii of 339 μm and 1013 μm and length of S (as much as the small knot circumference). The output spectrum of its drop port shows almost the same behavior to the comb filter in structure 1 with a following characteristics of FSR = 765 pm, quality factor ≅ 12000 and finesse = 6.37 as shown in Figure 4.12. Comparing Figure 4.10 and Figure 4.12, one can observe that manipulating the dimension of the structure results in different FSR bandwidths. Based on the results, the second structure, that has smaller dimensions compared to structure 1, generates wider FSR bandwidth.

University of Malaya

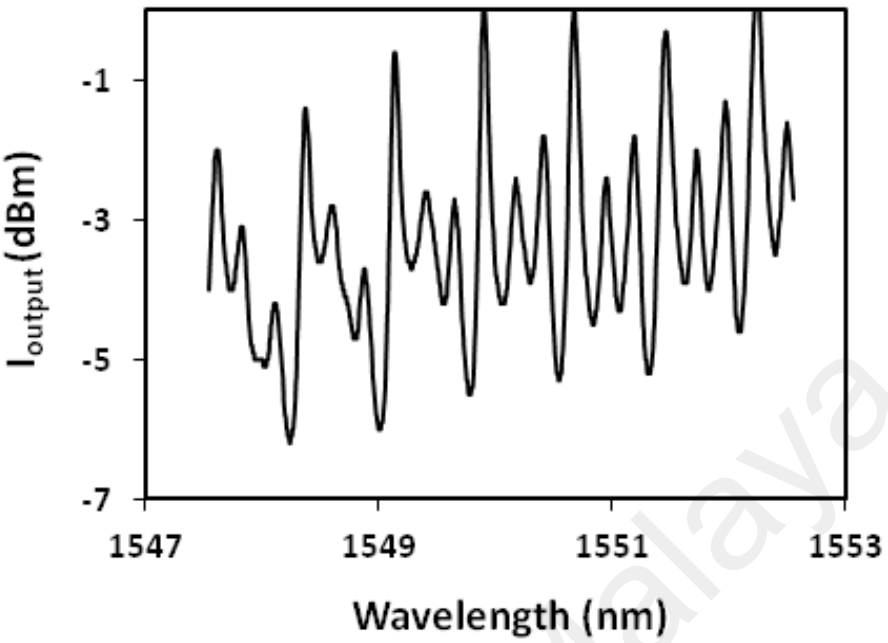

Figure 4.12: Drop port output spectrum of the hybrid structure 2.

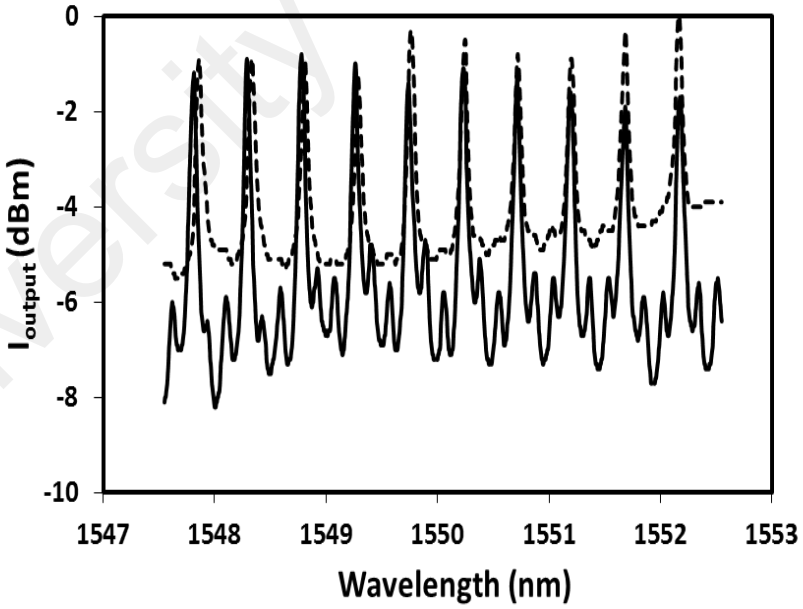

Figure 4.13: Drop port output spectra of the structure 3, before (bold line) and after (dashed line) manipulating the coupling regions of the knots.

University of Malaya

It is worth mentioning that it is also possible to modify and eliminate the ripples of the output comp filter by manipulating the coupling regions of the hybrid structure in order to improve the filtering. An additional investigation on modifying the ripples is also demonstrated in this experiment. Wherein, another hybrid microfiber resonance structure has been fabricated that included two knots having different radii of 555 μm and 1662 μm and the length S is as long as the circumference of the small knot, referred as (structure 3). Figure 4.13 demonstrates the waveforms of the output comb filter before and after manipulation for the same structure. The spectrum before manipulation shows the following characteristics of FSR = 460 pm, quality factor ≅ 30000 and finesse = 9.7. As it can be clearly seen from the comb filter of the spectrum before manipulation, it has lower band ripples with ER of about 1.5 dB. Altering the coupling regions of the big knot that has a radius of 1662 μm by decreasing the coupling lengths, the lower band ripples vanished while the quality factor and the finesse are reduced to 22000 and 6.8 respectively. Such result indicates that manipulating the coupling regions of the knot can eliminate the band ripples. That leads to improving the quality of the filter. The fabricated hybrid microfiber resonance structure based filters maintain the relative advantages of design simplicity and lower cost. This shows a large potential for application in photonic integrated circuits such as band-pass and stop-band filters. The coupling coefficients also have effects on the resonance. One of them is the fluctuation of resonant wavelength per period. Assuming $\boldsymbol{k_1 = k_3 = k_4}$, the effects of changing $\boldsymbol{k_1}$ $\boldsymbol{and}$ $\boldsymbol{k_2}$ on the output spectrum can be studies. Three cases are considered: $\boldsymbol{k_1 < k_2}$, $\boldsymbol{k_1 > k_2}$ and $\boldsymbol{k_1 = k_2}$ .Here, the effect of the coupling coefficients on the output spectrum is calculated through a figure of merit referred to as at the fluctuation ratio. This parameter is defined as the difference between two successive relative maxima and relative minima of functions $\boldsymbol{E_4 E_4^*}$ (left port) or $\boldsymbol{E_4 E_4^*}$

University of Malaya

(right port) on a period. Figure 4.14 (b) shows the fluctuation ratio versus the coupling coefficients when $\boldsymbol{k_1 = k_2}$. Under this situation, increment in the coupling coefficients increases the light feedback through the structure. This enhances the light interference in the structure. That leads to a sharp resonant at the output. For other conditions of $\boldsymbol{k_1 < k_2}$ or $\boldsymbol{k_1 > k_2}$, as shown in Figure 4.14 (b), increasing the difference of the coefficients (increasing or decreasing one of the coefficients), results in a smaller feedback. This reduces the fluctuation thereby improves the flatness of the output spectrum as shown in the results. This indicates that different spectra can be tailored by the structure to obtain the desired filtering characteristics for various applications in amplifiers such as laser and sensors

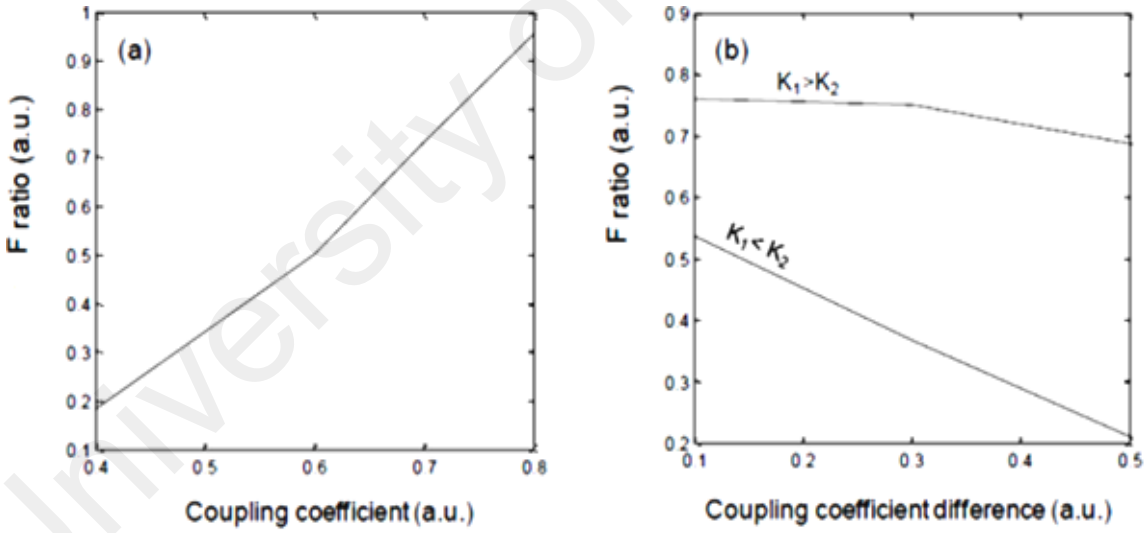

Figure 4.14: Flatness ratio versus (a) coupling coefficient ($\boldsymbol{k_1 = k_2}$) and (b) coupling coefficient difference under condition ($\boldsymbol{k_1 < k_2}$, $\boldsymbol{k_1 > k_2}$) when ($\mathbf{n = 4, 0.9, r_C = 200\ \mu m}$, $\boldsymbol{r_B = r_A = 800\ \mu m}$).

A smooth spectrum is required in amplifier so that the desired bandwidth filter can be equally amplified (Figure 4.15 (a)). A sharp and short resonant bandwidth is required in

University of Malaya

laser applications to create narrow line width laser (Figure 4.15 (b) and (c)), to omit a wavelength or have a band stop spectrum (Figure 4.15 (b)). Optimization for any application, which has been mentioned above, is possible by manipulation of the coupling coefficients. Here in Figures 4.15 (a), (b) and (c), three different through port output spectra from the same structure are depicted under three conditions: $k_1 = 0.4, k_2 = 0.9$, $k_1 = 0.8, k_2 = 0.5$ and $k_1 = k_2 = 0.7$ respectively. The structure has the following parameters: $n = 4, r_c = 200$ µm, $r_B = r_A = 800$ µm and $L = 1500$ µm.

As shown in Figure 4.15 (a), in-band ripple minimization is obtained when the coupling coefficient at the input section is smaller than that of at the output section. While condition at Figure 4.15 (b), $k_1 > k_2$, is useful for laser application.

University of Malaya

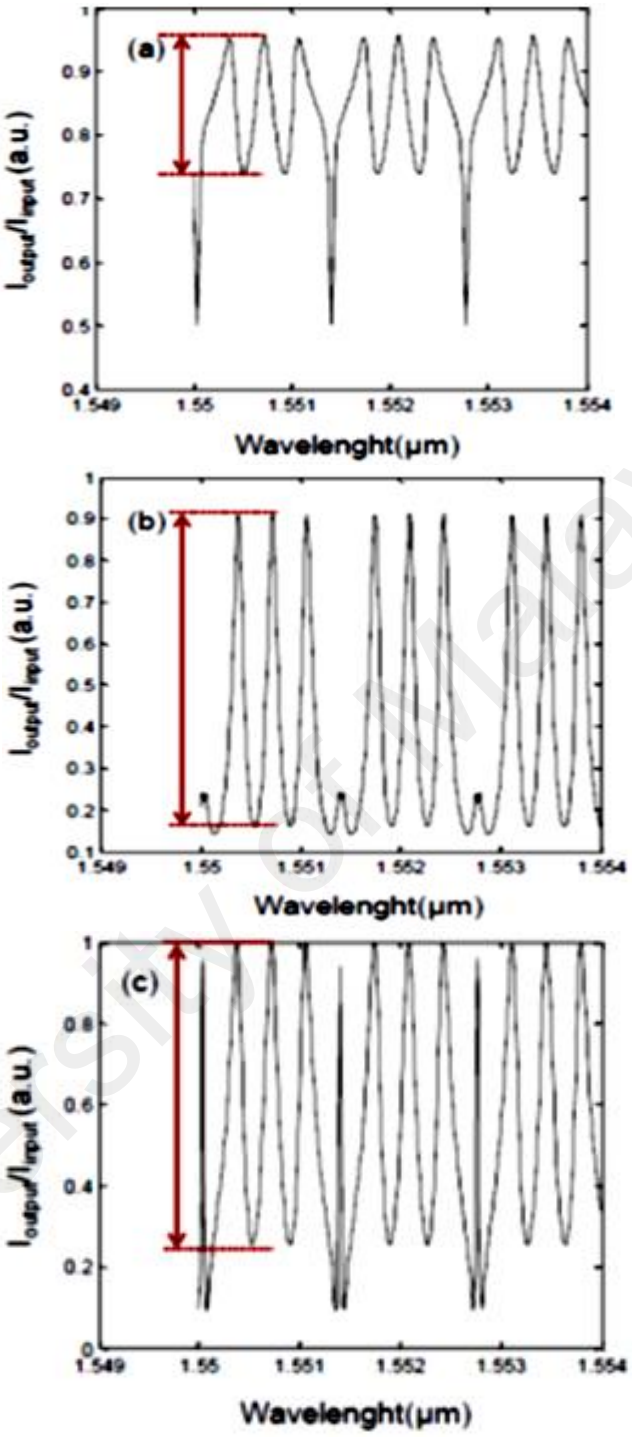

Figure 4.15: Left output/input versus wavelength when ($\mathbf{n = 4, 0.9, r_C = 200\ \mu m}$, $\boldsymbol{r_B = r_A = 800\ \mu m}$), (a) under condition ($\boldsymbol{k_1 = 0.4, k_2 = 0.9}$) ;(b) ($\boldsymbol{k_1 = 0.8, k_2 = 0.5}$) and (c) ($\boldsymbol{k_1 = k_2 = 0.7}$).

University of Malaya

4.4 Future Design and Fabrication

Based on the analysis in the previous sections, it was demonstrated that coupling coefficient plays a major role in shaping the output spectrum. To increase the degrees of freedom in designing specific filters, one can add an extra coupling region between the two knots in Figure 4.6. A proposed structure is shown in Figure 4.16.

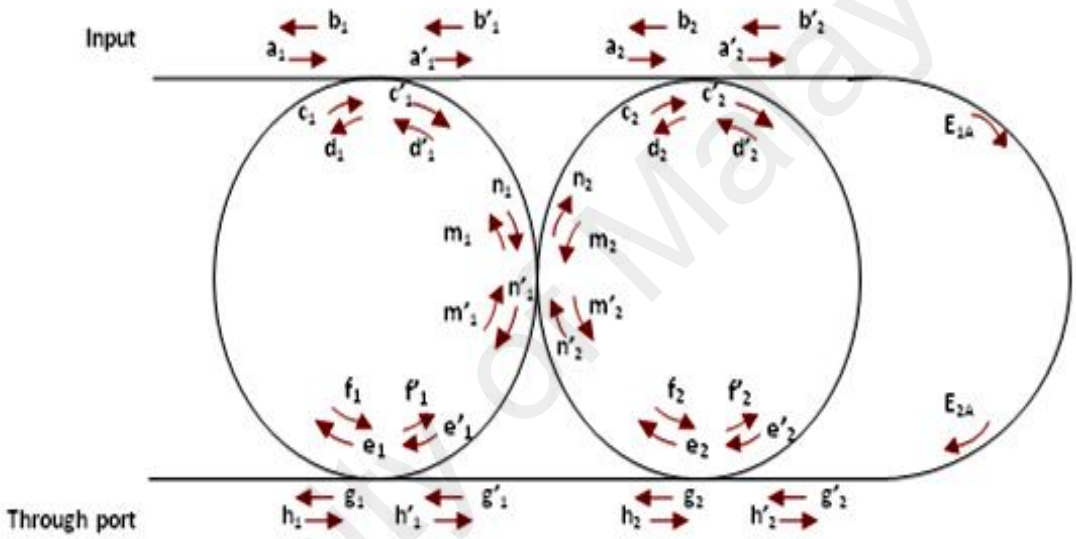

Figure 4.16: Schematic of the proposed structure using double coupled knots.

The labels $a_{1,2}, b_{1,2}, c_{1,2}, d_{1,2}, e_{1,2}, f_{1,2}, g_{1,2}, h_{1,2}, a'_{1,2}, b'_{1,2}, c'_{1,2}, d'_{1,2}, e'_{1,2}, f'_{1,2}, g'_{1,2}, h'_{1,2}$ are the field elements. They are related to each other the following matrix equations:

$$\begin{bmatrix} a_1 \\ b_1 \\ c_1 \\ d_1 \\ e_1 \\ f_1 \\ g_1 \\ h_1 \end{bmatrix} = T_1 \begin{bmatrix} a'_1 \\ b'_1 \\ c'_1 \\ d'_1 \\ e'_1 \\ f'_1 \\ g'_1 \\ h'_1 \end{bmatrix}, \begin{bmatrix} a'_1 \\ b'_1 \\ c'_1 \\ d'_1 \\ e'_1 \\ f'_1 \\ g'_1 \\ h'_1 \end{bmatrix} = T_2 \begin{bmatrix} a_2 \\ b_2 \\ c_2 \\ d_2 \\ e_2 \\ f_2 \\ g_2 \\ h_2 \end{bmatrix} \tag{4.16}$$

University of Malaya

$$T_1 = \begin{bmatrix} r & 0 & -ik & 0 & 0 & 0 & 0 & 0 \\ 0 & r & 0 & ik & 0 & 0 & 0 & 0 \\ -ik & 0 & r & 0 & 0 & 0 & 0 & 0 \\ 0 & ik & 0 & r & 0 & 0 & 0 & 0 \\ 0 & 0 & 0 & 0 & r & 0 & ik & 0 \\ 0 & 0 & 0 & 0 & 0 & r & 0 & -ik \\ 0 & 0 & 0 & 0 & ik & 0 & r & 0 \\ 0 & 0 & 0 & 0 & 0 & -ik & 0 & r \end{bmatrix} \tag{4.17}$$

$$T_2 = \begin{bmatrix} M_{11} & 0 & 0 & 0 & 0 & 0 & 0 & 0 \\ 0 & M_{22} & 0 & 0 & 0 & 0 & 0 & 0 \\ 0 & 0 & 0 & M_{34} & 0 & M_{36} & 0 & 0 \\ 0 & 0 & M_{43} & 0 & M_{45} & 0 & 0 & 0 \\ 0 & 0 & 0 & M_{54} & 0 & M_{56} & 0 & 0 \\ 0 & 0 & M_{63} & 0 & M_{65} & 0 & 0 & 0 \\ 0 & 0 & 0 & 0 & 0 & 0 & M_{77} & 0 \\ 0 & 0 & 0 & 0 & 0 & 0 & 0 & M_{88} \end{bmatrix} \tag{4.18}$$

$$M_{11} = e^{\frac{\alpha(R_1+R_2)}{2}+i\varphi_R}\,,\ M_{22} = e^{-\frac{\alpha(R_1+R_2)}{2}-i\varphi_R} \tag{4.19a}$$

$$M_{34} = \frac{ir}{k}e^{\frac{-\alpha L_1}{8}-\frac{i\varphi_1}{4}}e^{\frac{-\alpha L_2}{8}-\frac{i\varphi_2}{4}}\,,\ M_{36} = \frac{-i}{k}e^{\frac{-\alpha L_1}{8}-\frac{i\varphi_1}{4}}e^{\frac{\alpha L_2}{8}+\frac{i\varphi_2}{4}} \tag{4.19b}$$

$$M_{43} = \frac{-ir}{k}e^{\frac{\alpha L_1}{8}+\frac{i\varphi_1}{4}}e^{\frac{\alpha L_2}{8}+\frac{i\varphi_2}{4}}\,,\ M_{45} = \frac{i}{k}e^{\frac{+\alpha L_1}{8}+\frac{i\varphi_1}{4}}e^{\frac{-\alpha L_2}{8}-\frac{i\varphi_2}{4}} \tag{4.19c}$$

$$M_{54} = \frac{i}{k}e^{\frac{-\alpha L_1}{8}-\frac{i\varphi_1}{4}}e^{\frac{-\alpha L_2}{8}-\frac{i\varphi_2}{4}}\,,\ M_{56} = \frac{ir}{k}e^{\frac{-\alpha L_1}{8}-\frac{i\varphi_1}{4}}e^{\frac{\alpha L_2}{8}+\frac{i\varphi_2}{4}} \tag{4.19d}$$

$$M_{63} = \frac{-i}{k}e^{\frac{\alpha L_1}{8}+\frac{i\varphi_1}{4}}e^{\frac{\alpha L_2}{8}+\frac{i\varphi_2}{4}}\,,\ M_{65} = \frac{ir}{k}e^{\frac{\alpha L_1}{8}+\frac{i\varphi_1}{4}}e^{\frac{-\alpha L_2}{8}-\frac{i\varphi_2}{4}} \tag{4.19e}$$

$$M_{77} = e^{-\frac{\alpha(R_1+R_2)}{2}-i\varphi_R}\,,\ M_{88} = e^{\frac{\alpha(R_1+R_2)}{2}+i\varphi_R} \tag{4.19f}$$

$$b_2' = e^{\frac{-\alpha S}{2}-i\varphi_S}h_2'\,,\ d_2' = e^{\frac{-\alpha S}{2}-i\varphi_S}f_2' \tag{4.20a}$$

$$e_2' = e^{\frac{-\alpha S}{2}-i\varphi_S}c_2',\ g_2' = e^{\frac{-\alpha S}{2}-i\varphi_S}a_2' \tag{4.20b}$$

where α is the attenuation coefficient, $\varphi_{1,2} = \left(\frac{2\pi n}{\lambda}\right)\mathrm{L}_{1,2}, \varphi_R = \left(\frac{2\pi n}{\lambda}\right)\frac{(R_1+R_2)}{2}$ and $\varphi_S = \left(\frac{2\pi n}{\lambda}\right)$, S are the round trip phase, λ is the wavelength of light. n is the effective index of the

University of Malaya

microfiber, L ($L = 2\pi R$) is the round trip length of the knots, R is the radius of the knots and S is the length of the curved section.

In Figure 4.16, g_1 and b_1 are called through and reflection outputs. During this study both knot radii and coupling coefficients are considered as main factors that affect the characteristics of output spectrum.

Figure 4.17 (a) and (b) shows reflection from two structures composed of two knots with different radii. Figure 4.17 (a) shows the reflection from the knots with radii of $\boldsymbol{R_1 = 600\ \mu m, R_2 = 300\ \mu m}$ and $\boldsymbol{S = 1885\ \mu m}$. As it is demonstrated in the figure, the spectrum has a pass band of 650 pm, a stop band of 1300 pm and a suppression ratio of 0.6. Figure 4.17 (b) demonstrates the reflection where the knots have radii of $\boldsymbol{R_1 = 700\ \mu m, R_2 = 350\ \mu m}$ and $\boldsymbol{S = 2199\ \mu m}$. The structure produces a spectrum with a pass band of 400 pm, a stop band of 1100 pm and suppression ratio 0.64. In both structures, the coupling coefficients are considered to be 0.55. It is deduced from the figures that smaller knots provide wider bandwidth in both stop and pass bands.

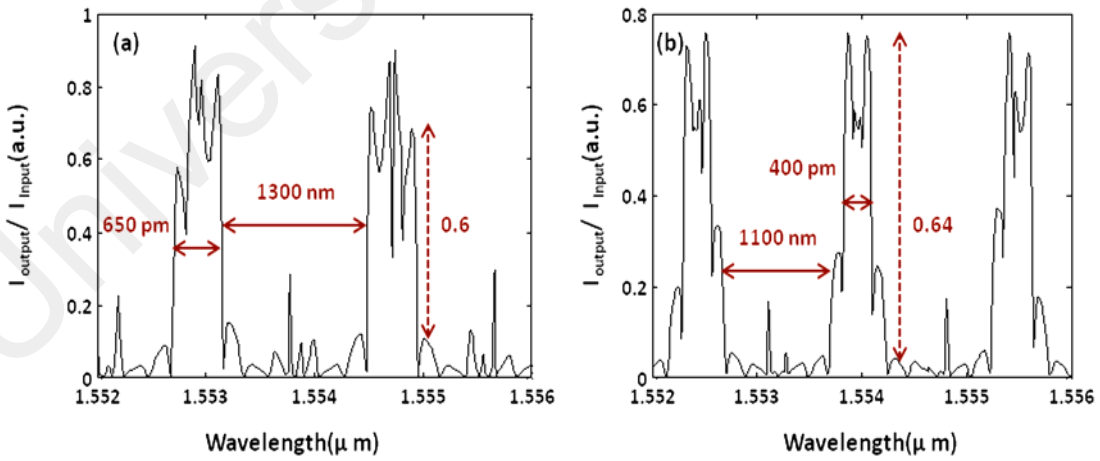

Figure 4.17: Simulation of reflection from a structure (a) the knots with radii of $\boldsymbol{R_1 = 600\ \mu m, R_2 = 300\ \mu m, S = 1885\ \mu m}$, (b) the knots with radii of $\boldsymbol{R_1 = 700\ \mu m, R_2 = 350\ \mu m, S = 2199\ \mu m}$.

University of Malaya

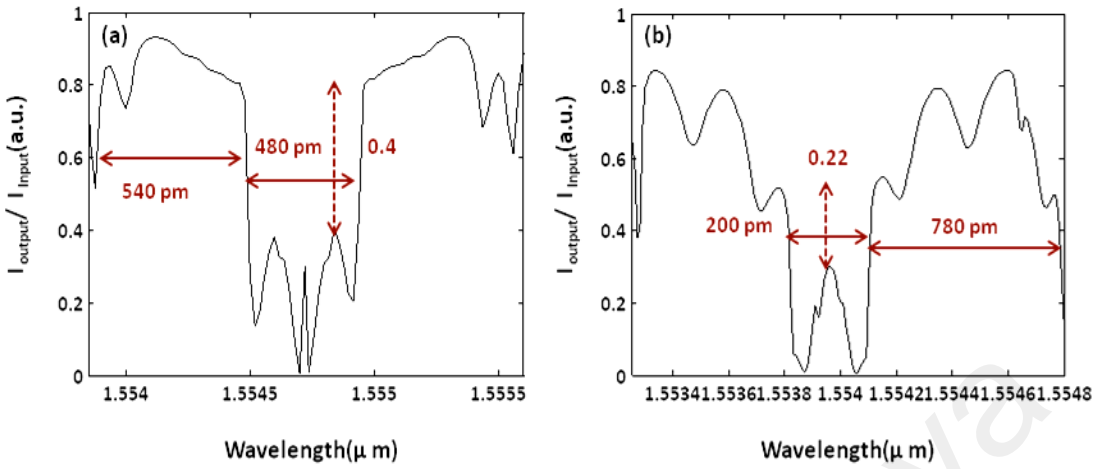

Figure 4.18: Simulation of through port from a structure (a) the knots with radii of $R_1 = 600\ \boldsymbol{\mu}\mathrm{m}, R_2 = 300\ \boldsymbol{\mu}\mathrm{m}, \mathrm{S} = 1885\ \boldsymbol{\mu}\mathrm{m}$, (b) the knots with radii of $R_1 = 700\ \mu\mathrm{m}, R_2 = 350\ \boldsymbol{\mu}\mathrm{m}, \mathrm{S} = 2199\ \boldsymbol{\mu}\mathrm{m}$.

The through spectra of both structures are depicted in Figure 4.18. The through spectrum from the first structure has a pass band of 540 pm, a stop band of 480 pm and a suppression ratio of 0.4. The second structure illustrates a spectrum with a pass band of 200 pm, a stop band of 780 pm and a suppression ratio of 0.22. Coupling coefficient is another important factor for the spectrum characteristics. Here, numerical calculations are performed to show the effect of the coupling on the output. Figures 4.19 (a) and (b) show the reflection from one structure with the following parameters: two knots with radii of $\boldsymbol{R_1 = 800\ \mu\mathrm{m}, R_2 = 400\ \mu\mathrm{m}}$ and $\boldsymbol{\mathrm{S} = 2513\ \mu\mathrm{m}}$. Figure 4.19 (a) shows that the spectrum has a pass band of 300 pm, stop band of 800 pm and a suppression ratio 0.42 when $\boldsymbol{k = 0.55}$. Figure 4.19 (b) demonstrates the reflection from the same structure considering $\boldsymbol{k = 0.8}$. The spectrum shows a pass band of 300 pm, a stop band of 550 pm and a suppression ratio of 0.58.

The through spectra of the structure for both coupling coefficients are demonstrated in Figure 4.20. The through spectrum from the structure at $\boldsymbol{k = 0.55}$ produces a pass band of

University of Malaya

500 pm, a stop band of 380 pm and a suppression ratio of 0.38. The produced spectrum shows a pass band of 200 pm, a stop band of 320 pm and a suppression ratio 0.4 when $\boldsymbol{k} = \mathbf{0.8}$.

By optimizing theses parameters, it is possible to design a defined or desired output for specific applications.

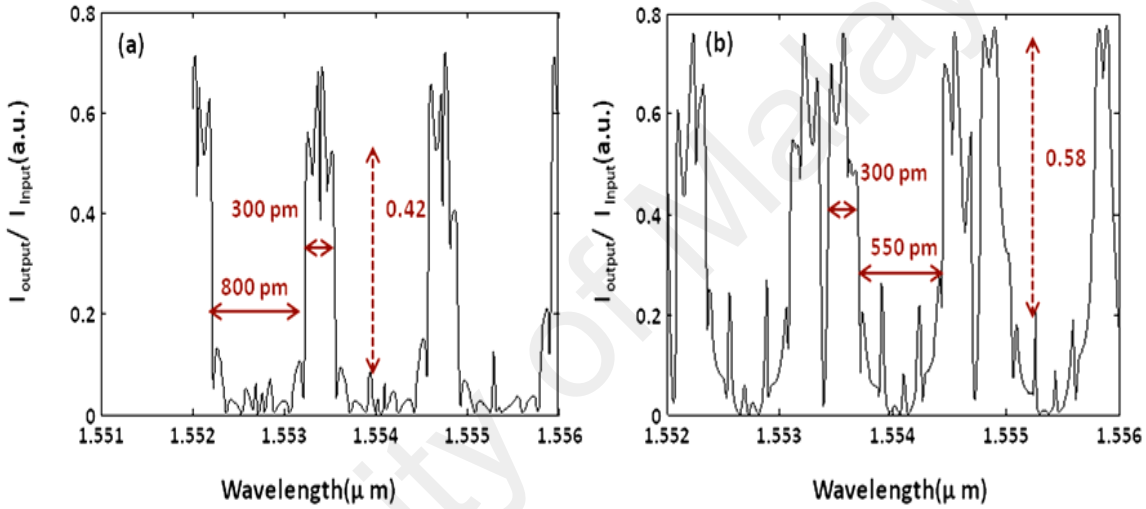

Figure 4.19: Simulation of reflection from a structure with the knots with radii of $R_1 = 6800\ \boldsymbol{\mu}\mathrm{m}, R_2 = 400\ \boldsymbol{\mu}\mathrm{m}, \mathrm{S} = 2513\ \boldsymbol{\mu}\mathrm{m}$, (a) with coupling coefficient of $k = 0.55$ (b) with coupling coefficient of $k = 0.55$.

University of Malaya

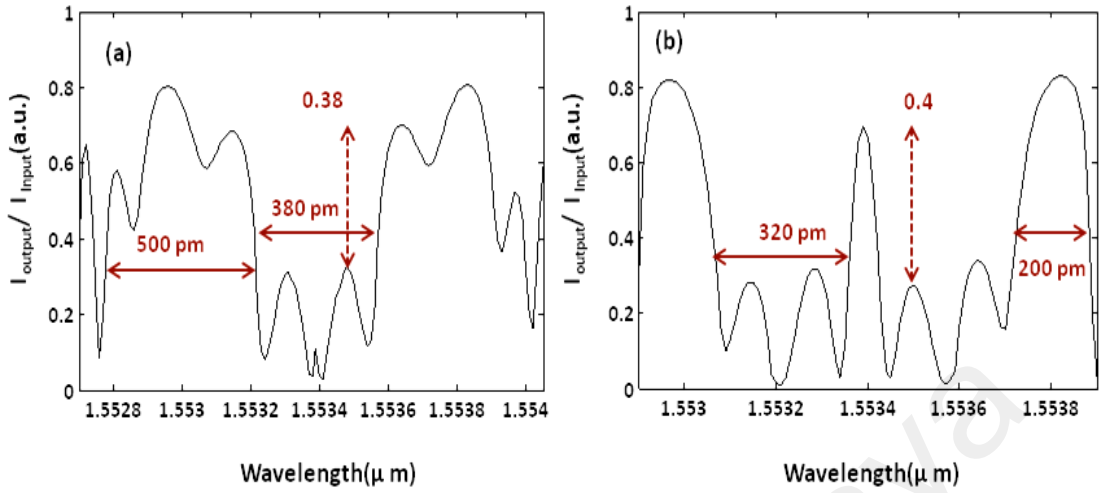

Figure 4.20: Simulation of through port from a structure with the knots with radii of $R_1 = 6800\ \boldsymbol{\mu}\mathrm{m}, R_2 = 400\ \boldsymbol{\mu}\mathrm{m}, \mathrm{S} = 2513\ \boldsymbol{\mu}\mathrm{m}$, (a) with coupling coefficient of $k = 0.55$ (b) with coupling coefficient of $\boldsymbol{k = 0.55}$.

4.5 Summery

This work proposes a novel design of a hybrid microfiber resonator, which can be used as a band-pass and band-stop filter in various applications such as fiber lasers. The structure comprises of two microfiber knot resonators with different sizes, which are surrounded by a semi loop structure with one input and two output ports. The utilization of the Vernier effect in the proposed structure showed noticeable enhancement of the free spectral range (FSR). The finesse has increased by a factor of three compared to the single knot providing a sharper roll-off. The filter bandwidth is adjustable as a result of the manipulation of the coupling length and rings' radii. The performance of the device is explained theoretically using transfer matrix analysis.

University of Malaya

In this chapter, a novel design of a hybrid microfiber resonator based filter is demonstrated. The structure comprises of a microfiber knot resonator and a loop. Using this combination, it is possible to design and fabricate some components with proper phase shift that produces a periodic spectrum. These structures are simple to fabricate and can be used for photonic integrated circuits. They can also be employed as optical switch, photonic logic gate, laser and amplifier. Their output spectrum characteristics such as resonance wavelength, bandwidth and resonance fluctuation ratio can be adjusted by manipulating the ring curvatures, coupling coefficients and the number of rings.This work investigates Vernier effect by a simple design of microfiber resonators. The structure, which includes one knot and a semi ring with 1763 μm radius also straight microfiber with 3766 μm length, can be used as a high order filter. A comparison between the structure and one knot resonators is demonstrated, which shows an increase in Free Spectral Range from 145 pm (knot resonators) to 440 pm (structure).

By combinating a microfiber knot and a loop, it is possible to design and fabricate some components which can obtain higher field enhancement. This causes sharper roll-off, higher finesse, wider FSR and filter undesirable wavelengths at the same time. Microfiber resonators are simple to fabricate and handle for photonic integrated circuits. Also they can be employed as optical switch, photonic logic gate, laser and amplifier. Their output spectrum characteristics such as resonance wavelength, resonance bandwidth and in band ripple can be adjusted by manipulating the ring curvatures, coupling coefficients and the number of knots.

University of Malaya

CHAPTER 5

DESIGN OF OPTICAL DEVICES USING MICROFIBER KNOT

5.1 Introduction

In previous chapters it has been mentioned that fiber ring resonator has been introduced and progressed as a basic component in photonics systems recently (Y. Zhang et al., 2010). Considering microfiber characteristics such as supporting single-mode operation (J. Y. Lou et al., 2014), low cost alternative waveguide and easy to form (X. Wu & Tong, 2013); a wide range of microfiber resonators have been proposed and fabricated (Sumetsky et al., 2006). Using a very simple design, microfiber loop twisting a 1μm-microfiber to shape a 1mm diameter loop with quality factor of 630000 has been demonstrated (Sumetsky et al., 2006). Theoretically, QF value of up to 10^{10} is predicated (Sumetsky, 2004) and the value of 470000 has been realized by fabrication of microfiber coil (Hsieh et al., 2012). Among these structures, microfiber knot shows more capability in applications such as modulators and convertors (X. L. Zhang et al., 2012; Y. Zhang et al., 2009), tunable lasers (Sulaiman et al., 2012b) and sensors (Yu Wu et al., 2009) due to stable light coupling (Sun et al., 2012), its firm structure and easy manipulation compare with the others. Also this structure has been considered as all pass filter and as an add-drop filter (including an extra microfiber beside the knot) with QF of 13000 (X. D. Jiang et al., 2007). At an output spectrum of a filter, the flatness and the width of both transmission and rejection regions on the spectrum are important characteristics in filtering especially for wavelength division multiplexing applications and notch filters (Grover et al., 2004; Liu et al., 2011). Sharp roll off, adjustable pass band and less in-band ripple spectrum provide a desired filter (Liu et al., 2011; Jan Niehusmann et al., 2004). The dimensions and coupling length of the ring are

University of Malaya

important but are not enough factors to achieve the desired filter characteristics. Multi-ring resonators have been proposed as a solution to obtain pass-band spectrum (Poon et al., 2004).

Also in section 5.2, an optical XOR is investigated. The optical nonlinearity is used in a microfiber knot to generate an all optical gate. Using the field enhancement inside the optical resonator obtains high power to stimulate the nonlinearity. This enhancement causes a significant decrease in the switching power threshold. This research compares the simulation results between passive and active microfiber knot. The calculations use coupled wave equations to predict the effect of the nonlinear refractive coefficient on threshold power.

5.2 Demonstration of a Periodic Pass-band Filter Based on Coupled Microfiber Knots

In this work a combination of microfiber knots are proposed to generate a periodic pass band filter. With proper control of the phase relation between the different rings, which depends on ring radius, the superposition of the individual spectra can result in a net enhancement of the resonance while suppressing others. This can be used in fiber laser due to stability requirement on a specific resonance wavelength. This stability has been demonstrated with an erbium doped microfiber knot in a few works (Sulaiman et al., 2012a). In this research, thermal effect is employed to tune the filter spectral response. It is found that the periodic pass band filter can be changed to an all pass filter by controlling optical path length difference via heating technique. Also the output spectrum from another two-knot sample and a three-knot sample are presented.

University of Malaya

These multi-resonator structures utilize coupled induced shift effect, which causes a displacement in the resonant wavelength of the different knot. That generates different pass band and stop band on the spectrum. The bandwidth of both pass band and stop band domains at the spectrum are adjustable by manipulating the size of the knot and the number of knots. Such structure can be used as a filter in fiber lasers, time delay, sensors and amplifier applications.

5.2.1 Concept and Fabrication of a Coupled-Knot Structure

The focus of this work is on the design and the realization of a coupled knot structure based periodic pass band filter, where the thermal effect is introduced in order to switch the response to an all pass filter. The structure includes two coupled microfiber knot (a microfiber knitted successively).

Figure 5.1 (a) shows a sketch of coupled knots with different radii. The forward and backward field elements, a_1, a_2, a'_1, a'_2, b_1, b_2 are shown inside the microfiber knots. Also a microscopic picture of the fabricated sample, with two knots is depicted in Figure 5.1 (b).

University of Malaya

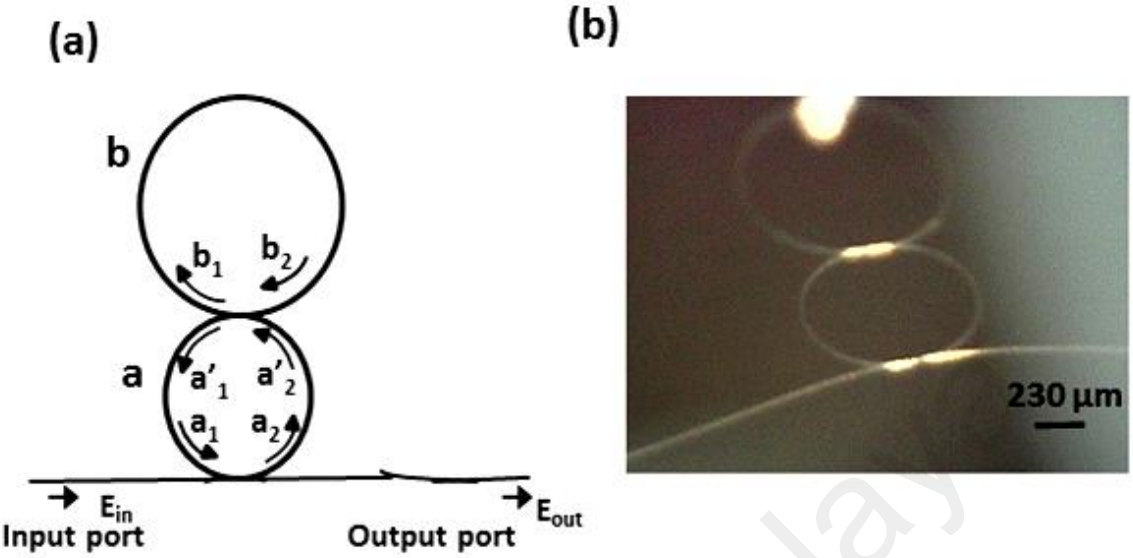

Figure 5.1: (a) Schematic diagram of the proposed structure (b) microscopic pictures from a coupled-knot.

Based on the transfer matrix, the relation between these field elements can be expressed as follows:

$$\begin{cases} E_{out} = ikE_{in} + ra_1 \\ a_2 = ika_1 + rE_{in} \\ a_2^{'} = \mathrm{e}^{-\propto\frac{\mathrm{L}a}{4}} e^{-i\left(\frac{2\pi n}{\lambda}\right)\frac{\mathrm{L}a}{2}} a_2 \\ a_1 = \mathrm{e}^{-\propto\frac{\mathrm{L}a}{4}} e^{-i\left(\frac{2\pi n}{\lambda}\right)\frac{\mathrm{L}a}{2}} a_1^{'} \end{cases} \tag{5.1}$$

$$\begin{cases} b_1 = ikb_2 + ra_2 \\ a_1^{'} = ika_2 + rb_2 \\ b_2 = \mathrm{e}^{-\propto\frac{\mathrm{L_b}}{2}} e^{-i\left(\frac{2\pi n}{\lambda}\right)\mathrm{L_b}} b_1 \end{cases} \tag{5.2}$$

$$\begin{bmatrix} a_2 \\ a_1 \end{bmatrix} = T_1 \begin{bmatrix} E_{out} \\ E_{in} \end{bmatrix}, T_1 = \begin{bmatrix} \frac{-ik}{r} & \frac{1}{r} \\ \frac{1}{r} & \frac{ik}{r} \end{bmatrix} \tag{5.3}$$

University of Malaya

$$\begin{bmatrix} a'_2 \\ a'_1 \end{bmatrix} = T_2 \begin{bmatrix} a_2 \\ a_1 \end{bmatrix}, T_2 = \begin{bmatrix} \mathrm{e}^{-\propto \frac{\mathrm{L}_a}{4}} e^{-i(\frac{2\pi n}{\lambda})\frac{\mathrm{L}_a}{2}} & 0 \\ 0 & \mathrm{e}^{\propto \frac{\mathrm{L}_a}{4}} e^{i(\frac{2\pi n}{\lambda})\frac{\mathrm{L}_a}{2}} \end{bmatrix} \quad (5.4)$$

$$\begin{bmatrix} b_2 \\ b_1 \end{bmatrix} = T_3 \begin{bmatrix} a'_2 \\ a'_1 \end{bmatrix}, T_3 = \begin{bmatrix} \frac{ik}{r} & \frac{1}{r} \\ \frac{1}{r} & \frac{-ik}{r} \end{bmatrix} \quad (5.5)$$

It is possible to calculate the output spectrum of the filter by solving the following matrix equation:

$$\begin{bmatrix} \mathrm{e}^{-\propto \frac{\mathrm{L}_b}{2}} e^{-i(\frac{2\pi n}{\lambda})\mathrm{L}_b} b_1 \\ b_1 \end{bmatrix} = \begin{bmatrix} \frac{ik}{r} & \frac{1}{r} \\ \frac{1}{r} & \frac{-ik}{r} \end{bmatrix} \begin{bmatrix} \mathrm{e}^{-\propto \frac{\mathrm{L}_a}{4}} e^{-i(\frac{2\pi n}{\lambda})\frac{\mathrm{L}_a}{2}} & 0 \\ 0 & \mathrm{e}^{\propto \frac{\mathrm{L}_a}{4}} e^{i(\frac{2\pi n}{\lambda})\frac{\mathrm{L}_a}{2}} \end{bmatrix}_2 \begin{bmatrix} \frac{-ik}{r} & \frac{1}{r} \\ \frac{1}{r} & \frac{ik}{r} \end{bmatrix} \begin{bmatrix} E_{out} \\ E_{in} \end{bmatrix} \quad (5.6)$$

In which r is the transmission coefficient, k is the coupling coefficient and α is the round trip loss and $L_{a,b}$ is the length related to knots a and b in order.

Designing a periodical band-pass or all-pass filter using two knots, one needs to estimate their radii prior to fabrication. The radii of the knots have to be selected such that at least two resonant wavelengths of the individual knots are close to each other as shown in Figure 5.2. The coupled induced shift effect causes a displacement in the resonant wavelength of the knot (element b in Figure 5.1 (a)) that is not directly connected to the straight microfiber. The coupling coefficient between directly connected knot (a in Figure 5.1) and straight microfiber as well as the one between the two knots are important factors to generate the suppression at the resonance region. The coupling coefficients are calculated from the transfer matrix, which is derived from coupled mode theory. The estimated coupling coefficients can be roughly realized by manipulating the coupling length while observing the output spectrum. Based on the definition of free spectral range for a single

University of Malaya

ring resonator, $FSR = \frac{\lambda^2}{nL}$ when λ is the resonant wavelength, n is refractive index and L is the circumference of the knot. As shown, some of the resonant wavelengths from two fabricated knots with radii 460.01 µm and 230 µm are close to each other. The wavelength shift is in the order of few picometers.

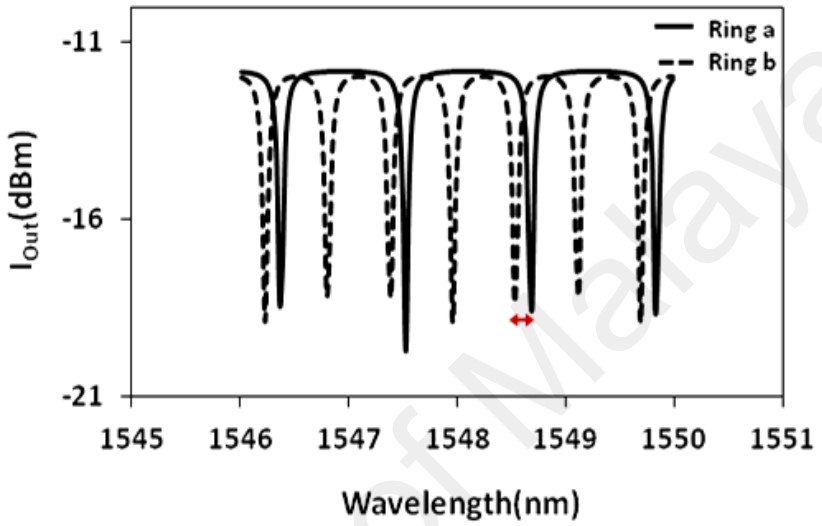

Figure 5.2: Simulation results from single knots with 460.01 µm (dashed line) and 230 µm (bold line) radii.

In Figure 5.2, spectrum suppression is expected at the two resonances around 1548.5 nm, marked with the red arrow in the figure. This is due to the superposition of the two modes related to the knots.

To fabricate the designed structure, a single mode fiber is tapered down to a 6-micrometer waist using flame-brushing method. The tapered fiber is cut to two parts; one part is shaped to the coupled knot by inter-twisting (knitting) the head of the microfiber twice. The second part of the microfiber is coupled to the first one by attaching the two microfibers end via Van Der Waals and electrostatic forces.

University of Malaya

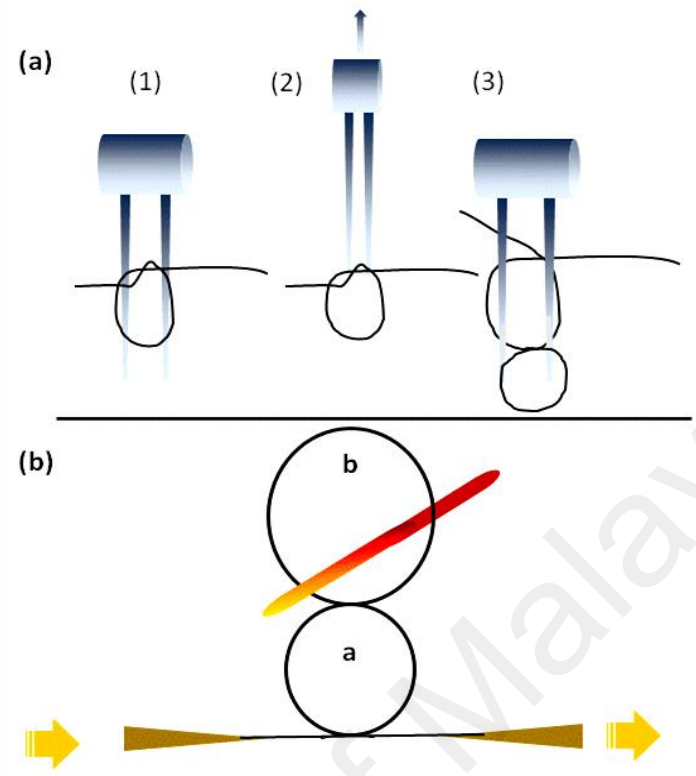

Figure 5.3: (a) Knot formation technique, (b) proposed setup using thermal effect for modulation.

Figure 5.3 shows the process of knitting. To obtain the estimated microfiber knot diameter, two nonstick bars are used to adjust the diameter and avoid microfiber sticking and breaking as it shown in Figure 5.3. For high precision fabrication, after inter-twisting the microfiber their ends are pulled with 10 μm resolution translation stages to obtain almost the desired radius.

The fabrication process was performed in free air at a fixed room temperature of 28 °C. To enhance the robustness of the structure the microfibers are placed on a glass that is coated with a Teflon liquid to provide low refractive index slab. In measuring the output spectrum, a broadband light source (ASE) and an optical spectrum analyzer (OSA) were used to record the output.

University of Malaya

5.2.2 Characterization of the Output Spectrum

Figure 5.4 shows the output spectrum from the fabricated fiber with two knots with 460.01 µm and 230 µm radii. Each knot can be considered as a feed-back loop which contributes to a pole in the transmission spectrum.

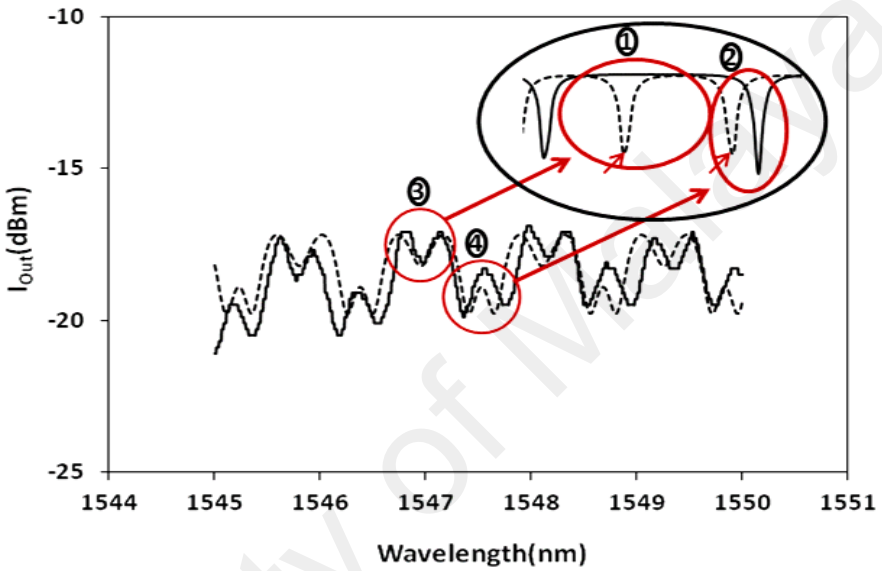

Figure 5.4: Experimental output spectrum from a double knot structure with radii 460.01.

µm and 230 µm radii including a sub-plot from two individual knots spectrum simulation. Due to coupling induced resonant wavelength shift, the poles are not generated at the exact resonant wavelength of the individual knots. Based on this effect and the mode superposition, the output spectrum from the coupled knot forms a periodic pass band filter. Figure 5.4 shows an output spectrum with 720 pm pass band and 425 pm band stop suppression ratio of 5.2 dB. The suppression ratio is strongly dependent on the coupling coefficient at the knitting point. The length of the knots however strongly affects the spectrum modulation. To tune the spectrum, the optical path needs to be altered. Here, the

University of Malaya

spectrum tuning is induced via the thermal effect as the setup shown in Figure 5.3 (b). The temperature increase is controlled by placing a hot metallic wire close to the knot b with a pitch of ~60 µm. As a result of the temperature increase from room temperature up to 28–30°C, the round trip length of knot (a and b) extended to few nanometers based on thermal expansion of a fiber glass.

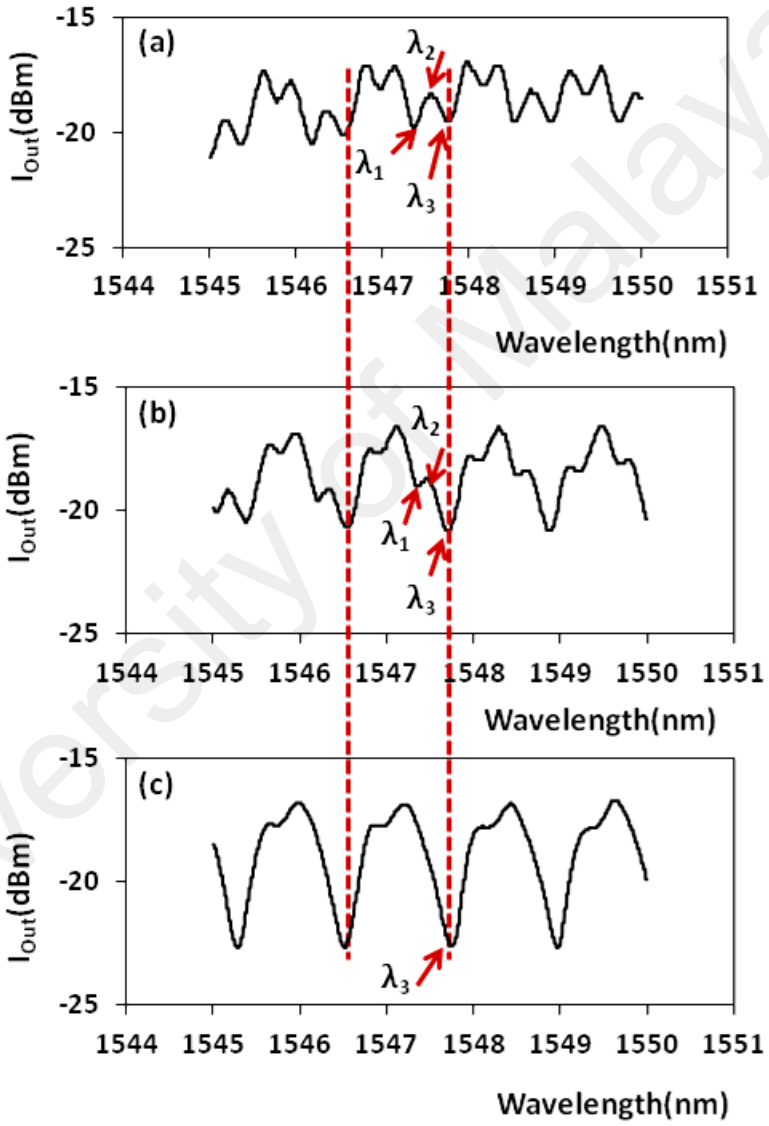

Figure 5.5: Spectrum from the coupled knot with radii of 460.01 µm and 230 µm at (a) 28 ^{o}C, (b) 29 ^{o}C and (c) 30 ^{o}C.

University of Malaya

Figure 5.5 (a), (b) and (c) show the spectra from the coupled knots at temperatures of 28, 29 and 30 degrees respectively. As shown from the plots in Figure 5.5, the resonance pole at λ_1 and λ_2 are suppressed with increasing the temperature. At the highest temperature the extension ratio increases from 3 dB to 6 dB at λ_3. Increasing the temperature changes the optical path and that causes the new spectral modulation. The new spectrum comes from the superposition of the related modes from the extended resonators. A calculation based on transfer matrix, which is derived from coupled mode theory, demonstrates that knots a and b radii increase to 230.03 μm and 460.06 μm respectively. Increasing temperature causes a modulation, which turns the pass-band filter into all-pass filter as shown in Figure 5.5 (c). The all-pass filter has a FSR of1150 pm, a quality factor of 6000, a FWHD of 255 pm and a finesse of 4.5.

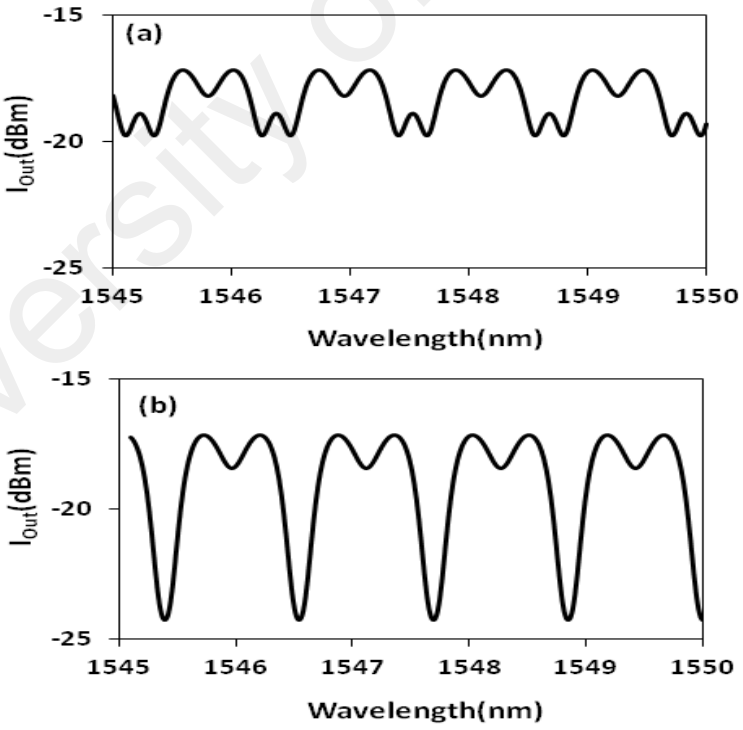

Figure 5.6: Simulation result of the coupled knot with radii of (a) 460.01 μm and 230 and (b) 460.06 μm and 230.03 μm.

University of Malaya

Figure 5.6 (a) demonstrates the simulation results of a structure that includes two knots with radii of 460.01 µm and 230 µm at 28 ºC. Figure 5.6 (b) depicts the calculated output spectrum of the same structure when the two radii change to 460.06 µm and 230.03 µm due to increase of the knot temperature up to 30 ºC

To increase the pass band, the structure should include knots with smaller radii in order to generate wider FSR. Figure 5.7 shows the spectrum from another sample. Wider pass-band is fabricated with two knots having radii of 114.98 µm and 456.92 µm.

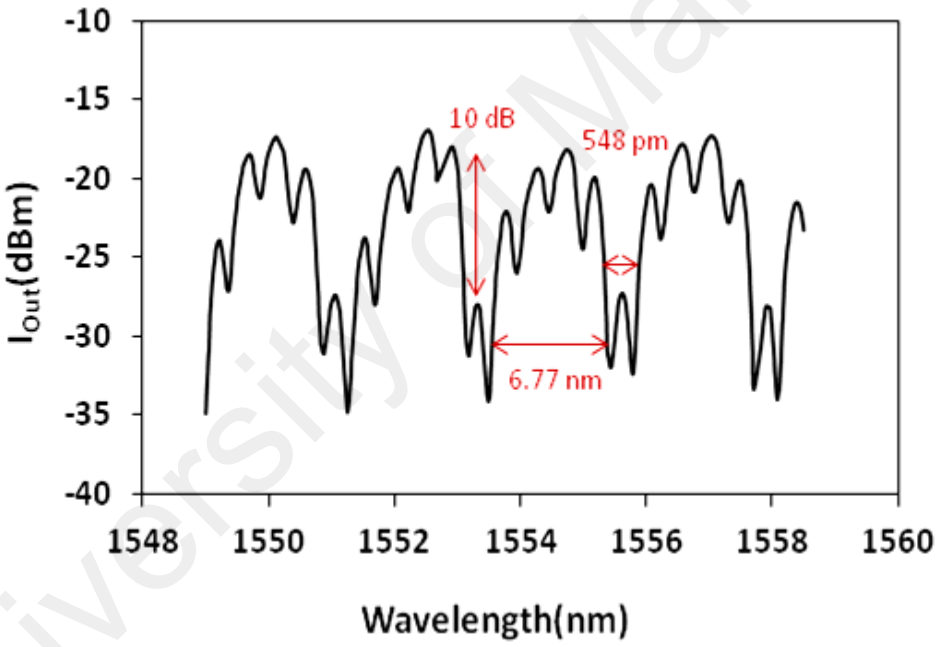

Figure 5.7: Spectrum from the coupled knot with radii of 114.98 µm and 456.92 µm.

University of Malaya

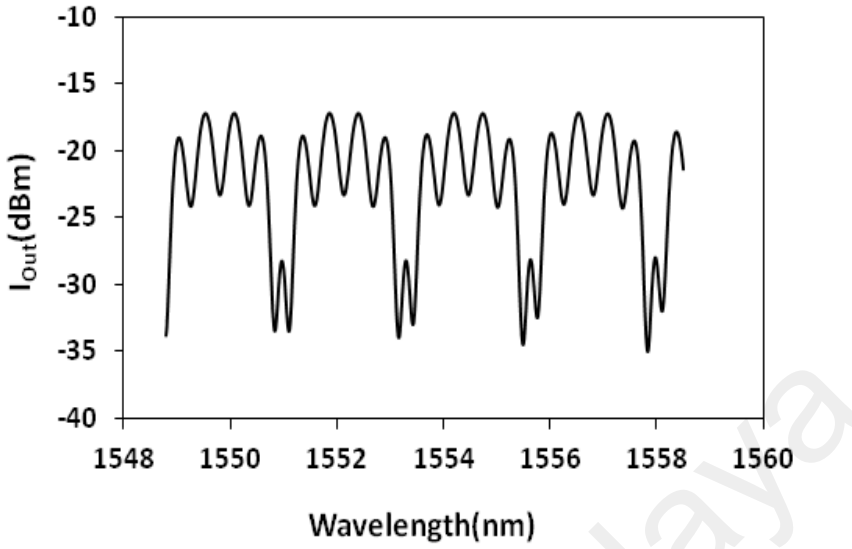

Figure 5.8: Simulation of response from the coupled knot with radii of 114.98 μm and 456.92 μm.

As shown in Figure 5.7, the spectrum has a pass band of 840 pm, stop band of 670 pm and suppression ratio 7 dB. Also the related simulation result has been shown in Figure 5.8. The simulation result is in a good agreement with the experimental result in Figure 5.7. The simulation result shows a pass band of 840 pm, stop band of 670 pm and suppression ratio 10 dB.

5.2.3 Concept and Fabrication of a Triple-knot Structure

Increasing the band stop is more challenging than that of the pass band. One important factor that causes wider band stop is to increase the number of knots. Figure 5.9 (a) and (b) show a sketch and a microscopic image of three knots sample in order.

University of Malaya

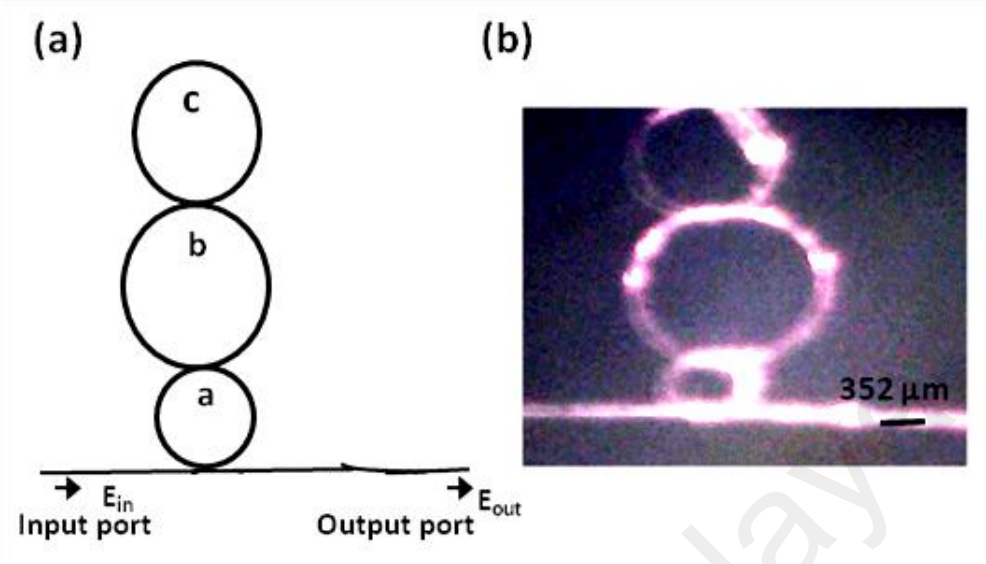

Figure 5.9: (a) Schematic diagram of a three coupled knots structure (b) microscopic pictures from the structure.

The transfer matrix for the triple-knot structure follows the same theory as the coupled-knot. With this condition the output follows equations (5.7), (5.8), (5.9):

$$\begin{cases} E_{out} = ikE_{in} + ra_1 \\ a_2 = ika_1 + rE_{in} \\ a_2^{'} = \mathrm{e}^{-\propto\frac{\mathrm{L}a}{4}} e^{-i\left(\frac{2\pi n}{\lambda}\right)\frac{\mathrm{L}a}{2}} a_2 \\ a_1 = \mathrm{e}^{-\propto\frac{\mathrm{L}a}{4}} e^{-i\left(\frac{2\pi n}{\lambda}\right)\frac{\mathrm{L}a}{2}} a_1^{'} \end{cases} \tag{5.7}$$

$$\begin{cases} b_1 = ikb_2 + ra_2 \\ a_1^{'} = ika_2 + rb_2 \\ b_1 = \mathrm{e}^{\propto\frac{\mathrm{L}b}{4}} e^{i\left(\frac{2\pi n}{\lambda}\right)\frac{\mathrm{L}b}{2}} b_1^{'} \\ b_2 = \mathrm{e}^{-\propto\frac{\mathrm{L}b}{4}} e^{-i\left(\frac{2\pi n}{\lambda}\right)\frac{\mathrm{L}b}{2}} b_2^{'} \end{cases} \tag{5.8}$$

$$\begin{cases} c_2 = ikc_1 + rb_1 \\ b_2 = ikb_1 + rc_1 \\ c_1 = \mathrm{e}^{-\propto\frac{\mathrm{L}c}{2}} e^{-i\left(\frac{2\pi n}{\lambda}\right)\mathrm{L}c} c_2 \end{cases} \tag{5.9}$$

University of Malaya

Re-arranging equation (5.7) to (5.9), the following matrix equations are deduced:

$$\begin{bmatrix} a_2 \\ a_1 \end{bmatrix} = T_1 \begin{bmatrix} E_{out} \\ E_{in} \end{bmatrix}, T_1 = \begin{bmatrix} \frac{-ik}{r} & \frac{1}{r} \\ \frac{1}{r} & \frac{ik}{r} \end{bmatrix} \tag{5.10}$$

$$\begin{bmatrix} a'_2 \\ a'_1 \end{bmatrix} = T_2 \begin{bmatrix} a_2 \\ a_1 \end{bmatrix}, T_2 = \begin{bmatrix} \mathrm{e}^{-\propto \frac{L_a}{4}} e^{-i(\frac{2\pi n}{\lambda})\frac{L_a}{2}} & 0 \\ 0 & \mathrm{e}^{\propto \frac{L_a}{4}} e^{i(\frac{2\pi n}{\lambda})\frac{L_a}{2}} \end{bmatrix} \tag{5.11}$$

$$\begin{bmatrix} b_2 \\ b_1 \end{bmatrix} = T_3 \begin{bmatrix} a'_2 \\ a'_1 \end{bmatrix}, T_3 = \begin{bmatrix} \frac{ik}{r} & \frac{1}{r} \\ \frac{1}{r} & \frac{-ik}{r} \end{bmatrix} \tag{5.12}$$

$$\begin{bmatrix} b'_2 \\ b'_1 \end{bmatrix} = T_4 \begin{bmatrix} b_2 \\ b_1 \end{bmatrix}, T_4 = \begin{bmatrix} \mathrm{e}^{\propto \frac{L_b}{4}} e^{i(\frac{2\pi n}{\lambda})\frac{L_b}{2}} & 0 \\ 0 & \mathrm{e}^{-\propto \frac{L_b}{4}} e^{-i(\frac{2\pi n}{\lambda})\frac{L_b}{2}} \end{bmatrix} \tag{5.13}$$

$$\begin{bmatrix} c_2 \\ c_1 \end{bmatrix} = T_5 \begin{bmatrix} b'_2 \\ b'_1 \end{bmatrix}, T_5 = \begin{bmatrix} \frac{ik}{r} & \frac{1}{r} \\ \frac{1}{r} & \frac{-ik}{r} \end{bmatrix} \tag{5.14}$$

The output spectrum can be obtained by solving the following equation (5.15):

$$\begin{bmatrix} c_2 \\ c_1 \end{bmatrix} = T_5 T_4 T_3 T_2 T_1 \begin{bmatrix} E_{out} \\ E_{in} \end{bmatrix} \tag{5.15}$$

Equations (5.15) show how an increase in the number of rings can add to the phase coefficient in the final matrix. That leads to an increase in the number of poles. It is possible to extend the stop band at the spectrum by increasing the number of knots.

University of Malaya

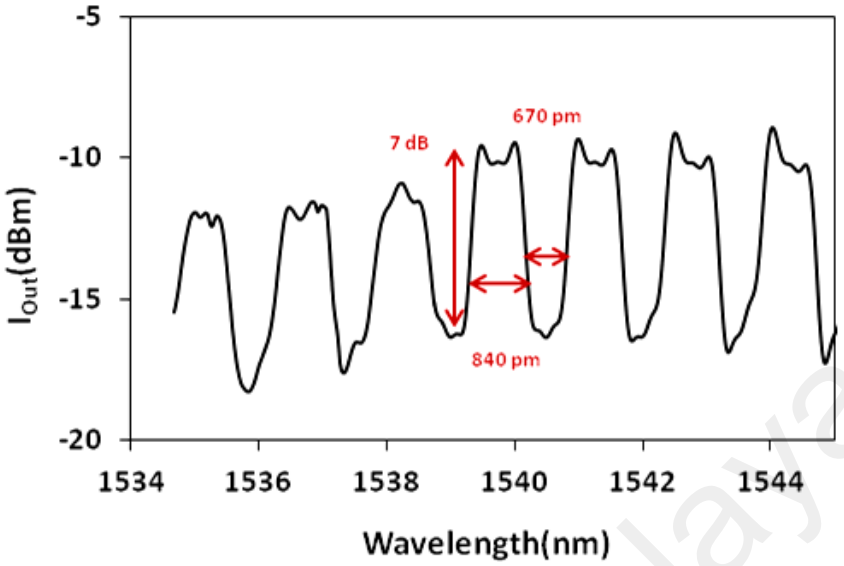

Figure 5.10: Spectrum from the coupled knot with 176 µm, 344 µm and 344 µm radii.

Figure 5.10 demonstrates the output spectrum with pass bandwidth of 840 pm, stop bandwidth of 670 pm and suppression ratio of 7 dB. This was obtained from a three-knot structure with 176 µm, 344 µm and 344 µm radii. The simulation result from the same structure is shown in Figure 5.11.

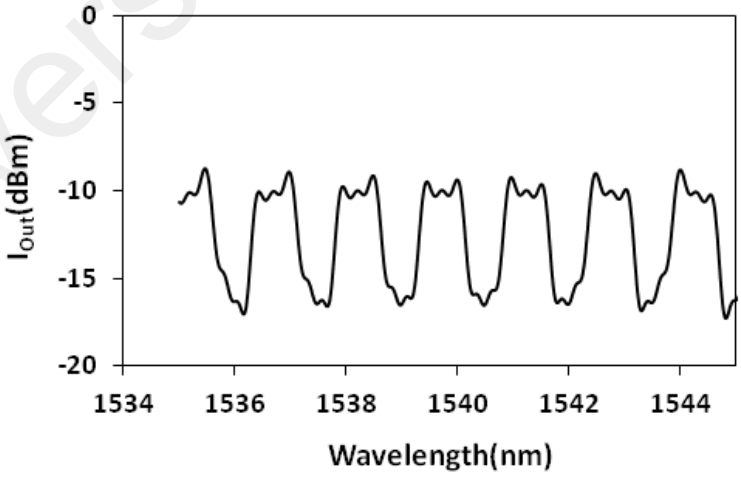

Figure 5.11: Simulation result from the coupled knot with 176 µm, 344 µm and 344 µm radii.

University of Malaya

5.3 Design of Optical Gate Using Nonlinearity in Erbium-doped Microfiber Knot

All optical switches and gates are important devices in photonics circuits (Bao et al., 2014; Mansouri-Birjandi et al., 2008). High switching power and complicated fabrication of the designed structure are two main limitations in achieving practical devices (Baba et al., 2003; Roy et al., 2014). Field enhancement inside optical resonators can provide a mean to decrease the threshold power (Barrios, 2004). Microring resonators have been used to achieve a low switching power to 6.mW due to strong light confinement (Barrios, 2004). Several studies of ring resonators in optical switching have been theoretically and experimentally proposed. In 2009, a nonlinear photonic crystal microring resonators was introduced theoretically as NOR gate by Isfehani (Isfahani et al., 2009). Implementation of NOR and NAND gates is achieved through the nonlinearity in the photonic crystals (Bao et al., 2014; Isfahani et al., 2009). In the same year, a nanofiber bend switch has been fabricated in which the turn-off and turn-on times of the proposed structure are about 500ms and 760ms in order (Yu et al., 2009). These times are not practical for optical switching applications.

This raises the need for alternative materials to enhance the nonlinearity and decreases the threshold power. This search leads to large variety of materials such as Erbium-doped glass in active fiber (J. Q. Li et al., 2004), polymers (Bloembergen, 1996; Hall et al., 1989) and glasses doped with metha nanocrystals (Haglund Jr et al., 1997). In 2004, an active nonlinear fiber ring resonator has been proposed and fabricated (J. Q. Li et al., 2004). The active ring resonator causes an increase in the finesse due to the gain medium. This causes an enhancement in the nonlinearity (C. F. Li et al., 2007; J. Q. Li et al., 2004). Following the same concept, a few works were proposed from 2004 to 2007 (J. Q. Li et al., 2005). These studies utilize Kerr effect in metamaterial, optical resonator and nonlinear photonic

University of Malaya

crystals. This leads to high contrast controllable, tunable and ultrafast low threshold switching (Chen et al., 2014; Fasihi, 2014; Hajizadegan et al, 2013; J. Q. Li et al., 2005).

In this section, erbium doped microfiber knot is considered as a nonlinear cavity to generate an all optical gate. This relies on the field enhancement inside the optical resonator. This enhancement causes a significant decrease in the switching power threshold. The nonlinear refractive coefficient of the erbium doped microfiber is larger (about 10^5 times) than that of the silica fiber (C. Li et al., 2006). This research compares the simulation results between passive and active microfiber knot. The calculations use coupled wave equations to predict the effect of the nonlinear refractive coefficient on threshold power.

5.3.1 Nonlinear Phase in Passive Microfiber Knot

Section 3.3 in chapter 3 focuses on the design and analysis of a single knot. As mentioned in the chapter, in/output and field elements inside the knot are coupled using coupled mode theory.

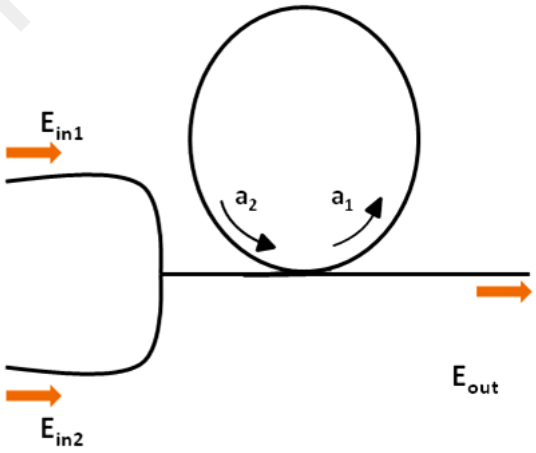

Figure 5.12: Schematic of knot resonator, including the relate field elements.

The following relations refer to the field elements in Figure 5.12 when $E_{in} = E_{in1} + E_{in2}$:

University of Malaya

$$\begin{cases} a_1 = rE_{in} + ika_2 \\ E_{out} = ra_2 + ikE_{in} \\ a_2 = e^{-\propto\frac{L}{2}}e^{-i(\frac{2\pi n}{\lambda})L}a_1 \end{cases} \tag{5.16}$$

where r, k are the transmission and coupling coefficients, respectively. The factor $\varphi = \frac{2\pi n}{\lambda}$L is referred to as the round trip phase. In which n is the refractive index and $L = 2\pi R$ is the circumference of the knot. Resonance occurs when the phase is a multiple of $(2n + 1)\pi$. The factor n and L are two main keys in phase definition. The last two chapters (chapter 3 and chapter 4) discussed the effect of resonator length on the output spectrum. This chapter focuses on the effect of the change of refractive index on the phase and output spectrum.

In this section the polarization response of material is considered in order to investigate the effect of external electromagnetic field on their refractive index.

It is described as follow:

$$p = \varepsilon_0\left[x^{(1)}E + x^{(2)}EE + x^{(3)}EEE^* + \cdots\right] \tag{5.17}$$

where p represents the polarization vector, $x^{(n)}$ denotes the nth order susceptibility and E the external electric field inside the medium.

The displacement vector is expressed as:

$$D = \varepsilon_0 E + p = \varepsilon_0(1 + x)E = \varepsilon E \tag{5.18}$$

The real part of ε can be expressed as $\varepsilon = n^2\varepsilon_0$.

Glass is an isotropic material that behaves like centrosymmetric material. With this kind of material, the second order of the sucessibility is negligible. The refractive index in such nonlinear medium (considering Kerr Effect) is defined as $n = n_0 + n_2 I$, in which n_0 as linear refractive index, $n_2 I$ as nonlinear terms of the index and I is the intensity of light inside the microfiber knot. Following this definition, the factor phase is involved with the linear part and nonlinear part as follows:

University of Malaya

$$\varphi = \varphi_0 + \Delta\varphi = \frac{2\pi n_0 \mathrm{L}}{\lambda} + \frac{2\pi n_2 \mathrm{L}}{\lambda} \mathrm{I} \tag{5.19}$$

in which I is the circulating intensity inside resonator.

5.3.2 Nonlinear Effective Phase Shift

Considering equation (3.15) the normalized output intensity is:

$$\frac{E_{out}}{E_{in}} = \frac{ik\mathrm{e}^{\propto\frac{\mathrm{L}}{2}}e^{i\varphi}+1}{\mathrm{e}^{\propto\frac{\mathrm{L}}{2}}e^{i\varphi}-ik} \tag{5.20}$$

in which φ is single-pass phase. As mentioned, resonance occurs when $\varphi = (2\mathrm{n}+1)\pi$. The phase shift that is obtained when light passes through the resonator and is recorded from the final port, is called the effective phase shift. Equation (3.15) can be rewritten as equation (5.21):

$$\frac{E_{out}}{E_{in}} = \frac{ik\mathrm{e}^{\propto\frac{\mathrm{L}}{2}}e^{i\varphi}+1}{\mathrm{e}^{\propto\frac{\mathrm{L}}{2}}e^{i\varphi}-ik} = e^{-i\varphi}\frac{\mathrm{e}^{-\propto\frac{\mathrm{L}}{2}}+ke^{-i\varphi-\mathrm{i}\frac{\pi}{2}}}{1+k\mathrm{e}^{-\propto\frac{\mathrm{L}}{2}}e^{-i\varphi-\mathrm{i}\frac{\pi}{2}}} = Ee^{-i\Phi} \tag{5.21}$$

in which Φ is the effective phase shift and E is output amplitude. Equation (5.22) can be derived as a solution of equation (5.21) as follows:

$$\Phi = -\varphi + tan^{-1}\left(\frac{-ksin(\varphi)}{e^{-\propto\frac{L}{2}}+k\,cos(\varphi)}\right) + tan^{-1}\left(\frac{-ke^{-\propto\frac{L}{2}}sin(\varphi)}{1+ke^{-\propto\frac{L}{2}}cos(\varphi)}\right) \tag{5.22}$$

The dependency of effective phase shift to single pass phase is plotted in Figure 5.13. The curves indicate three coupling coefficients; $k = 0$ (bold line), $k = 75$ (dashed line) and $k = 95$ (dotted line).

University of Malaya

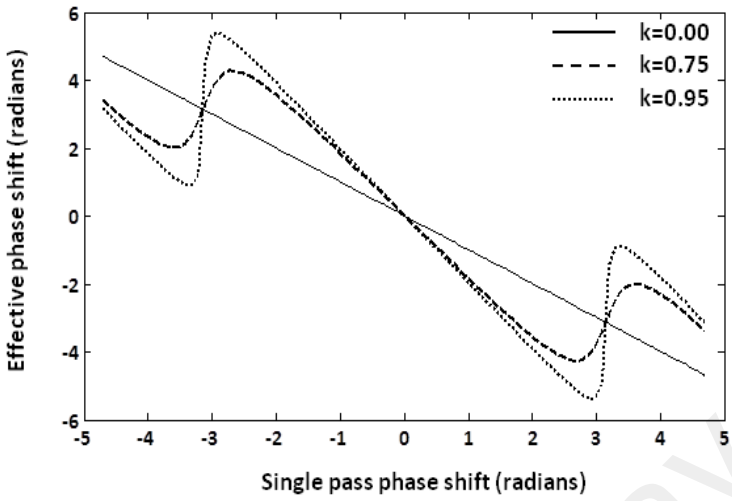

Figure 5.13: Effective phase shift of a knot with radius of 200 µm with three different coupling coefficients versus a single round phase.

As shown in Figure 5.13 the curves have a sharp slop near resonance condition ($\varphi = (2n + 1)\pi$). It means the structure shows high phase sensitivity at this region. Mathematical formalism of phase sensitivity can be obtained through differentiating equation (5.22) as follows:

$$\Phi' = \frac{d\Phi}{d\varphi} = \frac{(1-k^2)e^{-\propto L}}{1+2ke^{-\propto\frac{L}{2}}\cos(\varphi)\left(\frac{1+e^{-\propto L}}{2}\right)+k^2e^{-\propto L}+k^2\sin^2(\varphi)(1-e^{-\propto L})^2-1+e^{-\propto L}} \tag{5.23}$$

At resonance condition when loss is negligible ($\varphi = (2n + 1)\pi, e^{-\propto L} = 1$), equation (5.23) can be reduced to equation (5.24):

$$\frac{d\Phi}{d\varphi} = \frac{1+k}{1-k} \tag{5.24}$$

which shows the dependency of the phase sensitivity on the coupling coefficient.

University of Malaya

5.3.3 Design a XOR Gate Using Microfiber Knot

In this section, an XOR logic gate based on a single microfiber knot is proposed. To design the gate, the nonlinear effect (Kerr effect) is used. In this design (Figure 5.12), when the power is launched through the knot at input 1, $E_{in} = E_{in1}$(input 1 is "1" and input 2 is "0"), the circulating field experiences a linear phase and the output has resonance at a certain wavelength, λ_c (gate output is "1"). While adding the power through input 2, $E_{in} = E_{in1} + E_{in2}$(input 1 is "1" and input 2 is "1") stimulates the nonlinear terms of the phase ($\frac{2\pi n_2 \mathrm{L}}{\lambda}$ I). When the phase experiences a shift of π ($\Delta\varphi = \pi$), it changes the resonance condition and resonance wavelength. In this situation λ_c is no more at the resonance condition (gate output is "0").

5.3.4 Microfiber Geometry

To achieve the required nonlinear phase shift (π radians), the threshold intensity inside the resonator is $I_{th} = \frac{\lambda}{2n_2 \mathrm{L}}$. The definition of intensity in terms of power is $I_{th} = \frac{P}{A}$, where P is the power inside the resonator and A is the cross section of the microfiber. This indicates that high intensity is achievable by reducing the cross section of the microfiber at a constant power. There is a limitation on the size of the cross section of the microfiber as a waveguide. A microfiber is not able to transfer light when its waist becomes less than a certain diameter (M. Sumetsky et al., 2006). When the diameter of microfiber is small enough (near the launched wavelength), power confinement is reduced. The performance of the microfiber as a waveguide is practical when loss is small. The minima size of the tapered fiber, as a waveguide, can be calculated using equation (5.25) as propagation of loss ($\mathcal{L}$) (M. Sumetsky et al., 2006):

University of Malaya

$$\mathcal{L} = \frac{\pi^{1/2}}{4\left(\frac{1}{2}l\lambda{\gamma_0}^2\right)^{1/2}} e^{-\left(\frac{1}{2}l\lambda{\gamma_0}^2\right)}, \beta_0 = \frac{2}{W} = \frac{1.65}{r_0}.exp\left(-0.0713\frac{\lambda^2}{r_0^2}\right) \quad (5.25)$$

where β_0 is the propagation constant, W is the mode field diameter, r_0 is the radius of the microfiber and l is the length of the microfiber. Theoretically, the threshold loss is calculated at the condition $\mathcal{L}\sim 1$. Based on this equation, the limit for a microfiber radius with a length of one hundred km at an erbium region is 100 nm.

As mentioned in section 5.3, a resonator made by nonlinear material has a phase with two terms: linear and nonlinear. Equation (5.19) expresses the phase in a material with third-order nonlinearity.

The threshold power, inside the resonator, to stimulate the nonlinearity for a complete switch ($\Delta\varphi = \pi$) is expressed as follows:

$$P_{2th} = \frac{\lambda S}{2Ln_2} \quad (5.26)$$

To calculate the input power threshold, derivation of the effective phase shift to power is expressed as follow:

$$\frac{d\Phi}{dP_1} = \frac{d\Phi}{d\varphi}\frac{d\varphi}{dP_2}\frac{dP_2}{dP_1} = \frac{2\pi Ln_2}{\lambda S}\left(\frac{1+k}{1-k}\right)^2 \quad (5.27)$$

The threshold power is deduced from equation (5.27) as follows:

$$P_{1th} = \frac{\pi^2\lambda S}{8Ln_2\left(\frac{1+k}{1-k}\right)^2} \quad (5.28)$$

Figure 5.14 shows the dependency of the threshold power of a passive microfiber knot at the condition of a very small loss. The microfiber knot has a radius of 3.7 μm, waist of 0.2 μm and a nonlinear refractive index of 3×10^{-20}. The threshold power is recorded at resonance wavelength of 1553 nm. As shown in the figure, the minimum circulating power

University of Malaya

inside the knot to stimulate the nonlinearity is in order of a few mW. It clearly shows that the required power is decreased by reducing the size microfiber waist.

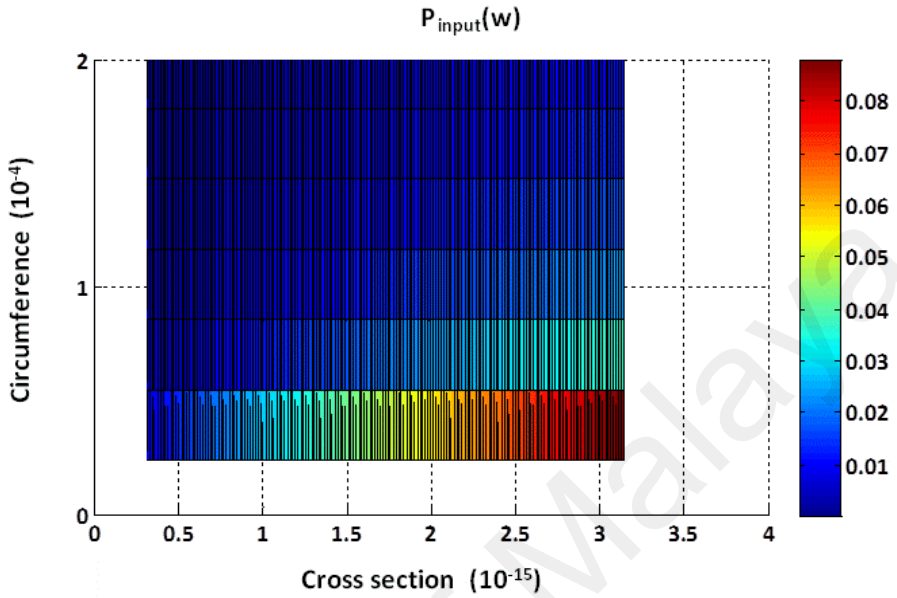

Figure 5.14: The threshold of input power of passive knot versus its circumference and cross section.

The following section focuses on relations between threshold power with spectrum factors such as field enhancement and finesse. It also considers the effect of knot parameters such as coupling coefficient, ring radius and loss on these factors.

5.3.5 Knot Parameters

In this section the trade-off between field enhancement and resonator factor such as ring radius coupling coefficient and loss are investigated. The following calculations demonstrate the effect of the different parameters of the structure such as ring radius, microfiber waist, coupling coefficient and loss on field enhancement inside the knot. Based on equation (5.16), the field intensity inside a resonator (a_2) is expressed by:

$$\frac{a_2}{E_{in}} = \frac{r}{-ik+e^{\propto\frac{L}{2}+i\varphi}}, \tag{5.29}$$

University of Malaya

which is called field enhancement. Higher field enhancement causes sharp roll-off and large extension ratio. Figure 5.15 (b) shows the dependency of the field enhancement on the coupling coefficient.

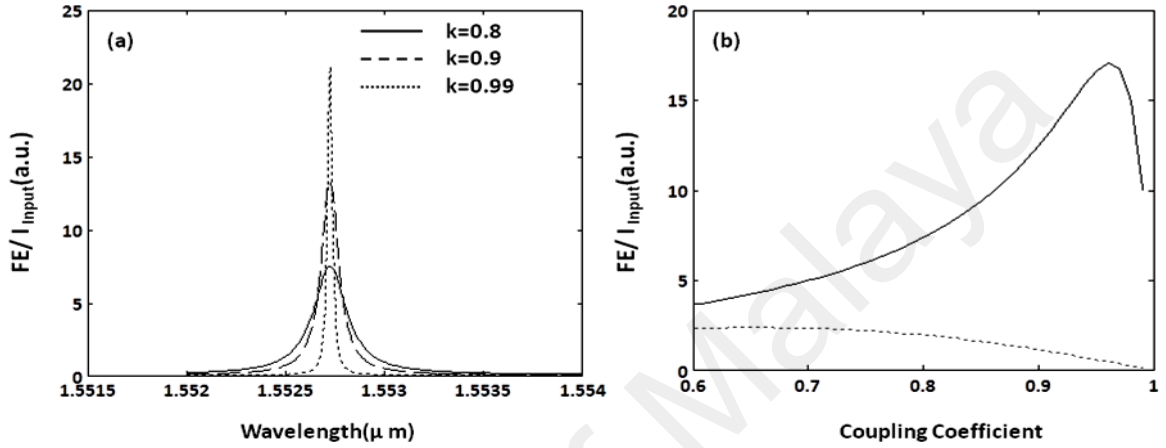

Figure 5.15: (a) Normalized field enhancement inside the knot (intensity of light inside the knot/ Input intensity) versus wavelength at three coupling coefficients (k=0.8, 0.9 and 0.99), (b) normalized field enhancement on a resonant wavelength of 1.553 μm versus the coupling coefficient.

Based on Figure 5.15, considering a knot with a defined radius, maximum field enhancement happens at a certain value of the coupling coefficient. The maximum normalized field enhancement ($I_{inside\ resonator}/I_{input}$) for a knot with a radius of 100 μm is about 23 at a coupling coefficient of 0.99.

Based on the field enhancement definition, there are two other effective parameters in the denominator L and α as resonator circumference and loss coefficient in order. Figure 5.16 (a) shows the output spectrum from three knots with circumferences of 54 μm (the bold line), 178 μm (the dashed line) and 465 μm (the dot line). Increasing the length of the knot causes a drop in the field enhancement due to the round trip loss, $e^{-\propto L}$, as shown in Figure

University of Malaya

5.16 (b). To increase the field enhancement inside the knot, the minimum ring circumference is desired. Based on the resonance condition at a certain wavelength, $(2m + 1)\lambda_m/2 = nL$, the minimum circumference can be obtained when $m = 1$. In this situation it is $\lambda_1 = \frac{2}{3}nL$.

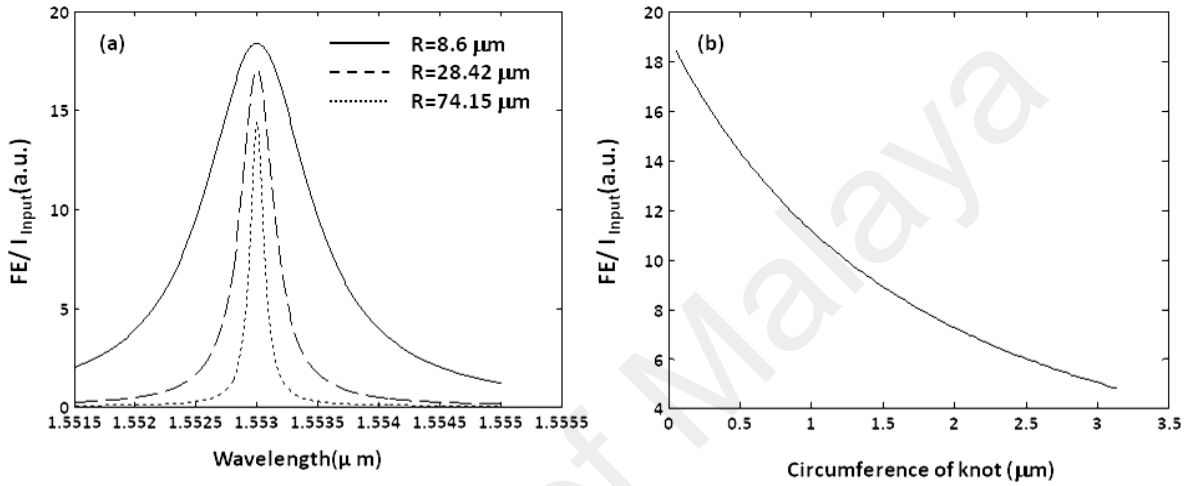

Figure 5.16: (a) Normalized field enhancement inside the knot (intensity of light inside the knot/ Input intensity) versus wavelength, (b) normalized field enhancement on a resonant wavelength of 1.553 µm versus the circumference of a knot with different radii.

Figure 5.16 (b) demonstrates that there is a dramatic decrease in the generated field enhancement inside a knot with increasing the length of the resonator. The minimum circumference of the knot is desired in order to decrease the round trip loss. The effect of loss on the output of a knot with radius of 100 µm at resonant wavelength of 1552.73 nm is theoretically calculated as depicted in figures 5.17 (a) and (b).

University of Malaya

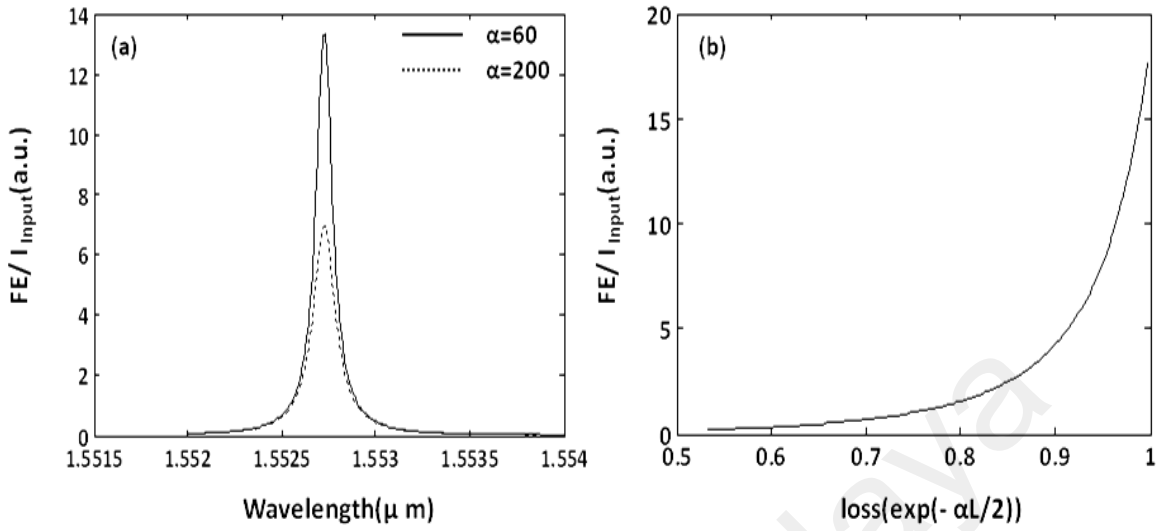

Figure 5.17: (a) Normalized field enhancement inside the knot (intensity of light inside the knot/ Input intensity) versus wavelength at different loss coefficients, (b) normalized field enhancement inside the knot versus loss.

Finesse is another spectrum factor that is important in controlling the power threshold. As mentioned in chapter 3, for knot resonators, the bandwidth around resonance is expressed by:

$$\delta\lambda_{FWHM} \approx \frac{\lambda^2(1-re^{-\frac{L}{2}})}{\pi nL\sqrt{re^{-\frac{L}{2}}}} \tag{5.30}$$

The free spectral range (FSR) is defined as:

$$\Delta\lambda_{FSR} = \frac{\lambda^2}{nL} \tag{5.31}$$

The finesse is the ratio of free spectral range (FSR) to FWHM or the ratio of 2π to $\delta\varphi$. It can be expressed as follows:

University of Malaya

$$f = \frac{\Delta\lambda_{FSR}}{\Delta\lambda_{FWHM}} = \frac{\pi\sqrt{re^{-\frac{L}{2}}}}{1-re^{-\frac{L}{2}}} \cong \frac{\pi}{2}\frac{1+k}{1-k} \tag{5.32}$$

It is clear that the finesse is not dependent on the dimensions of the resonator. It is however a function of the coupling coefficient and the loss. Figure 5.18 shows the finesse as a function of the coupling coefficient considering round trip losses of 0.95 (bold line) and 0.85 (dashed line). The curves show a noticeable increase in the finesse when coupling coefficient increase.

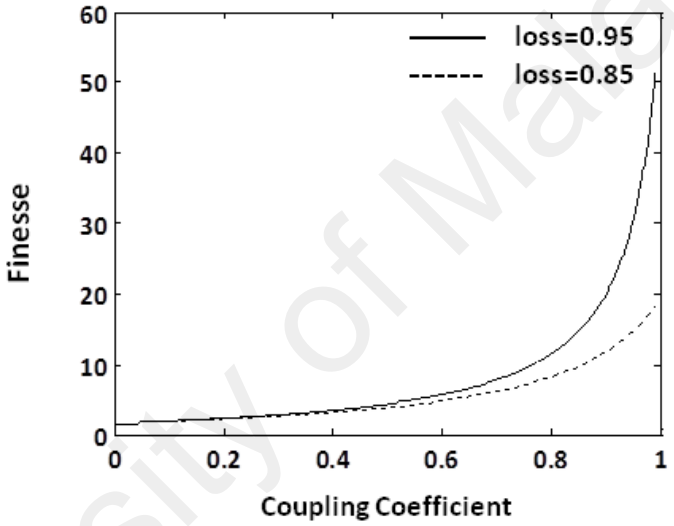

Figure 5.18: Finesse versus coupling coefficient considering two different loss coefficients.

The relation between the threshold power and finesse is obtained using equations (5.26) and (5.28) as follows:

$$P_{1th} = \frac{\pi^2\lambda S}{8Ln_2f^2} \tag{5.33}$$

Considering equations (5.28) and (5.33), Figure 5.19 (a) and (b) show the effect of the coupling and finesse on the power threshold respectively. Increasing the coupling causes a dramatic decrease in the power threshold.

University of Malaya

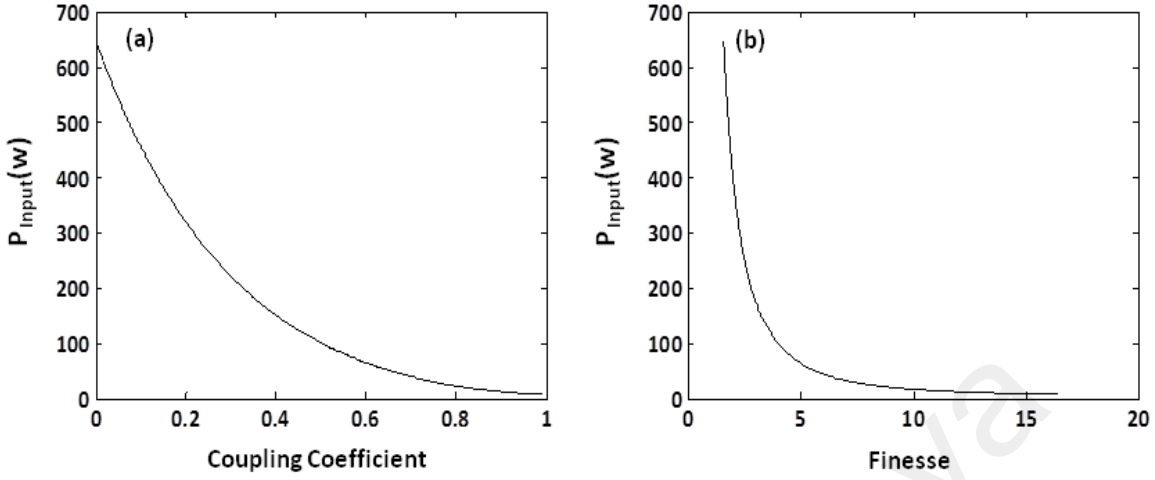

Figure 5.19: (a) Threshold power of input light versus coupling coefficient, (b) threshold power of input light versus finesse in a passive microfiber knot

5.3.6 Erbium Doped Microfiber Knot as an XOR Gate

The previous sections considered passive glass to design an XOR gate. In this section, erbium doped glass is proposed for the same structure. As previously mentioned, the nonlinear refractive index in erbium doped glass is in order of 10^{-15}. That is five times bigger that passive glass. Figure 5.14 shows the dependency of the threshold power of an erbium doped microfiber knot at the condition of a very small loss. The microfiber knot has a radius of 3.7 μm, waist of 0.2 μm and nonlinear refractive index of 6.9×10^{-15}. Considering equation (5.28), the threshold power versus microfiber waist and ring radius is shown in Figure 5.20. The minima power is in order of 10^{-7}, which is dramatically decreased considering Figure 5.14.

University of Malaya

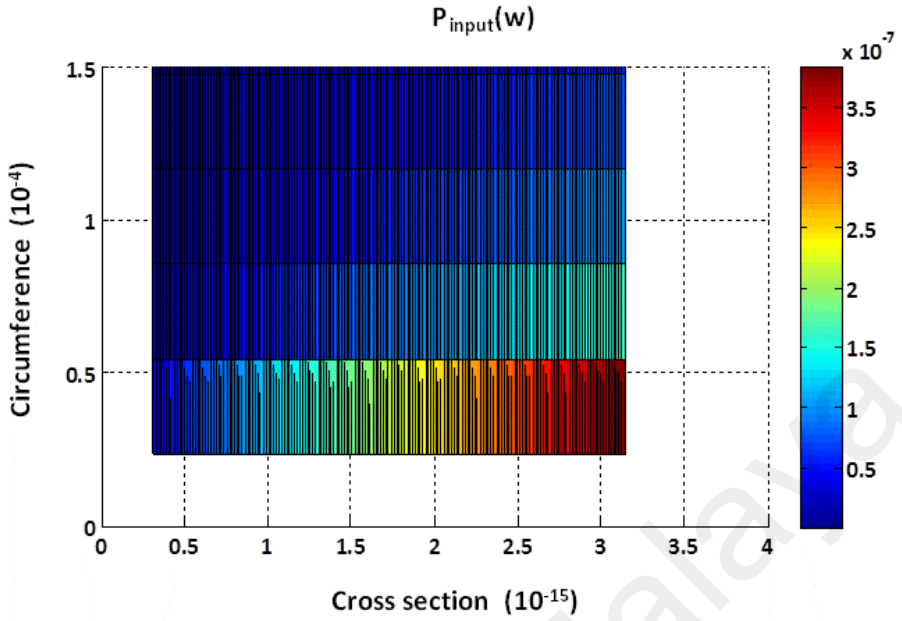

Figure 5.20: Threshold of input power inside an erbium knot versus its circumference and cross section.

Figure 5.21 shows the dependency of threshold power to coupling coefficient and finesse at the condition of active glass nonlinear refractive index.

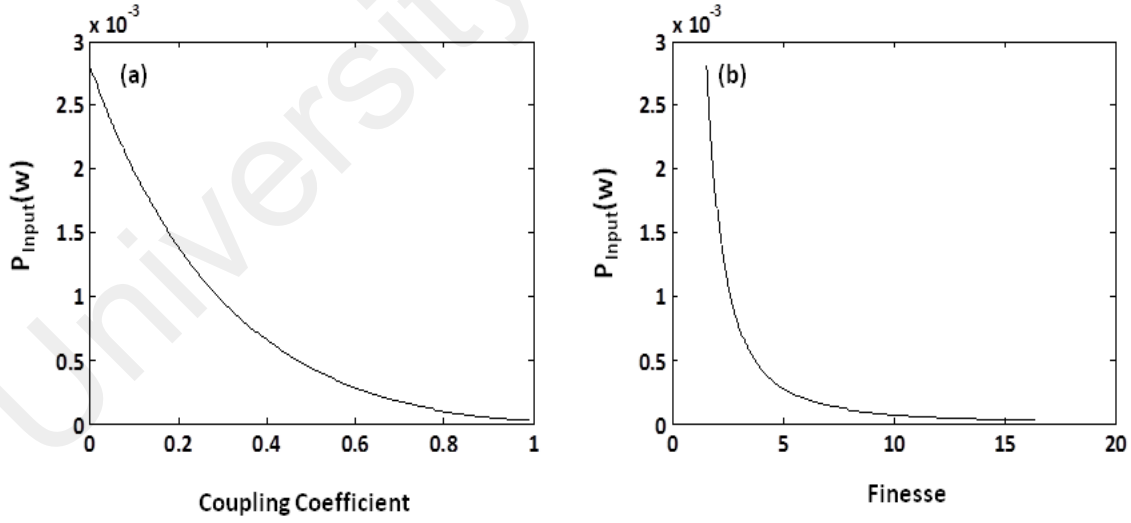

Figure 5.21: (a) Threshold power of input light versus coupling coefficient and (b) threshold power of input light versus finesse in an erbium doped microfiber knot.

University of Malaya

Figure 5.22 shows gate output for a structure with following characteristics; radius of 3.7 μm, waist of 0.2 μm and a nonlinear refractive index of 6.9×10^{-15}. The bold line demonstrates the output when the structure shows linear phase. In this condition, structure has resonance at wavelength of 1553 nm. The dashed line indicate output of the structure when nonnlinear phase is stimulated. The threshold power to change phase as much as π is about 1×10^{-7} W. as shown in the figure, wavelength 1553 nm is not on resonance at this condition.

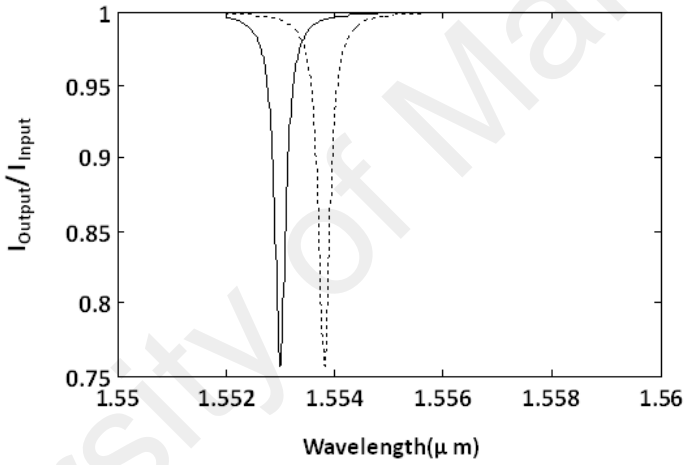

Figure 5.22: Normalized output spectrum at linear refractive index (bold line) and nonlinear refractive index (dot line).

5.4 Summery

In this chapter, a periodical pass-band filter based microfiber structure is proposed. The structure is made of successive microfiber knot resonators. Periodical spectral filtering is obtained as a result of superposition of different knots' modes and coupling induced resonance wavelength shift. This work demonstrates an experimental investigation of the thermal effect on the spectral modulation of this structure. The fabricated resonator consists

University of Malaya

of two knots with radii 460.01 μm and 230 μm, which are knitted successively in a column. This results in a periodic spectrum with 720 pm pass-band, 425 pm stop-band and suppression ratio of 5.2 dB. Increasing the optical path, using a hot metal bar with a temperature of 30^{o} close to the big knot, the periodic pass band filter switches to all pass filter with free spectral range of 1150 pm and quality factor 6000. The section as well demonstrates experimentally how to enhance the pass-band and stop-band widths through decreasing the knot's radii as well as increasing the number of knots.

Section 5.3 focuses to enhance the capability of microfiber in terms of nonlinearity. Using nonlinearity helps to switch the resonant wavelength through changing in refractive index by stimulating nonlinear refractive index. Resonators are considered as all optical switches due to the high field enhancement inside them. This effect leads to high power inside the resonators, which stimulates the nonlinear effect, and decrease the input power threshold for such phenomena.

Indeed, fiber glass in an alternative material, which boost the nonlinear refractive coefficients through material dopant such as rare earth elements. Because the nonlinear refractive coefficient of the EDF,10^{-15}, is much larger that of the silica fiber, 10^{-20}, micro-Er doped-fiber may be a good alternative due to shaping easiness and low switching power threshold compare the fabricated structure so far. The refractive index in such nonlinear medium (considering Kerr Effect) is defined n_0 as linear refractive index, $n_2 I$ as nonlinear terms of the index.

An XOR logic gate based on a single microfiber knot is proposed. To design the gate, the nonlinear effect (Kerr effect) is used. In this design, when the power is launched through the knot at input 1, the circulating field experiences a linear phase and the output has resonance at a certain wavelength, λ_c. Adding the power through input 2 stimulates the

University of Malaya

nonlinear terms of the phase. When the phase experiences a shift of π ($\Delta\varphi = \pi$), it changes the resonance condition and resonance wavelength. In this situation λ_c is no more at the resonance condition.

The required nonlinear phase shift (π radians), the threshold intensity inside the resonator is dependent on ring radius and the cross section of the microfiber. This indicates that high intensity is achievable by reducing the cross section of the microfiber at a constant power.

Some calculations showed the threshold power of a passive microfiber knot. As it is demonstrated the minimum circulating power inside the knot to stimulate the nonlinearity is in the order of a few mW. It is clearly shown that the required power is decreased by reducing the size microfiber waist. To increase the field enhancement inside the knot, the minimum ring circumference is desired.

Finally, an erbium doped glass is proposed for to design an XOR gate. As mentioned, the nonlinear refractive index in erbium doped glass is in order of 10^{-15}. This index has a noticeable effect to decrease power threshold of nonlinearity stimulation. To compare the result in an active medium with the one in passive medium, the dependency of the threshold power of an erbium doped microfiber knot at the condition of a very small loss was shown. The minima power is in order of 10^{-7} W, which is dramatically decreased, consider to the result in passive microfiber knot.

University of Malaya

CHAPTER 6

CONCLUSION AND FUTURE WORK

6.1 Conclusion

This dissertation proposed novel designs and new applications of microfiber knot structures as optical filters for communication systems. Chapter 1 presents an overview about microfiber structures and their applications in general. Chapter 2 explains the development of the different methods of microfiber fabrication. It refers as well to the fabrication, design and application of micro-knot fiber structure in the recent decade. In this work, four novel structures were proposed and studied. Double knots structure, Mach-Zender-knot structure and coupled knot structure were illustrated in chapter 3. The first section, in chapter 3, focused on theoretical characterization of a single knot output spectrum. The coupled mode theory was used to model the performance of the micro-fiber knot. Some of the most important characteristics of the output spectrum of a knot resonator were introduced; the free spectral range (FSR), the full width at half maximum (FWHM) and the extinction ratio (ER). These characteristics depend strongly on the microfiber knot parameters such as ring radius and coupling coefficient. This dependency limits the spectral tuning of the resonator, finesse and ER. Thermal effect and multi-resonators were proposed to overcome these limitations.

Based on the defined phase by the resonator, resonant wavelengths are generated. Changing the phase tunes the resonators such that certain resonant wavelength was changed. Dependency of the phase on the length of the resonator causes optical path variation when length changes. It generates different resonant wavelengths. By taking advantage of this fact, it is possible to tune the resonant wavelength on the spectrum by any change of the

University of Malaya

physical condition of the surrounding medium. Temperature was one of the environment factor considered in chapter 3. This research used linear expansion of microfiber in presence of thermal source to correct optical path. This change in optical path tunes the structure responses. It was experimentally observed that a change in temperature of about 1 degree centigrade increases the microfiber length of the order of nanometers. This change stimulates few picometers changes at a certain resonant wavelength that is noticeable. A combined microfiber MZ-knot was fabricated. The obtained finesse of this structure was twice bigger than the one of a single knot. To tune the response of the structure, a DC current was applied as thermal source near by the knot. The response of the structure showed a change in extension ratio from 2 dB to 10 dB by increasing the DC from 0 A to 1.22 A.

In the same chapter, a double-knot resonator was proposed and fabricated. Two-cascaded knots were assembled based on two single tapered microfibers with radii of 357.66 μm and 357.73 μm. The response from the single knot has an extinction ratio of 6 dB. The combination of the knots in a row causes the extinction ratio to diminish from 6 dB to around 3.5 dB. This owns to a slight mismatch in the radii of the knots of about ~ 70 nm, which correspond to a significant phase difference between the two spectra. With proper control of the phase relation between the different rings, the superposition of the individual spectra can result in a net enhancement of the resonance peaks due to Vernier effect. This effect causes an increase of the finesse at some peaks while suppressing others.

Heating up the smaller knot (with radii 357.66) leads to a flat comb filter with finesse of about 9.5 and extinction ratio of 15 dB. The result indicated that thermal effect can help to tune the output spectrum characteristics, possibility eliminating unwanted attenuated wavelengths and to enhance some other parts of the spectrum.

University of Malaya

Chapter 4 focuses on hybrid microfiber structure. The structure includes one knot, semi ring and straight microfiber. One structure was fabricated with the following parameters; knot and semi ring radii of 1763 µm and straight microfiber distance of 3766 µm. The structure obtained a FSR of 440 pm and a finesse of around 5.17 that is 3 times bigger than that of a knot structure.

To achieve sharp roll-off and less in band ripple some parameters were engineered such as number of knots, coupling coefficients and size of knot radius. A new hybrid structure included two knots were fabricated. The knots had radii of 549 µm (ER of 6 dB) and 1643 µm (ER of 3 dB). The small knot provided FSR of 465 pm and finesse of 2.73 while the big knot had FSR of 150 pm and finesse of 2.1. The combined structure showed a FSR of 465 pm, a quality factor of approximately 25000 and finesse of 8. Based on these results the structure obtained sharper roll-off compared to the small knot. The ER in this case was kept at the same value of a single knot, 6 dB. Based on the experimental result, smaller knots produced wider FSR. A structure was fabricated with radii of 339 µm and 1013 µm. The output spectrum of its drop port showed the following characteristics: FSR about 765 pm, a quality factor of 12000 and a finesse of about 6.37.

Another hybrid microfiber resonance structure were demonstrated that included two knots having different radii of 555 µm and 1662 µm and the length S is as long as the circumference of the small knot. The spectrum obtained the following characters of FSR about 460 pm, quality factor of around 30000, finesse of 9.7 and in band ripple 1.5. By manipulating the coupling regions of the big knot that has radius of 1662 µm via decreasing the coupling lengths, in band ripples vanished while the quality factor and the finesse are reduced to 22000 and 6.8 respectively. Such result indicates that by manipulating the

University of Malaya

coupling regions of the knot can eliminate the band ripple filter, which leads to filter quality improvement.

In chapter 5, thermal effect was examined on another structure comprises of two coupled knots. In this work a combination of microfiber knots was proposed to generate a periodic pass band filter.

Coupled induced shift effect in these multi-resonator structures causes a displacement in the resonant wavelength of the different knot. This effect was used to generate different pass band and stop band in the spectrum.

The proposed structure consists of two knots with 460.01 μm and 230 μm radii. The output spectrum of the structure demonstrated 720 pm pass band and 425 pm band stop suppression ratio of 5.2 dB. It was observed that the length of the knots strongly affected the spectrum modulation. The spectrum tuning was induced via the thermal effect. Increasing the temperature was controlled by placing a hot metallic wire close to one of the knots. As a result of the temperature increase of the metallic wire from the room temperature of 28–30°C, the extension ratio increased from 3 dB to 6 dB at certain wavelength. Increasing the temperature changes the optical path and causes a new spectral modulation. Increasing temperature caused a modulation which turned a pass-band filter to all-pass filter. The produced all-pass filter has the following characteristics; FSR= 1150 pm, quality factor≅ 6000, FWHD = 255 pm and a finesse of 4.5. Few structures with different knots radii were fabricated to provide response filter with different pass-band and band stop.

To increase the pass band, the structure should include knots with smaller radius that generates wider FSR. Wider pass-band was obtained with two knots having radii of 114.98 μm and 456.92 μm. The produced spectrum from the structure has a pass band of 840 pm

University of Malaya

and stop band 670 pm. The result demonstrated the increasing ring number makes it possible to extend the stop band at the spectrum. A three-knot structure with 176 μm, 344 μm and 344 μm radii has been fabricated. The result demonstrates an output spectrum with the pass bandwidth of 840 pm, stop bandwidth of 670 pm and suppression ratio of 7 dB.

This chapter also starts a new subject to enhance the capability of microfiber in terms of nonlinearity. Taking advantage of nonlinearity helps to switch the resonant wavelength through change in refractive index by stimulating nonlinear refractive index. Field enhancement inside resonator leads to high power inside it which stimulates the nonlinear effect and decrease the input power threshold for such phenomena. Passive and active microfiber knots were considered to investigate nonlinearity in the structures.

In the first section the polarization response of material was reviewed in order to calculate the effect of external electromagnetic field on their refractive index.

The effect of the change of refractive index on the phase and output spectrum was demonstrated. An XOR logic gate based on a single microfiber knot is proposed. To design the gate, the nonlinear effect (Kerr effect) was used. Based on the design when nonlinearity causes a change in phase as much as π, the resonant wavelength experiences a shift and the response of the structure changes.

The theory and results showed the threshold intensity inside the resonator depends on the ring radius and the cross section of the microfiber. This indicates that high intensity is achievable by reducing the cross section of the microfiber at a constant power.

Some calculations showed the threshold power of a passive microfiber knot. It was demonstrated that the minimum circulating power inside the knot to stimulate the nonlinearity is in order of a few mW. Following the investigation, the relations between threshold power with spectrum factors such as field enhancement and finesse were

University of Malaya

considered. The effect of knot parameters such as coupling coefficient, ring radius and loss on these factors were demonstrated. Based on these results, in a knot with a defined radius, maximum field enhancement happens at a certain value of the coupling coefficient.

These results indicate that increasing the length of the knot causes a drop in the field enhancement due to the round trip loss. To increase the field enhancement inside the knot, the minimum ring circumference was recommended. Based on the calculation, the minimum circumference can be obtained by multiplying by 3/2 of the ratio of a certain resonant wavelength to refractive index.

The theory showed that the finesse is not dependent on the dimensions of the resonator. It is however a function of the coupling coefficient and the loss. Results indicated a noticeable increase in the finesse when coupling coefficient increase.

The relation between the threshold power and coupling coefficient was obtained as well. It showed that increase in the coupling causes a dramatic decrease in the power threshold.

In final section an erbium doped glass was proposed for the design of a XOR gate. As mentioned, the nonlinear refractive index in erbium doped glass is five times bigger than passive glass. This index has a noticeable effect to decrease power threshold of nonlinearity stimulation. To compare the result in an active medium with the one in passive medium, the dependency of the threshold power of an erbium doped microfiber knot at the condition of a very small loss was shown. The minima power was in order of 10^{-7} W which was dramatically decreased compared to the result in passive microfiber knot.

6.2 Future works

The proposed future work is about design of new multi-resonator microfiber structures for filtering application. Also more investigation on coupling coefficients and number of resonators provide a wide range of filters with different pass band and band stop. Focusing

University of Malaya

on Vernier effect is helpful to obtain large extinction ratio for laser application. Also stimulation of field enhancement inside these structures is desired. Using the result may be help to design nonlinear optical gates with low threshold power.

University of Malaya

Reference

A.J.C.Grellier. (1998). Heat transfer modeling in CO2 laser processing of optical fibers. *Optics Communications, 152*, 324-328.

Arjmand, M., Ahmadi, V., & Karimi, M. (2012). Wavelength-Selective Optical Amplifier Based on Microfiber Coil Resonators. *Journal of Lightwave Technology, 30*(16), 2596-2602.

Aryanfar, I., Lim, K. S., Chong, W. Y., Harun, S. W., & Ahmad, H. (2012). Add-Drop Filter Based on Microfiber Mach-Zehnder/Sagnac Interferometer. *Ieee Journal of Quantum Electronics, 48*(11), 1411-1414.

Baba, T., & Iwai, T. (2003). Enhancement of third order nonlinearity calculated for two-dimensional photonic crystal. *Japanese Journal of Applied Physics Part 1-Regular Papers Short Notes & Review Papers, 42*(4A), 1603-1608.

Bao, J. J., Xiao, J., Fan, L., Li, X. X., Hai, Y. F., Zhang, T., & Yang, C. B. (2014). All-optical NOR and NAND gates based on photonic crystal ring resonator. *Optics Communications, 329*, 109-112.

Barrios, C. A. (2004). High-performance all-optical silicon microswitch. *Electronics Letters, 40*(14), 862-863.

Bloembergen, N. (1996). Nonlinear optics of polymers: fundamentals and applications. *Journal of Nonlinear Optical Physics & Materials, 5*(01), 1-7.

Bo, L., O'Mahony, C. C., Semenova, Y., Gilmartin, N., Wang, P. F., & Farrell, G. (2014). Microfiber coupler based label-free immunosensor. *Optics Express, 22*(7), 8150-8155.

Boeck, Robi, Jaeger, Nicolas A, Rouger, Nicolas, & Chrostowski, Lukas. (2010). Series-coupled silicon racetrack resonators and the Vernier effect: theory and measurement. *Optics express, 18*(24), 25151-25157.

Broderick, N. G. R. (2008). Optical Snakes and Ladders: Dispersion and nonlinearity in microcoil resonators. *Optics Express, 16*(20), 16247-16254.

Chao, Chung-yen, & Guo, L Jay. (2002). Polymer microring resonators fabricated by nanoimprint technique. *Journal of Vacuum Science & Technology B, 20*(6), 2862-2866.

Chen, F., & Yao, D. Z. (2014). Tunable multiple all-optical switch based on multi-nanoresonator-coupled waveguide systems containing Kerr material. *Optics Communications, 312*, 143-147.

University of Malaya

Chen, G. Y., Newson, T. P., & Brambilla, G. (2013). Optical microfibers for fast current sensing. *Optical Fiber Technology, 19*(6), 802-807.

Chen, George Y, Ding, Ming, Newson, Trevor P, & Brambilla, Gilberto. (2013). A review of microfiber and nanofiber based optical sensors. *Open Optic. J, 7*, 32-57.

Chen, N. K., Yang, T. H., Chen, Y. N., Guo, T., & Guan, B. O. (2013). High sensitivity stretched-abrupt-tapered Mach-Zehnder interferometer with optical attractive force for active microsensing applications. *Applied Physics Letters, 102*(17).

Chen, S. Q., Chen, Y., Wu, M., Li, Y., Zhao, C. J., & Wen, S. C. (2014). Stable Q-Switched Erbium-Doped Fiber Laser Based on Topological Insulator Covered Microfiber. *Ieee Photonics Technology Letters, 26*(10).

Chen, Y. H., Wu, Y., Rao, Y. J., Deng, Q. A., & Gong, Y. A. (2010). Hybrid Mach-Zehnder interferometer and knot resonator based on silica microfibers. *Optics Communications, 283*(14), 2953-2956.

Chen, Y., Yan, S. C., Xu, F., & Lu, Y. Q. (2013). A Compact Microfiber Coupler Based Sagnac Loop. *2013 12th International Conference on Optical Communications and Networks (Icocn)*.

Chen, Yuan, Ma, Zhe, Yang, Qing, & Tong, Li-Min. (2008). Compact optical short-pass filters based on microfibers. *Optics letters, 33*(21), 2565-2567.

Delage, A., Xu, D. X., McKinnon, R. W., Post, E., Waldron, P., Lapointe, J., Schmid, J. H. (2009). Wavelength-Dependent Model of a Ring Resonator Sensor Excited by a Directional Coupler. *Journal of Lightwave Technology, 27*(9), 1172-1180.

Digonnet, M. J. F. (2011). Rotation Sensitivity of Gyroscopes Based on Distributed-Coupling Loop Resonators. *Journal of Lightwave Technology, 29*(20), 3048-3053.

Dimmick, T. E. (1999). Carbon dioxide laser fabrication of fused fiber couplers and tapers. *Applied Optics, 38*, 6845-6848.

Durfee III, CG, Lynch, J, & Milchberg, HM. (1995). Development of a plasma waveguide for high-intensity laser pulses. *Physical Review E, 51*(3), 2368.

Fan, W., Gan, J. L., Zhang, Z. S., Wei, X. M., Xu, S. H., & Yang, Z. M. (2012). Narrow linewidth single frequency microfiber laser. *Optics Letters, 37*(20), 4323-4325.

Fasihi, K. (2014). High-Contrast All-Optical Controllable Switching and Routing in Nonlinear Photonic Crystals. *Journal of Lightwave Technology, 32*(18), 3126-3131.

University of Malaya

Gouveia, M. A., Lee, T., Ismaeel, R., Ding, M., Broderick, N. G. R., Cordeiro, C. M. B., & Brambilla, G. (2013). Second harmonic generation and enhancement in microfibers and loop resonators. *Applied Physics Letters, 102*(20).

Griffel, Giora. (2000). Vernier effect in asymmetrical ring resonator arrays. *Photonics Technology Letters, IEEE, 12*(12), 1642-1644.

Grover, R., Ibrahim, T. A., Kanakaraju, S., Lucas, L., Calhoun, L. C., & Ho, P. T. (2004). A tunable GaInAsP-InP optical microring notch filter. *Ieee Photonics Technology Letters, 16*(2), 467-469.

Grover, R., Van, V., Ibrahim, T. A., Absil, P. P., Calhoun, L. C., Johnson, F. G., Ho, P. T. (2002). Parallel-cascaded semiconductor microring resonators for high-order and wide-FSR filters. *Journal of Lightwave Technology, 20*(5), 872-877.

Guo, Xin, Ying, Yibin, & Tong, Limin. (2013). Photonic nanowires: From subwavelength waveguides to optical sensors. *Accounts of chemical research, 47*(2), 656-666.

Haglund Jr, Richard F, Rodriguez, Carmen N Afonso, Battaglin, Giancarlo, Godbole, Mukund, Gonella, Francesco, Hamilton, John D, Osborne Jr, Dannie H. (1997). *Effects of laser and particle beams on the synthesis and nonlinear optical response of nanostructures.* Paper presented at the Photonics West'97.

Hajizadegan, M., Fathi, D., & Sakhdari, M. S. (2013). All-optical metamaterial switch based on Kerr effect with MWCNT composite. *Physica E-Low-Dimensional Systems & Nanostructures, 48*, 1-6.

Hall, DW, Newhouse, Mark A, Borrelli, Nicholas F, Dumbaugh, WH, & Weidman, DL. (1989). Nonlinear optical susceptibilities of high-index glasses. *Applied Physics Letters, 54*(14), 1293-1295.

Hryniewicz, JV, Absil, PP, Little, BE, Wilson, RA, & Ho, PT. (2000). Higher order filter response in coupled microring resonators. *IEEE Photonics Technology Letters, 12*(3), 320-322.

Hsieh, Y. C., Peng, T. S., & Wang, L. A. (2012). Millimeter-Sized Microfiber Coil Resonators With Enhanced Quality Factors by Increasing Coil Numbers. *Ieee Photonics Technology Letters, 24*(7), 569-571.

Isfahani, B. M., Tameh, T. A., Granpayeh, N., & Javan, A. R. M. (2009). All-optical NOR gate based on nonlinear photonic crystal microring resonators. *Journal of the Optical Society of America B-Optical Physics, 26*(5), 1097-1102.

Ismaeel, R., Lee, T., Al-Saab, F., Jung, Y. M., & Brambilla, G. (2012). A self-coupling multi-port microcoil resonator. *Optics Express, 20*(8), 8568-8574.

University of Malaya

Ismaeel, R., Lee, T., Ding, M., Broderick, N. G. R., & Brambilla, G. (2012). Nonlinear microfiber loop resonators for resonantly enhanced third harmonic generation. *Optics Letters, 37*(24), 5121-5123.

Jasim, A. A., Harun, S. W., Muhammad, M. Z., Arof, H., & Ahmad, H. (2013). Current sensor based on inline microfiber Mach-Zehnder interferometer. *Sensors and Actuators a-Physical, 192*, 9-12.

Jasim, A. A., Muhammad, M. Z., Zulkifli, A. Z., Ahmad, F., Ahmad, H., & Harun, S. W. (2012). Fabrication and characterization of 2 x 2 microfiber coupler. *Optoelectronics and Advanced Materials-Rapid Communications, 6*(1-2), 7-11.

Jerman, JH, & Clift, DJ. (1991). *Miniature Fabry-Perot interferometers micromachined in silicon for use in optical fiber WDM systems.* Paper presented at the Solid-State Sensors and Actuators, 1991. Digest of Technical Papers, TRANSDUCERS'91., 1991 International Conference on.

Jiang, X. D., Chen, Y., Vienne, G., & Tong, L. M. (2007). All-fiber add-drop filters based on microfiber knot resonators. *Optics Letters, 32*(12), 1710-1712.

Jiang, X. S., Song, Q. H., Xu, L., Fu, J., & Tong, L. M. (2007). Microfiber knot dye laser based on the evanescent-wave-coupled gain. *Applied Physics Letters, 90*(23).

Jiang, X. S., Tong, L. M., Vienne, G., Guo, X., Tsao, A., Yang, Q., & Yang, D. R. (2006). Demonstration of optical microfiber knot resonators. *Applied Physics Letters, 88*(22).

Jiang, X. S., Yang, Q., Vienne, G., Li, Y. H., Tong, L. M., Zhang, J. J., & Hu, L. L. (2006). Demonstration of microfiber knot laser. *Applied Physics Letters, 89*(14).

Jiang, Xiaoshun, Chen, Yuan, Vienne, Guillaume, & Tong, Limin. (2007). All-fiber add-drop filters based on microfiber knot resonators. *Optics letters, 32*(12), 1710-1712.

Jin, W., Xuan, H. F., & Jin, W. (2013). Birefringent Microfiber-Based Fiber Loop Mirrors for Tunable Filters and Refractive Index Sensors. *Fifth European Workshop on Optical Fibre Sensors, 8794*.

Jin, W., Xuan, H. F., Wang, C., & Jin, W. (2013). High Sensitivity Pressure Sensor Based on a Birefringent Microfiber Loop Mirror. *Fourth Asia Pacific Optical Sensors Conference, 8924*.

Jung, Yongmin, Brambilla, Gilberto, Murugan, Ganapathy Senthil, & Richardson, David J. (2011). Optical racetrack ring-resonator based on two U-bent microfibers. *Applied Physics Letters, 98*(2), 021109.

Kakarantzas, G, Dimmick, TE, Birks, TA, Le Roux, R, & Russell, P St J. (2001). Miniature all-fiber devices based on CO 2 laser microstructuring of tapered fibers. *Optics Letters, 26*(15), 1137-1139.

University of Malaya

Kawazoe, T., Yatsui, T., & Ohtsu, M. (2006). Nanophotonics using optical near fields. *Journal of non-crystalline solids, 352*(23), 2492-2495.

Kou, J. L., Ding, M., Feng, J., Lu, Y. Q., Xu, F., & Brambilla, G. (2012). Microfiber-Based Bragg Gratings for Sensing Applications: A Review. *Sensors, 12*(7), 8861-8876.

Lee, T., Broderick, N. G. R., & Brambilla, G. (2013). Resonantly enhanced third harmonic generation in microfiber loop resonators. *Journal of the Optical Society of America B-Optical Physics, 30*(3), 505-511.

Lepetit, L, Cheriaux, G, & Joffre, M. (1995). Linear techniques of phase measurement by femtosecond spectral interferometry for applications in spectroscopy. *JOSA B, 12*(12), 2467-2474.

Li, C. F., Dou, N., & Yupapin, P. P. (2006). Milliwatt and nanosecond all-optical switching in a double-coupler ring resonator containing an EDFA. *Journal of Optics a-Pure and Applied Optics, 8*(9), 728-732.

Li, C. F., Xu, G. M., Dou, N., & Wang, F. (2007). Low-power all-optical switching using a fiber Sagnac interferometer with a pumped nonlinear coupler. *Journal of Nonlinear Optical Physics & Materials, 16*(1), 101-110.

Li, J., Sun, L. P., Gao, S., Ran, Y., & Guan, B. O. (2012). Enhancement of Refractive Index Sensitivity for Rectangular-microfiber Sagnac Loop Sensors. *2012 Photonics Global Conference (Pgc)*.

Li, J. Q., Bananej, A., Li, Q. H., Chen, Q., & Li, C. F. (2004). An all-optical switch of Mach-Zehnder interferometer type using an active fibre ring resonator. *Chinese Physics, 13*(7), 1046-1051.

Li, J. Q., Li, L., Zhao, J. Q., & Li, C. F. (2005). Ultrafast, low power, and highly stable all-optical switch in MZI with two-arm-sharing nonlinear ring resonator. *Optics Communications, 256*(4-6), 319-325.

Li, T., Dong, X. Y., Chan, C. C., Zhao, C. L., & Zu, P. (2012). Humidity Sensor Based on a Multimode-Fiber Taper Coated With Polyvinyl Alcohol Interacting With a Fiber Bragg Grating. *Ieee Sensors Journal, 12*(6), 2205-2208.

Li, X. L., & Ding, H. (2012). All-fiber magnetic-field sensor based on microfiber knot resonator and magnetic fluid. *Optics Letters, 37*(24), 5187-5189.

Li, X. L., & Ding, H. (2013). Investigation of the Thermal Properties of Optical Microfiber Knot Resonators. *Instrumentation Science & Technology, 41*(3), 224-235.

University of Malaya

Li, Y. H., Vienne, G., Jiang, X. S., Pan, X. Y., Liu, X., Gu, P. F., & Tong, L. M. (2006). Modeling rare-earth doped microfiber ring lasers. *Optics Express, 14*(16), 7073-7086.

Liao, C. R., Chen, H. F., & Wang, D. N. (2014). Ultracompact Optical Fiber Sensor for Refractive Index and High-Temperature Measurement. *Journal of Lightwave Technology, 32*(14).

Liao, C. R., Wang, D. N., & Wang, Y. (2013). Microfiber in-line Mach-Zehnder interferometer for strain sensing. *Optics Letters, 38*(5), 757-759.

Lim, K. S., Chiam, Y. S., Phang, S. W., Chong, W. Y., Pua, C. H., Zulkifli, A. Z., Ahmad, H. (2013). A Polyaniline-Coated Integrated Microfiber Resonator for UV Detection. *Ieee Sensors Journal, 13*(5), 2020-2025.

Lim, K. S., Harun, S. W., Damanhuri, S. S. A., Jasim, A. A., Tio, C. K., & Ahmad, H. (2011). Current sensor based on microfiber knot resonator. *Sensors and Actuators a-Physical, 167*(1), 60-62.

Lim, K. S., Harun, S. W., Jasim, A. A., & Ahmad, H. (2011). Fabrication of Microfiber Loop Resonator-Based Comb Filter. *Microwave and Optical Technology Letters, 53*(5), 1119-1121.

Lim, K. S., Jasim, A. A., Damanhuri, S. S. A., Harun, S. W., Rahman, B. M. A., & Ahmad, H. (2011). Resonance condition of a microfiber knot resonator immersed in liquids. *Applied Optics, 50*(30), 5912-5916.

Lim, S. D., Lee, S. G., Lee, K., & Lee, S. B. (2010). A Tunable-Transmission Sagnac Interferometer Using an Optical Microfiber. *Japanese Journal of Applied Physics, 49*(8).

Little, BE, Chu, ST, Absil, PP, Hryniewicz, JV, Johnson, FG, Seiferth, F, Trakalo, M. (2004). Very high-order microring resonator filters for WDM applications. *Photonics Technology Letters, IEEE, 16*(10), 2263-2265.

Liu, Hsi-Chun, & Yariv, Amnon. (2011). Synthesis of high-order bandpass filters based on coupled-resonator optical waveguides (CROWs). *Optics express, 19*(18), 17653-17668.

Lou, J. Y., Wang, Y. P., & Tong, L. M. (2014). Microfiber Optical Sensors: A Review. *Sensors, 14*(4), 5823-5844.

Lou, Jingyi, Tong, Limin, & Ye, Zhizhen. (2005). Modeling of silica nanowires for optical sensing. *Optics express, 13*(6), 2135-2140.

Ma, C. J., Ren, L. Y., & Xu, Y. P. (2012). Slow-light element for tunable time delay based on optical microcoil resonator. *Applied Optics, 51*(26), 6295-6300.

University of Malaya

Madsen, Christi K, & Zhao, Jian H. (1999). *Optical filter design and analysis*: Wiley-Interscience.

Mansouri-Birjandi, M. A., Moravvej-Farshi, M. K., & Rostami, A. (2008). Ultrafast low-threshold all-optical switch implemented by arrays of ring resonators coupled to a Mach-Zehnder interferometer arm: based on 2D photonic crystals. *Applied Optics, 47*(27), 5041-5050.

McKinnon, W. R., Xu, D. X., Storey, C., Post, E., Densmore, A., Delage, A., Janz, S. (2009). Extracting coupling and loss coefficients from a ring resonator. *Optics Express, 17*(21), 18971-18982.

Morgner, U, Drexler, W, Kärtner, FX, Li, XD, Pitris, C, Ippen, EP, & Fujimoto, JG. (2000). Spectroscopic optical coherence tomography. *Optics letters*, *25*(2), 111-113.

Niehusmann, J., Vorckel, A., Bolivar, P. H., Wahbink, T., Henschel, W., & Kurz, H. (2004). Ultrahigh-quality-factor silicon-on-insulator microring resonator. *Optics Letters, 29*(24), 2861-2863.

Poon, J. K. S., Huang, Y. Y., Paloczi, G. T., & Yariv, A. (2004). Soft lithography replica molding of critically coupled polymer microring resonators. *Ieee Photonics Technology Letters, 16*(11), 2496-2498.

Poon, J. K. S., Scheuer, J., Mookherjea, S., Paloczi, G. T., Huang, Y. Y., & Yariv, A. (2004). Matrix analysis of microring coupled-resonator optical waveguides. *Optics Express, 12*(1), 90-103.

Popovíc, Miloš A, Barwicz, Tymon, Watts, Michael R, Rakich, Peter T, Socci, Luciano, Ippen, Erich P, Smith, Henry I. (2006). Multistage high-order microring-resonator add-drop filters. *Optics letters, 31*(17), 2571-2573.

Roy, J. N., & Rakshit, J. K. (2014). Design of micro-ring resonator-based all-optical logic shifter. *Optics Communications, 312*, 73-79.

Shao, M., Qiao, X. G., Fu, H. W., Liu, Y. G., Zhao, X., & Yao, N. (2014). High sensitivity refractive index sensing of Mach-Zehnder interferometer based on multimode fiber core sandwiched between two waist-enlarged fiber tapers. *Optics Communications, 311*, 359-363.

Shi, L., Chen, X. F., Liu, H. J., Chen, Y. P., Ye, Z. Q., Liao, W. J., & Xia, Y. X. (2006). Fabrication of submicron-diameter silica fibers using electric strip heater. *Optics Express, 14*(12), 5055-5060.

Shi, L., Xu, Y. H., Tan, W., & Chen, X. F. (2007). Simulation of optical microfiber loop resonators for ambient refractive index sensing. *Sensors, 7*(5), 689-696.

University of Malaya

Smith, Robert B. (1976). Analytic solutions for linearly tapered directional couplers. *JOSA, 66*(9), 882-892.

Snyder, Allan W, & Love, J. (2012). *Optical waveguide theory*: Springer Science & Business Media.

Snyder, Allan W, & Love, John D. (1976). Goos-Hänchen shift. *Applied optics, 15*(1), 236-238.

Sulaiman, A., Harun, S. W., Ahmad, F., & Ahmad, H. (2014). Nonadiabatic microfiber based mode-locked erbium-doped fiber laser using graphene. *Microwave and Optical Technology Letters, 56*(7), 1670-1673.

Sulaiman, A., Harun, S. W., Ahmad, F., Norizan, S. F., & Ahmad, H. (2012a). Electrically Tunable Microfiber Knot Resonator Based Erbium-Doped Fiber Laser. *Ieee Journal of Quantum Electronics, 48*(4), 443-446.

Sulaiman, A., Harun, S. W., Ahmad, F., Norizan, S. F., & Ahmad, H. (2012b). Tunable laser generation with erbium-doped microfiber knot resonator. *Laser Physics, 22*(3), 588-591.

Sulaiman, A., Harun, S. W., & Ahmad, H. (2012). Erbium-Doped Fiber Laser With a Microfiber Coupled to Silica Microsphere. *Ieee Photonics Journal, 4*(4), 1065-1070.

Sulaiman, A., Harun, S. W., Desa, J. M., & Ahmad, H. (2012). Demonstration of DC Current Sensing through Microfiber Knot Resonator. *2012 10th Ieee International Conference on Semiconductor Electronics (Icse)*, 378-380.

Sulaiman, A., Harun, S. W., Muhammad, M. Z., & Ahmad, H. (2013). Compact Dual-Wavelength Laser Generation Using Highly Concentrated Erbium-Doped Fiber Loop Attached to Microfiber Coupler. *Ieee Journal of Quantum Electronics, 49*(7), 586-588.

Sulaiman, A., Muhammad, M. Z., Harun, S. W., Arof, H., & Ahmad, H. (2013). Demonstration of acoustic vibration sensor based on microfiber knot resonator. *Microwave and Optical Technology Letters, 55*(5), 1138-1141.

Sumetsky, M. (2008). Basic elements for microfiber photonics: Micro/nanofibers and microfiber coil resonators. *Journal of lightwave technology, 26*(1), 21-27.

Sumetsky, M, Dulashko, Y, Fini, JM, Hale, A, & DiGiovanni, DJ. (2006). The microfiber loop resonator: theory, experiment, and application. *Lightwave Technology, Journal of, 24*(1), 242-250.

University of Malaya

Sumetsky, M, Dulashko, Y, & Hale, A. (2004). Fabrication and study of bent and coiled free silica nanowires: Self-coupling microloop optical interferometer. *Optics Express, 12*(15), 3521-3531.

Sumetsky, M. (2004). Optical fiber microcoil resonator. *Optics Express, 12*(10), 2303-2316.

Sumetsky, M. (2005). Uniform coil optical resonator and waveguide: transmission spectrum, eigenmodes, and dispersion relation. *Optics Express, 13*(11), 4331-4340.

Sumetsky, M. (2010). Whispering gallery modes in a microfiber coil with an n-fold helical symmetry: classical dynamics, stochasticity, long period gratings, and wave parametric resonance. *Optics Express, 18*(3), 2413-2425.

Sumetsky, M., Dulashko, Y., Fini, J. M., & Hale, A. (2005). Optical microfiber loop resonator. *Applied Physics Letters, 86*(16).

Sumetsky, M., Dulashko, Y., Fini, J. M., Hale, A., & DiGiovanni, D. J. (2006). The microfiber loop resonator: Theory, experiment, and application. *Journal of Lightwave Technology, 24*(1), 242-250.

Sun, L. P., Li, J., Tan, Y. Z., Shen, X., Xie, X. D., Gao, S., & Guan, B. O. (2012). Miniature highly-birefringent microfiber loop with extremely-high refractive index sensitivity. *Optics Express, 20*(9).

Ta, V. D., Chen, R., & Sun, H. D. (2014). Coupled Polymer Microfiber Lasers for Single Mode Operation and Enhanced Refractive Index Sensing. *Advanced Optical Materials, 2*(3), 220-225.

Tan, Y. Z., Sun, L. P., Jin, L., Li, J., & Guan, B. O. (2013). Microfiber Mach-Zehnder interferometer based on long period grating for sensing applications. *Optics Express, 21*(1), 154-164.

Tian, Bozhi, Xie, Ping, Kempa, Thomas J, Bell, David C, & Lieber, Charles M. (2009). Single-crystalline kinked semiconductor nanowire superstructures. *Nature nanotechnology, 4*(12), 824-829.

Tien, Ming-Chun, Mizumoto, Tetsuya, Pintus, Paolo, Kromer, Herbert, & Bowers, John E. (2011). Silicon ring isolators with bonded nonreciprocal magneto-optic garnets. *Optics express, 19*(12), 11740-11745.

Tong, Limin, Gattass, Rafael R, Ashcom, Jonathan B, He, Sailing, Lou, Jingyi, Shen, Mengyan, Mazur, Eric. (2003). Subwavelength-diameter silica wires for low-loss optical wave guiding. *Nature, 426*(6968), 816-819.

Tong, Limin, Lou, Jingyi, Gattass, Rafael R, He, Sailing, Chen, Xuewen, Liu, Liu, & Mazur, Eric. (2005). Assembly of silica nanowires on silica aerogels for microphotonic devices. *Nano letters, 5*(2), 259-262.

University of Malaya

Tong, Limin, & Sumetsky, Michael. (2011). *Subwavelength and nanometer diameter optical fibers*: Springer Science & Business Media.

Vienne, G., Grelu, P., Li, Y., Chen-Perdereau, X., & Tong, L. (2008). Bistable Device based on the Kerr Effect in a Microfiber Resonator. *Aoe 2007: Asia Optical Fiber Communication & Optoelectronic Exposition & Conference, Conference Proceedings*, 570-572.

Vienne, G., Grelu, P., Pan, X. Y., Li, Y. H., & Tong, L. M. (2008). Theoretical study of microfiber resonator devices exploiting a phase shift. *Journal of Optics a-Pure and Applied Optics, 10*(2).

Vienne, G., Li, Y. H., Tong, L. M., & Grelu, P. (2008). Observation of a nonlinear microfiber resonator. *Optics Letters, 33*(13), 1500-1502.

Vienne, G., Li, Y., & Tong, L. (2007). Effect of host polymer on microfiber resonator. *Ieee Photonics Technology Letters, 19*(17-20), 1386-1388.

Wang, G. H., Shum, P. P., Tong, L. M., Li, C. M., & Lin, C. L. (2010). Polarization Effects in Microfiber Loop and Knot Resonators. *Ieee Photonics Technology Letters, 22*(8), 586-588.

Wang, P., Gu, F. X., Zhang, L., & Tong, L. M. (2011). Polymer microfiber rings for high-sensitivity optical humidity sensing. *Applied Optics, 50*(31), G7-G10.

Wang, S. S., Hu, Z. F., Li, Y. H., & Tong, L. M. (2009). All-fiber Fabry-Perot resonators based on microfiber Sagnac loop mirrors. *Optics Letters, 34*(3), 253-255.

Wei, Z. T., Song, Z. Q., Song, R., Zhang, X. L., & Meng, Z. (2014). Measurement of the optical absorption coefficient for liquid based on optical microfiber. *Optik, 125*(12), 2880-2884.

Wong, KY, Marhic, ME, Uesaka, K, & Kazovsky, LG. (2002). Polarization-independent fiber optical parametric amplifier. *OECC 2001*, 1-5.

Wu, J. X., Miao, Y. P., Lin, W., Song, B. B., Zhang, K. L., Zhang, H., . . . Yao, J. Q. (2014). Magnetic-field sensor based on core-offset tapered optical fiber and magnetic fluid. *Journal of Optics, 16*(7).

Wu, Xiaoqin, & Tong, Limin. (2013). Optical microfibers and nanofibers. *Nanophotonics, 2*(5-6), 407-428.

Wu, Y., Chen, Y. H., Rao, Y. J., Zhang, T. H., & Gong, Y. (2011). Microscopic multiple-point temperature sensing based on microfiber double-knot resonators. *21st International Conference on Optical Fiber Sensors, 7753*.

University of Malaya

Wu, Y., Rao, Y. J., Chen, Y. H., & Gong, Y. (2009). Miniature fiber-optic temperature sensors based on silica/polymer microfiber knot resonators. *Optics Express, 17*(20), 18142-18147.

Wu, Y., Zeng, X., Hou, C. L., Bai, J., & Yang, G. G. (2008). A tunable all-fiber filter based on microfiber loop resonator. *Applied Physics Letters, 92*(19). doi: Artn 191112

Wu, Y., Zhang, T. H., Rao, Y. J., & Gong, Y. (2011). Interferometric humidity sensors based on microfiber knot resonators. *21st International Conference on Optical Fiber Sensors, 7753*.

Xu, F., & Brambilla, G. (2007a). Embedding optical microfiber coil resonators in Teflon. *Optics Letters, 32*(15), 2164-2166.

Xu, F., & Brambilla, G. (2007b). Manufacture of 3-D microfiber coil resonators. *Ieee Photonics Technology Letters, 19*(17-20), 1481-1483.

Xu, Fei, Pruneri, Valerio, Finazzi, Vittoria, & Brambilla, Gilberto. (2008). An embedded optical nanowire loop resonator refractometric sensor. *Optics Express, 16*(2), 1062-1067.

Xu, Y. P., Ren, L. Y., Liang, J., Ma, C. J., Wang, Y. L., Chen, N. N., & Qu, E. S. (2014). A simple, polymer-microfiber-assisted approach to fabricating the silica microfiber knot resonator. *Optics Communications, 321*, 157-161.

Xu, Y. P., Ren, L. Y., Ma, C. J., & Liang, J. (2014). Theoretical study on slow light in different structures of optical microfiber knot resonators (OMKRs). *Optik, 125*(12), 2856-2861.

Xu, Y. P., Ren, L. Y., Ma, C. J., Wang, Y. L., Liang, J., & Qu, E. S. (2014). Wide-bandwidth zero-dispersion slow light in MKRs with a two-ring parallel connection structure based on an analogue of electromagnetically induced transparency. *Journal of Modern Optics, 61*(13), 1109-1114.

Xu, Yi-Ping, Ren, Li-Yong, Liang, Jian, Ma, Cheng-Ju, Wang, Ying-Li, Kong, Xu-Dong, & Lin, Xiao. (2015). Wideband slow light in microfiber double-knot resonator with a parallel structure. *Journal of Applied Physics, 118*(7), 073105.

Yang, Q., Jiang, X. S., Guo, X., Chen, Y., & Tong, L. M. (2009). Hybrid structure laser based on semiconductor nanowires and a silica microfiber knot cavity. *Applied Physics Letters, 94*(10).

Yao, B. C., Wu, Y., Wang, Z. G., Cheng, Y., Rao, Y. J., Gong, Y., Li, Y. R. (2013). Demonstration of complex refractive index of graphene waveguide by microfiber-based Mach-Zehnder interferometer. *Optics Express, 21*(24), 29818-29826.

University of Malaya

Yariv, A. (1973). Coupled-mode theory for guided-wave optics. Quantum Electronics, IEEE Journal of, 9(9), 919-933.

Yariv, Amnon, Xu, Yong, Lee, Reginald K, & Scherer, Axel. (1999). Coupled-resonator optical waveguide: a proposal and analysis. *Optics letters, 24*(11), 711-713.

Yu, J. H., Feng, R. H., & She, W. L. (2009). Low-power all-optical switch based on the bend effect of a nm fiber taper driven by outgoing light. *Optics Express, 17*(6), 4640-4645.

Zeng, X., Wu, Y., Hou, C. L., Bai, J., & Yang, G. G. (2009). A temperature sensor based on optical microfiber knot resonator. *Optics Communications, 282*(18), 3817-3819.

Zhang, Jiejun, Sun, Qizhen, Liang, Ruibing, Wo, Jianghai, Liu, Deming, & Shum, Perry. (2012). Microfiber Fabry–Perot interferometer fabricated by taper-drawing technique and its application as a radio frequency interrogated refractive index sensor. *Optics letters, 37*(14), 2925-2927.

Zhang, X. L., Belal, M., Chen, G. Y., Song, Z. Q., Brambilla, G., & Newson, T. P. (2012). Compact optical microfiber phase modulator. *Optics Letters, 37*(3), 320-322.

Zhang, Y., Xu, E. M., Huang, D. X., & Zhang, X. L. (2009). All-Optical Format Conversion From RZ to NRZ Utilizing Microfiber Resonator. *Ieee Photonics Technology Letters, 21*(17), 1202-1204.

Zhang, Y., Zhang, X. L., Chen, G. J., Xu, E. M., & Huang, D. X. (2010). A Microwave Photonic Notch Filter Using a Microfiber Ring Resonator. *Chinese Physics Letters, 27*(7).

Zhang, Y., Zhang, X. L., Zhang, F. Z., Wu, J. A., Wang, G. H., & Shum, P. P. (2011). Photonic generation of millimeter-wave ultra-wideband signal using microfiber ring resonator. *Optics Communications, 284*(7), 1803-1806.

Zhang, Z. S., Fan, W., Gan, J. L., Li, C., & Yang, Z. M. (2013). Single-Frequency Microfiber Single-Knot Laser. *Applied Physics Express, 6*(4).

Zhou, G. R., Feng, G. Y., Zhou, H., Deng, G. L., Zhang, Y., & Ma, Z. (2011). Experimental investigation of supercontinuum generated from microfiber loop wound on Al-coated silica rod. *Optics Communications, 284*(19), 4769-4772.

Zou, Z., Zhou, L. J., Li, X. W., & Chen, J. P. (2014). Channel-spacing tunable silicon comb filter using two linearly chirped Bragg gratings. *Optics Express, 22*(16).

University of Malaya

LIST OF PUBLICATIONS AND PAPARES PRESENTED

PUBLICATIONS:

1. Nodehi, S., Mohammed, W. S., Ahmad, H., & Harun, S. W, "Demonstration of a periodic pass-band filter based on coupled microfiber knots," Photonics Technology letter, IEEE, 10, 1061-1064, 2016.
2. Nodehi, S., Mohammed, W. S., Ahmad, H., & Harun, S. W, "Realization of Spectral Tunable Filter Based on Thermal Effect in Microfiber Structure," Optical Fiber Technology, Elsevier, 28, 38-41, 2016.
3. Nodehi, S., Mohammed, W. S., Ahmad, H., & Harun, S. W, "Fabrication and characterization of high order filter based on resonance in hybrid multi-knots microfiber structure," Optics & Laser Technology, 78, 120-124, 2016.
4. Nodehi, S., Mohammed, W. S., Ahmad, H., & Harun, S. W," Investigation of thermal effects in a resonance condition of microfibre double-knot resonators as high-order filter," Micro & Nano Letters, IET, 10(10), 580-582, 2015.
5. Lokman, S. Nodehi, M. Batumalay, H. Arof, H. Ahmad, and S. W. Harun, "Optical Fiber Humidity Sensor Based on a Tapered Fiber with Hydroxyethylcellu Lose/Polyvinylidenefluoride Composite," Microwave and Optical Technology Letters, vol. 56, pp. 380-382, 2014.

PAPARES PRESENTED:

1. "Study of Vernier Effect Using Microfiber Structure", International Conference on Photonic, Kuala lumpur, Malaysia 2014.
2. "Micro-telecommunication amplifier using erbium doped micro-ring waveguide structures" AUN/SEED-NET Conference on Electrical Engineering, kuala lumpur, Malaysia, 2014.

University of Malaya